COLLOIDAL SURFACE-ENHANCED RAMAN SPECTROSCOPY STUDY OF HYBRID GROUPER EPIDERMAL MUCUS AS A NON-INVASIVE METHOD OF MUCUS PROFILING

By

NATHANIEL LEONG JENN KWANG

Thesis Submitted to the School of Graduate Studies, Universiti Putra Malaysia, in Fulfilment of the Requirements for the Degree of Master of Science

February 2024

FK 2024 5

Abstract of thesis presented to the Senate of Universiti Putra Malaysia in fulfilment of the requirement for the degree of Master of Science

COLLOIDAL SURFACE-ENHANCED RAMAN SPECTROSCOPY STUDY OF HYBRID GROUPER EPIDERMAL MUCUS AS A NON-INVASIVE METHOD OF MUCUS PROFILING

By

NATHANIEL LEONG JENN KWANG

February 2024

Chairman : Mohd. Adzir bin Mahdi, PhD
Faculty : Engineering

Fish epidermal mucus is an important component in the innate immune defence against pathogens. Due to its significance in the fish physiology, detailed profiling of fish epidermal mucus will give valuable insight into fish health. However, conventional proteomics and metabolomics profiling of the biomolecules in fish epidermal mucus is time consuming. Therefore, realising the need for a rapid and minimally invasive method to profile fish epidermal mucus, this study explored a label-free colloidal surface-enhanced Raman spectroscopic (SERS) method to profile grouper epidermal mucus. The standard citrate reduction method was used to synthesise the gold nanoparticles. UV-Visible spectroscopy, dynamic light scattering, and transmission electron microscopy were used to characterise the gold nanoparticles. Acidified sodium sulphate (Na_2SO_4) at pH 3 was chosen as the

aggregating agent due to its low affinity to form bonds with gold nanoparticles. The gold nanoparticles were preconcentrated prior to SERS analysis and 9.5 µL of the preconcentrated gold nanoparticles were mixed with 10 µL of the analyte solution followed by 0.5 µL of the aggregating agent. The SERS efficacy of the synthesised gold nanoparticles and Na_2SO_4 was tested with three different analyte solutions, namely, Rhodamine 6G (R6G), lysozyme and hybrid grouper (*Epinephelus fuscoguttatus* x *Epinephelus lanceolatus*) mucus. Based on the results, the optimal concentration of Na_2SO_4 to obtain the highest SERS enhancement for R6G and grouper mucus was 1 M, while the concentration for lysozyme was 0.1 M. This indicates that lysozyme induces a higher degree of aggregation of gold nanoparticles. There were a few overlapping peaks in the SERS spectrum of lysozyme and grouper mucus, namely, 818, 1283, 1454 and 1542 cm^{-1}. The peaks at 818, 1283, and 1542 cm^{-1} may be good candidates for the detection of lysozyme in grouper epidermal mucus. Overall, the SERS protocol proposed in this work offers great potential for rapid and minimally invasive analysis of fish epidermal mucus.

Keywords: Gold nanoparticles, grouper epidermal mucus, Surface-enhanced Raman spectroscopy (SERS)

SDG: GOAL 14: Life Below Water

Abstrak tesis yang dikemukakan kepada Senat Universiti Putra Malaysia sebagai memenuhi keperluan untuk ijazah Master Sains

KAJIAN SPEKTROSKOPI RAMAN DIPERTINGKATKAN PERMUKAAN KOLOID BAGI LENDIR EPIDERMIS KERAPU HIBRID SEBAGAI KAEDAH PEMPROFILAN LENDIR YANG KURANG INVASIF

Oleh

NATHANIEL LEONG JENN KWANG

Februari 2024

Pengerusi : Mohd. Adzir bin Mahdi , PhD
Fakulti : Kejuruteraan

Lendir epidermis ikan merupakan komponen penting dalam sistem pertahanan imunisasi semula jadi terhadap patogen. Oleh sebab kepentingannya dalam fisiologi ikan, profil terperinci lendir epidermis ikan dapat memberikan informasi bernilai mengenai kesihatan ikan. Namun begitu, kaedah pemprofilan proteomik dan metabolomik konvensional bagi biomolekul dalam lendir epidermis ikan mengambil masa yang lama. Oleh itu, bagi memenuhi keperluan kaedah pemprofilan lendir epidermis ikan secarapantas dan kurang invasif, , kajian ini meneroka kaedah Spektroskopi Raman Dipertingkatkan Permukaan (SERS) koloid tanpa label untuk memprofil lendir epidermis ikan kerapu. Kaedah standard pengurangan sitrat digunakan untuk mensintesis nanozarah emas. Spektroskopi ultraungu tampak (UV-Visible), penyebaran cahaya dinamik dan mikroskopi elektron penghantaran digunakan untuk mencirikan nanozarah emas. Natrium sulfat (Na_2SO_4) yang diasidkan pada pH 3 dipilih sebagai

agen pengagregatan disebabkan sifatnya yang lemah untuk membentuk ikatan dengan nanozarah emas.. Larutan nanozarah emas dipekatkan terlebih dahulu sebelum menjalani analisis SERS.9.5 µL larutan nanozarah emas pekat tersebut dicampur dengan 10µL larutan analit diikuti dengan 0.5 µL agen pengagregatan. Keberkesanan SERS terhadap nanozarah emas yang tersintesis dan Na_2SO_4telah diuji dengan tiga larutan analit iaitu, Rhodamina 6G (R6G), lisozim dan lendir epidermis kerapu hibrid (*Epinephelus fuscogattus* × *Epinephelus lanceolatus*). Berdasarkan keputusan kajian, kepekatanoptimal Na_2SO_4 untuk mendapatkan peningkatan SERS tertinggi bagi R6G dan lendir epidermis kerapu ialah 1 M, manakala kepekatan bagi lisozim ialah 0.1 M. Hal inimenunjukkan bahawa lisozim mencetuskan tahap pengagregatan yang lebih tinggidalam nanozarah emas. Terdapat beberapa puncak yang bertindih dalam spektrumlisozim SERS dan lendir kerapu iaitu 818, 1283,1454 dan 1542 cm^{-1}. Puncak yang dicatatkan pada 818, 1283 dan 1542 cm^{-1} mungkin merupakan puncak yang baik bagi pengesanan lisozim dalam lendir epidermis kerapu. Kesimpulannya, protokol SERS yang dicadangkan dalam kajian inimenawarkan potensi untuk analisis pantas dan kurang invasif terhadap lendir epidermis ikan.

Kata Kunci: Lendir epidermis kerapu, nanozarah emas, Spektroskopi Raman Dipertingkatkan Permukaan (SERS)

SDG: MATLAMAT 14: Hidupan Bawah Air

ACKNOWLEDGEMENTS

The funding for this research is provided by the Ministry of Higher Education of Malaysia under the Transdisciplinary Research Grant Scheme (TRGS/1/2020/UPM/02/1/1). I would like to express my gratitude to my supervisors, Prof. Dr. Mohd. Adzir bin Mahdi and Assoc. Prof. Dr. Mohd. Hanif bin Yaacob for their continuous support throughout my research work. I would also like to thank Prof. Dr. Ahmad. Rifqi Md Zain and Dr. Tengku Abdul Aziz for providing technical advice and support for conducting surface-enhanced Raman spectroscopy analysis.

Many thanks also the other members of the research group namely, Dr. Chong Chou Min, Dr. Annie Christianus and Ellia Kartini Mujar, for providing support in acquiring the grouper mucus samples.

Additionally, I would like to express my sincerest gratitude to my parents, Lily Muh and Leong Kon Min, for their support in my research career and for being my emotional bedrock.

Not forgetting the appreciation for the lab members of the Photonics Systems Engineering for their support in making my research journey easier.

This thesis was submitted to the Senate of Universiti Putra Malaysia and has been accepted as fulfilment of the requirement for the degree of Master of Science. The members of the Supervisory Committee were as follows:

Mohd Adzir Mahdi, PhD
Professor
Faculty of Engineering
Universiti Putra Malaysia
(Chairman)

Mohd. Hanif Yaacob, PhD
Associate Professor
Faculty of Engineering
Universiti Putra Malaysia
(Member)/

Ahmad Rifqi Md Zain
Associate Professor
Institute of Microengineering and Nanoelectronics
Universiti Kebangsaan Malaysia
(Member)

Tengku Hasnan Tengku Abdul Aziz
Doctor
Institute of Microengineering and Nanoelectronics
Universiti Kebangsaan Malaysia
(Member)

ZALILAH MOHD SHARIF, PhD
Professor and Dean School of Graduate Studies Universiti Putra Malaysia

Date: 11 July 2024

TABLE OF CONTENTS

LIST OF TABLES

LIST OF FIGURES

LIST OF ABBREVIATIONS

$AgNO_3$	Silver nitrate
AOZ	3-amino-2-oxazolidinone
APTMS	(3-aminopropyl)trimethoxysilane
AuNp	gold nanoparticles
BC	Breast cancer
CaF_2	Calcium fluoride
CCl_4	Carbon tetrachloride
DLS	Dynamic light scattering
EF	Enhancement factor
FUZD	Furazolidone
$HAuCl_4$	Gold (III) chloride
HCC	Hepatocellular carcinoma
IR	Infrared
KBr	Potassium bromide
LDA	Linear discriminant analysis
LSPR	Localised surface plasmon resonance
MPD-SPME	Mechanical power-driven solid phase microextraction
MPTMS	(3-mercaptopropyl)trimethoxysilane
Na_2SO_4	Sodium sulphate
Na_3Ct	Sodium citrate
NaCl	Sodium chloride
NED	N-(1-naphthyl) ethylenediamine dihydrochloride
PCA	Principal component analysis

Phe	Phenylalanine
R6G	Rhodamine 6G
rpm	Rotations per minute
SEM	Scanning electron microscopy
SERRS	Surface-ehnanced resonant Raman scattering
SERS	Surface-enhanced Raman spectroscopy
TEM	Transmission electron microscopy
Trp	Tryptophan
Tyr	Tyrosine

CHAPTER 1

INTRODUCTION

1.1 Research Background

Raman scattering is an inelastic scattering of photons when light impinges on a material. As a result of the scattering, both the energy and direction of the photons are changed. There are two types of Raman scattering: Stokes and anti-Stokes Raman scattering. The former refers to the phenomenon where the photons lose their energy to the molecules while the latter refers to the phenomenon where the photons gain energy from the molecules. The amount of energy lost, or gain is highly dependent on the vibrational energy of the molecular bonds, which are reflected in the change in wavelength of the incident photons. Therefore, the change in wavelength, measured as the Raman shift, allows for the fingerprinting of a material based on the Raman shift. In most application, the Stokes Raman scattering is used due to the low probability of anti-Stokes Raman scattering occurring. This is due to the Boltzmann distribution. Molecules will need to be in a higher energy state to transfer their energy to the incident photons and at low temperatures, the number of molecules in the excited state is low.

Infrared spectroscopy is another vibrational spectroscopic method used to obtain the spectral fingerprint of a substance. However, infrared and Raman spectroscopy differ in fundamental ways. Infrared spectroscopy depends on the change in dipole moment while Raman spectroscopy depends on the

change in polarizability of the molecular bond (Exline, 2013). Raman spectroscopy has one unique advantage over infrared spectroscopy, namely, water is a weak Raman scatterer, therefore, interference from water in minimal in Raman spectroscopy (E. Smith & Dent, 2005). Therefore, Raman spectroscopy has a unique advantage in analysing biological samples where the most common solvent is water. Drying of biological samples often alter their properties, for example, proteins will undergo conformational change upon dehydration (Prestrelski et al., 1993). Therefore, Raman spectroscopy allows for the analysis of biological samples in their native state. However, fluorescence interference and weak sensitivity are significant disadvantages of Raman spectroscopy in analytical applications.

Experimentally in the 1970s, the tremendous enhancement of Raman scattering of analyte adsorbed on the surface of roughened metal has been described. Thus, surface-enhanced Raman spectroscopy (SERS) has been developed to address the weak sensitivity of Raman spectroscopy. SERS also has the added advantage of quenching the fluorescence of fluorophores adsorbed on noble metal surface, leading to an improved Raman spectrum quality (Shan et al., 2017). Various types of SERS substrates has been developed, ranging from fabricated nanostructures on noble metal surface (Fujiwara et al., 2022; Lv et al., 2021), deposited metallic nanoparticles (Almehmadi et al., 2019; Zeiri et al., 2012), colloidal solution (Xue et al., 2018; Zhou et al., 2019) and cost-effective substrates such as nanoparticles-loaded paper-based substrate (Moram et al., 2018) and deposited nanoparticles on Blu-Ray DVD disc (Chamuah et al., 2019). Colloidal system remains is the

simplest method as it simply requires mixing the metal colloid with the analyte solution, making it ideal for analysing biofluid. However, aggregation plays an important role in the SERS efficiency (Cyrankiewicz et al., 2007). Common aggregating agents are halide salts. However, they pose the issue of competitive binding to the nanoparticle surface, diminishing the adsorption of analyte. Sulphate ions on the other hand, have low affinity towards metallic nanoparticles surface, thus, lower tendency to competitively bind to the nanoparticle surface. (X. X. Han et al., 2009).

Fish epidermal mucus is an important first line of defence against pathogen as it is in constant contact with the environment. The mucus is composed primarily of mucin and a host of immunological compounds such as antimicrobial proteins, antibodies, peptides, lysozyme and lectins (Dash et al., 2018). Analysis of fish epidermal mucus offers a non-invasive method to determine fish health status. SERS is an ideal platform to analyse fish epidermal mucus due to the aforementioned weak Raman scattering of water and the minimal sample preparation required, allowing for the possibility to conduct in-situ analysis.

1.2 Problem Statements

Fish epidermal mucus contains a wide range of anti-microbial compounds and any changes in the fish physiology will be reflected in the change in epidermal mucus composition. Therefore, a detailed profiling of the epidermal mucus can provide great insight into fish health status. The conventional methods to

profile fish epidermal mucus includes Fourier-transform infrared (FTIR) spectroscopy, and the omics tools such as proteomic and metabolomic profiling. However, these methods have significant drawbacks; namely, water is a strong infrared absorber (Magalhães et al., 2021) and the omics tools are time consuming (Natnan et al., 2021)

Therefore, SERS is proposed as a non-invasive, rapid, and cost-effective method to profile fish epidermal mucus. SERS of biological fluids can be conducted in two ways: using dried biofluid on a solid SERS substrate and in liquid form in a colloidal system. In the latter system, aggregating agents play an important role in forming the SERS hot-spots (Turzhitsky et al., 2018) and the suitable aggregating agent highly depends on the analyte (Xie et al., 2020; Ye et al., 2023). To date, the colloidal SERS of grouper epidermal mucus has yet to be studied in detail and the ideal choice of aggregating agent has yet to be determined.

1.3 Research Objectives and Research Questions

This study aims to determine the optimised aggregating agent and sample preparation methods to achieve the best SERS efficiency of grouper mucus. The specific objectives are as follows:

1. To evaluate the viability of acidified (pH 3) sodium sulphate solution as aggregating agent for the colloidal SERS of grouper mucus.

2. To determine the ideal concentration of aggregating agent to obtain the highest SERS efficiency of desired biomolecules in grouper mucus, namely, proteins.

3. To conduct characterisation and profiling of grouper epidermal mucus using SERS spectrum.

The research questions are as follows:

1. How does acidified (pH 3) sodium sulphate solution perform as aggregating agent for colloidal SERS of grouper epidermal mucus compared to halide salt such as sodium chloride?
2. What is the optimal concentration of sodium sulphate solution to obtain the best SERS efficiency of grouper epidermal mucus?
3. Is it possible to detect specific proteins such as lysozyme from the multiplexed SERS spectrum of grouper mucus by identifying the overlapping peaks?

1.4 Significance of Study

Colloidal system SERS is the most straight-forward method for the SERS analysis of fish epidermal mucus. This method does not require any fabrication of SERS substrates and is relatively quick and cost-efficient. However, due to the limited study of SERS analysis of fish epidermal mucus, this study aims to elucidate the optimised sample preparation and aggregating agent to obtain the best SERS efficiency from fish epidermal mucus.

This study aims to serve as the groundwork for future SERS analysis of fish epidermal mucus and to demonstrate the possibility of in-situ analysis of fish epidermal mucus using SERS using a portable Raman spectroscopy setup using commercially available equipment.

1.5 Scope and Limitations

This work will be focusing on grouper mucus due to the limited availability of mucus from other fish species. It is assumed that the findings of this work will apply to the SERS analysis of mucus from marine fish. The chosen aggregating agent is sodium sulphate solution with concentration ranging from 2 M to 0.1 M with the pH value adjusted to 3 using dilute sulphuric acid. The performance of the aggregating agent will be evaluated using the following analytes:

1. A fluorescent dye, Rhodamine 6G (R6G) with concentration of 0.1 mM.
2. 300 µg/ml lysozyme solution in water.
3. Epidermal mucus from grouper.

This study will only perform basic characterisation of grouper mucus based on the peaks present and correlated to the functional groups and then correlated to the possible biomolecules present based on the functional groups. The spectrum from the mucus will be matched with the spectrum of lysozyme to identify the overlapping peaks to determine if lysozyme is one of the

biomolecules present in the mucus. A diagnosis of the fish health status will not be performed due to the limited samples available for a statistically significant number of samples to build a statistical and predictive model. Specificity to a specified biomolecule is beyond the scope of this study.

1.6 Outline of Thesis

This thesis is divided into five chapters: introduction, literature review, methodology, results and discussion, and conclusion. The research background and objectives are discussed in this chapter. The research questions that will be addressed in this work is also discussed in this chapter. This chapter also clearly defines the significance of this work and the scope and limitations of this study.

The theoretical background for Raman spectroscopy and SERS is discussed in Chapter 2. In addition, some examples of SERS substrates and SERS in a colloidal system is discussed in this chapter. Subsequently, applications of SERS in bioanalysis and aquaculture are also discussed in this chapter. Thus, this chapter concludes with the identified gap in the available research.

Chapter 3 covers the materials and reagents, synthesis of gold nanoparticles, mucus sample collection, sample preparation for SERS analysis, experimental setup, and spectral processing.

In Chapter 4, the experimental results are discussed. The result covers the

evaluation of two different salt solution as the aggregating agent for colloidal SERS and the appropriate aggregating agent was chosen for subsequent experimental work. This chapter discusses the efficacy of the synthesised gold nanoparticles and chosen aggregating agent to perform colloidal SERS using three different analytes: R6G, lysozyme and grouper epidermal mucus.

The characterisation of grouper mucus using SERS spectrum is also discussed in this chapter.

Chapter 5 summarises the research findings and highlights the important experimental results and provides some recommendations for future research.

CHAPTER 2

LITERATURE REVIEW

2.1 Raman Spectroscopy

Raman scattering is first observed by Chandrasekhara Venkata Raman and Kariamanikam Srinivasa Krishnan in 1928 when they showed that frequency of light changes after it is being scattered by benzene as shown in Figure 2.1 (Singh, 2002).

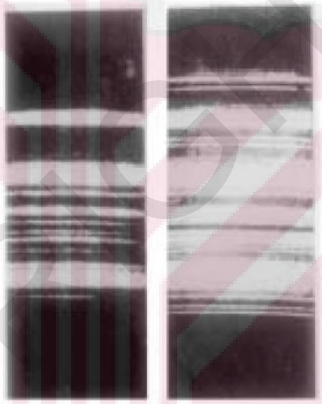

Figure 2.1: Spectrum of quartz mercury lamp with wavelength above 4358 Å being filtered off (left) and spectrum of the lamp after passing through benzene (right).
(Singh, 2002)

When photons impinge on a material, the photons are absorbed and re-emitted in various directions. This phenomenon is known as scattering. Elastic scattering events are known as Rayleigh scattering, where the energy of the photons does not change. Raman scattering are inelastic scattering events where both the energy and direction of the photon changes. The energy change in the photons may be lost of energy to the molecule when it relaxes to an excited state, or the photon may gain energy from molecules in the

excited state. The former is known as Stokes Raman scattering while the latter is known as anti-Stokes Raman scattering (E. Smith & Dent, 2005). The vibrational energy level transition of a molecule in each scattering events is shown in Figure 2.2.

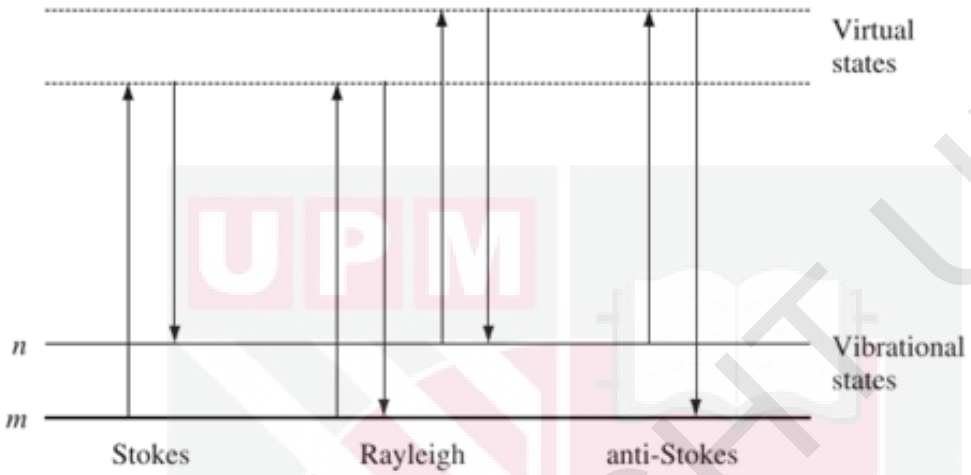

Figure 2.2: Vibrational energy level transition in Rayleigh scattering, Stokes and anti-Stokes Raman scattering.
(Ferraro et al., 2003)

Typically, Raman scattering occurs in one every 10^7 photons. Stokes Raman scattering is more probable due to the low number of molecules in the excited state at room temperature due to the Boltzmann distribution. Due to the low probability of Raman scattering, a laser source is often necessary to obtain a meaningful spectrum (E. Smith & Dent, 2005). Advancements in detector technology, optical filters, laser diodes, and optical fibre coupling has improved the feasibility of routine analysis using Raman spectroscopy (Crocombe, 2018). Figure 2.3(a) shows an example of the experimental setup to collect the Raman signal in the perpendicular direction.

The change in energy is measured as the Raman shift expressed in

$$Raman\ shift\ [cm^{-1}] = \frac{10^7}{\lambda_{excitation}[nm]} - \frac{10^7}{\lambda_{Raman}[nm]} \quad (1)$$

where $\lambda_{excitation}$ and λ_{Raman} are the excitation and Raman signal wavelength respectively. The Raman spectrum of CCl_4 is shown in Figure 2.3(b). The energy shift in Raman scattering depends on the vibrational energy of the molecular bonds in the molecule. Therefore, the Raman spectrum can elucidate information about the molecular structure of a material.

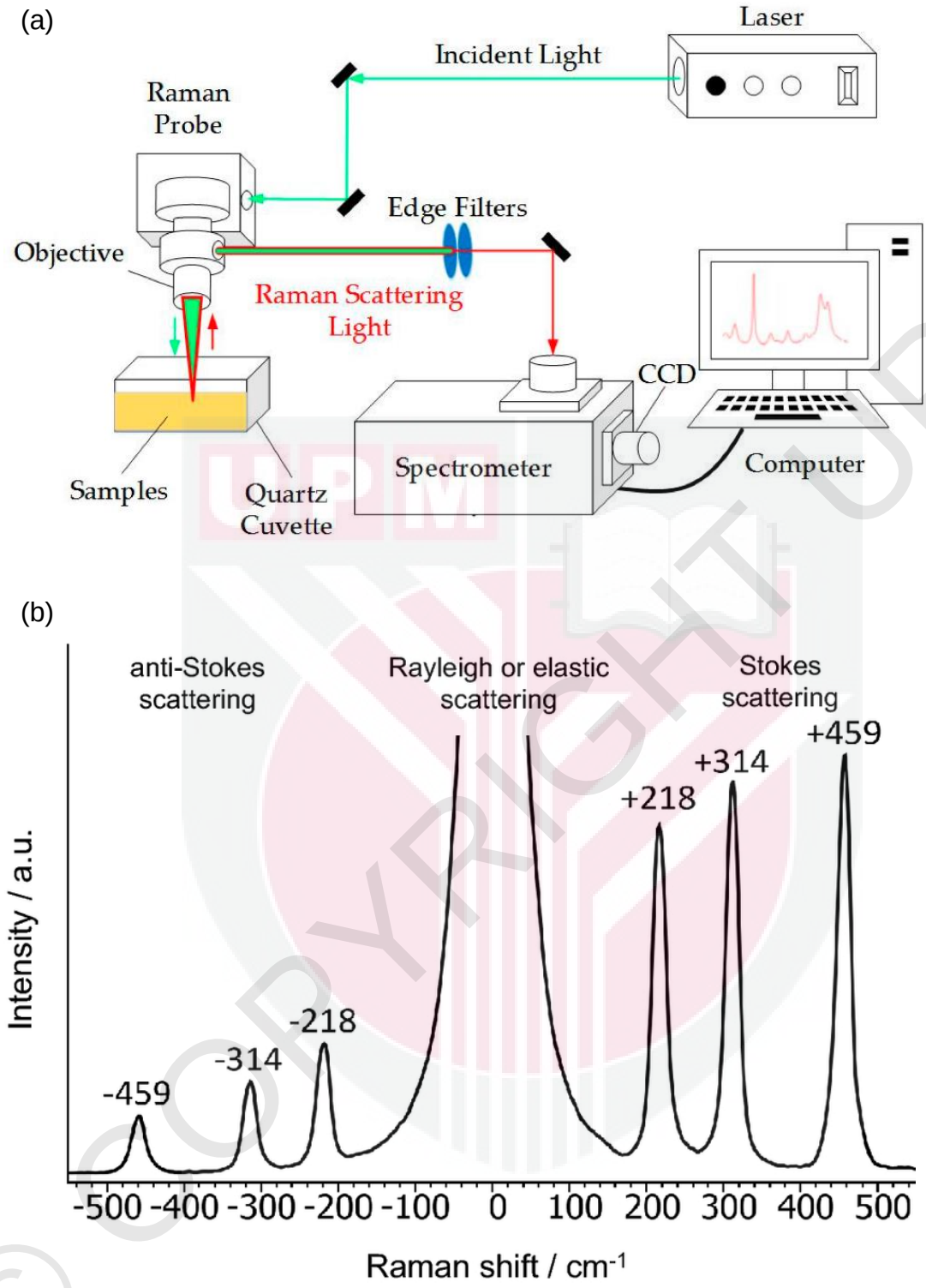

Figure 2.3: (a) Example of Raman scattering experimental setup (Wan et al., 2017) and (b) Raman spectrum of CCl_4.
(Campanella et al., 2021)

Due to the non-invasive and sensitive nature of Raman spectroscopy, the technique has been used in clinical, chemical and biological analysis. Tissue analysis and diagnosis (Hanna et al., 2021), blood analyte detection (Q. Wang et al., 2021) and cellular examination (Elumalai et al., 2020) has been performed using Raman spectroscopy. In mice, Raman spectroscopy enables non-destructive quantification of atherosclerotic plaque composition with good agreement with histological results (van de Poll et al., 2001). In addition, Raman spectroscopy has demonstrated good results in diagnosing benign and malignant skin tumours (Bratchenko et al., 2021). In most cases, Raman spectroscopy alone is sufficient to identify biological samples, but it is often complementary to IR spectroscopy (Kalasinsky & Kalasinsky, 2005). Fluorescence and low sensitivity (especially for aqueous samples) are the main hurdles in Raman spectroscopy (Baena & Lendl, 2004).

2.2 Surface-Enhanced Raman Spectroscopy (SERS)

2.2.1 Mechanism of Surface-Enhanced Raman Spectroscopy

As stated in the previous section, due to fluorescence and poor sensitivity of Raman spectroscopy for aqueous samples, Raman spectroscopy is rarely used. With the aid of noble metal nanoparticles, the hurdles of Raman spectroscopy can be overcome using the surface enhancement effect.

In pursuit for a minimally invasive, highly reliable and sensitive analysis methods for biological samples, surface-enhanced Raman spectroscopy has

been shown to be a promising approach (Zong et al., 2018). SERS is first observed experimentally in 1973, where the Raman signal from pyridine adsorbed on roughed silver is enhanced by 6000 times (Fleischmann et al., 1974).

Localised surface plasmon resonance (LSPR) plays an important role in understanding the mechanism behind SERS. Figure 2.4(a) illustrates the LSPR on metallic nanoparticles. In the presence of electromagnetic field, electrons on the metallic nanoparticle will oscillate. This is possible due to the delocalised electrons on the metal surface. The collective oscillation of the electrons is known as surface plasmon. When the frequency of the surface plasmon is equal to the incoming electromagnetic wave, resonance occurs. This phenomenon is known as LSPR. During LSPR, the electromagnetic field at the nanoparticle surface is greatly enhanced and the optical extinction is maximum (Ke et al., 2021). These two factors play an important role in SERS.

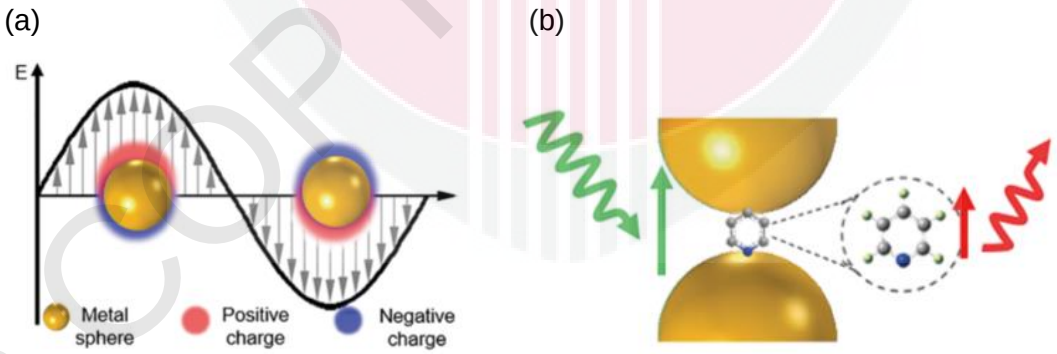

Figure 2.4: (a) Local surface plasmon resonance (LSPR) and (b) SERS of a molecule adsorbed on the metal nanoparticle surface.
(Zong et al., 2018)

The analyte molecule must be very close to the metal nanoparticle surface for SERS to occur as shown in Figure 2.4(b). This is due the electromagnetic field strength being proportional to the inverse of the cube of distance from the surface of the metal nanoparticle. The mechanism behind SERS can be understood in two ways: electronic and chemical enhancement. In electronic enhancement, the enhancement arises from the intense near-field electromagnetic field on the metal nanoparticle surface, leading the greater interaction between the electromagnetic field and molecular bonds. While in chemical enhancement, the enhancement arises from the formation of bonds between the metal and molecule, leading to formation of surface species with increased polarizability. These surface species are believed to be resonant intermediates for Raman scattering. There is evidence for both electronic and chemical enhancement, but electronic enhancement is believed to play a major role (E. Smith & Dent, 2005).

2.2.2 Surface-Enhanced Raman Spectroscopy Substrates

The key to a SERS substrates functionality is the large surface area for the adsorption of molecules. Typically, SERS substrates are fabricated from roughed noble metals, nanoparticles colloid and lithographic and non-lithographic methods to form nanostructures on a solid substrate (Betz et al., 2014). Metal surfaces can be roughened using electrochemical method or chemical etching. A silver or gold electrode can be roughed using an oxidation-reduction cycle (Tuschel et al., 1986). This process involves immersing the electrode into a redox media such as sodium chloride solution and connecting

it to a power source and signal generator. By applying an alternating voltage to the electrode, redox reaction will roughen the surface. The redox media and voltage play an important role in the surface morphology of the electrode. After the roughening process, the electrode is immersed in the analyte solution and allowed to dry before spectral acquisition. The chemical etching method is a wet etching method where the metal electrode, such as silver electrode, is etched using an acid such as nitric acid (Wijesuriya et al., 2016). This method has fallen out of favour due to the emergence of more efficient and reliable SERS substrates (Sauer et al., 2000).

Solid SERS substrates can be fabricated immobilising metal nanoparticles on a solid substrate and by fabricating nanostructures on a solid substrates using nanomachining and lithographic methods (Mosier-Boss, 2017). Gold or silver nanoparticles can be immobilised on a quartz or glass surface using a silane linker such as (3-mercaptopropyl)trimethoxysilane (MPTMS) and (3-aminopropyl)trimethoxysilane (APTMS) (Péron et al., 2009). Nanostructures directly fabricated on a solid substrate can also be used for SERS substrate. Silicon or glass substrate is ablated using femtosecond pulsed laser in air followed by a deposition of silver (Y. Han et al., 2009; Lin et al., 2009). Nanosphere lithography is another method of fabricating SERS substrates. This method is cheap, has high-throughput and produces a uniform two-dimensional, highly ordered metallic nanoparticles array. The process begins with deposition of a suspension of polystyrene or silica nanospheres on a conductive surface. The spheres self-assemble to form a mask for deposition of gold or silver. Physical vapour deposition of gold or silver can form a

nanoparticle over film array. Alternatively, the mask can be lifted off to form an array of uniform array of triangular nanoparticles.

The gold or silver may also be electrodeposited, followed by a removal the mask to form a hexagonal array of circular voids. The process is summarised in Figure 2.5 (Wu et al., 2008).

Figure 2.5: Schematic of the nanosphere lithography to form SERS substrate. The process can be used to form three types of substrates: a gold or silver film over nanospheres (FON), an array of triangular nanoparticles and an array of circular voids.
(Wu et al., 2008).

Electron beam lithography is a well-established technique in semiconductor fabrication and can be used to fabricate metallic nanostructures on a substrate. The process to fabricate SERS substrate is not too dissimilar compared to the semiconductor fabrication. Where they differ is the deposition of noble metal after the writing on the resist and development of the resist. After the deposition of the metallic film, the resist is then removed using a solvent or plasma etching, leaving behind the metallic nanostructure. This process is

summarised in Figure 2.6 (Yue et al., 2012).

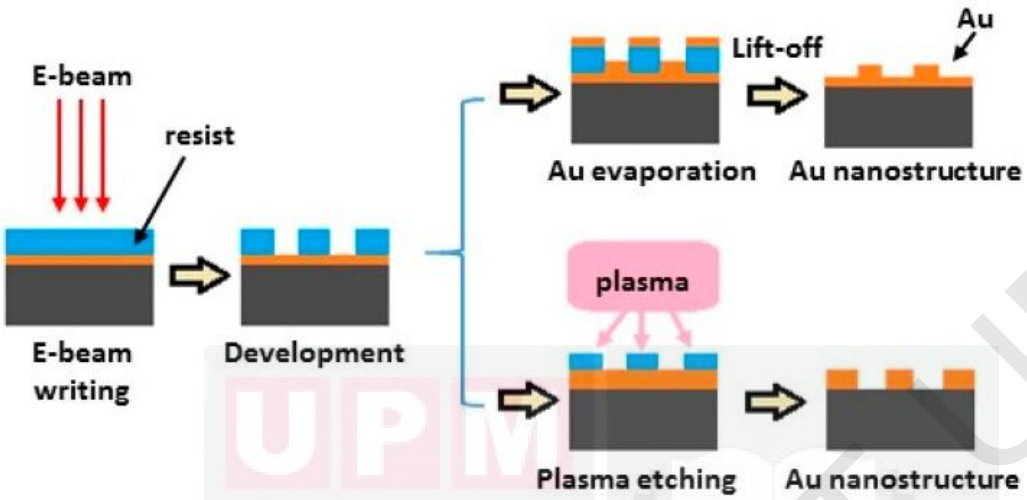

Figure 2.6: Schematic of electron beam lithography to fabricate SERS substrate.
(Yue et al., 2012)

The lithographic methods are often time-consuming, requiring multiple steps to fabricate SERS substrates. Cost-effective and quick methods to fabricate SERS substrates such as embedding nanoparticles in filter paper (Moram et al., 2018) and deposition of gold on a Blu-Ray DVD disc (Chamuah et al., 2019). These methods rely on the already present nanostructures in the substrate prior to the deposition of nanoparticles such as the network cellulose fibres in filter paper and the nano-islands and nanogaps on the Blu-Ray DVD discs. These solid substrates often require the drying of the analyte solution on the substrate before spectral acquisition of the analyte (Chamuah et al., 2019; Lin et al., 2009; Moram et al., 2018; Yue et al., 2012). The drying process facilitates the movement of the molecule on the substrate to achieve the optimum orientation for chemical enhancement (Fang et al., 2009). For a biological sample, the drying process often changes the properties of the sample. In addition, for a complex molecule with a three-dimensional structure

like protein, the orientation of the molecule on the substrate affects its SERS spectrum. On a solid substrate, the orientation of the molecule adsorbed on the metallic nanostructures will be random, leading to issues with repeatability due to the orientation dependent enhancement of the functional groups in the protein molecule (X. Yu et al., 2020). These two factors result in the poor repeatability of SERS of biological specimens.

2.2.3 Surface-Enhanced Raman Spectroscopy in Colloidal System

Metallic nanoparticle colloid is a useful SERS substrate particularly in chemical sensing. Metal nanoparticles can be synthesised using physical method, typically using laser ablation with a femtosecond laser (C. Li et al., 2020), and chemical reduction method using reducing agent such as sodium citrate and sodium borohydride as described by (P. C. Lee & Meisel, 1982). The gold and silver nanoparticles can also be conjugated with various capping agents to alter their surface chemistry. The ligands on the surface of the nanoparticles can improve selectivity and sensitivity (Israelsen et al., 2015). These noble metal colloids allow for the SERS analysis of biofluids simply by mixing the colloid with the analyte. This is advantageous for SERS analysis of samples that may be altered during the drying process which is often necessary for solid substrates. In addition, in a colloidal system, the orientation dependence of the SERS spectra may be eliminated because the formation of aggregates in the colloid traps the molecules in the nanogaps between the nanoparticles, leading to a uniform enhancement across the molecule as illustrated in Figure 2.7.

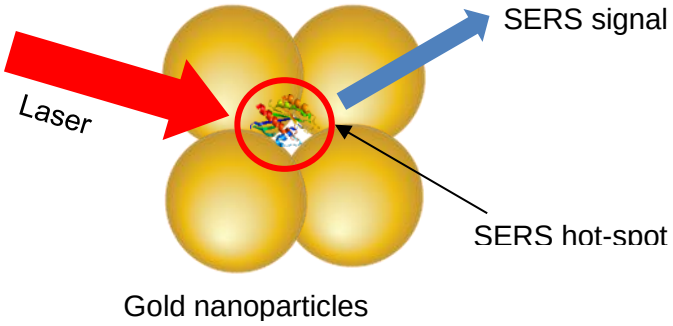

Figure 2.7: Schematic of molecules trapped in the nanogaps between aggregated nanoparticles.

SERS hot spots are the region of intense localised magnetic field produced by the coupling of LSPR of nanoparticles in the vicinity. These hot spots are present in the nanogaps between the nanoparticles and are fundamental to the surface-enhanced Raman scattering phenomena (H. Li et al., 2022). Evidently, a single nanoparticle is insufficient to produce a significant enhancement (Tay et al., 2010) and aggregation of nanoparticles play an important role in colloidal SERS (Dou et al., 1999; Siiman & Feilchenfeld, 1988). For optimal enhancement, the aggregates need to be small to trap the molecules between the nanogaps between the aggregates. Large aggregates will shield the hot spots. The formation of aggregates is dependent on the concentration, amount and the type of aggregating salts used (Turzhitsky et al., 2018).

The aggregation of metallic nanoparticles occurs due to the displacement of the surface stabilising agent (such as citrate) by the aggregating salts, depletion of the surface charge which allows the Van der Waals attraction to overcome the electromagnetic repulsion (Shi et al., 2018). In addition to aggregation, the size, shape and morphology of the nanoparticles also play a

role in the enhancement efficiency. Gold nanoparticles with diameter of 46 nm is shown to have the highest SERS enhancement but 74 nm gold nanoparticles exhibit the highest factor per unit surface area when the data is corrected for surface area (Bell & McCourt, 2009). Faceted nanoparticles such as gold nanocubes (Ding et al., 2017) and nanostars (Mahmoud et al., 2020) exhibit higher enhancement due to the larger hot-spots and larger surface area for adsorption. The simulated SERS hot spots between gold nanospheres and nanocubes is shown in Figure 2.8.

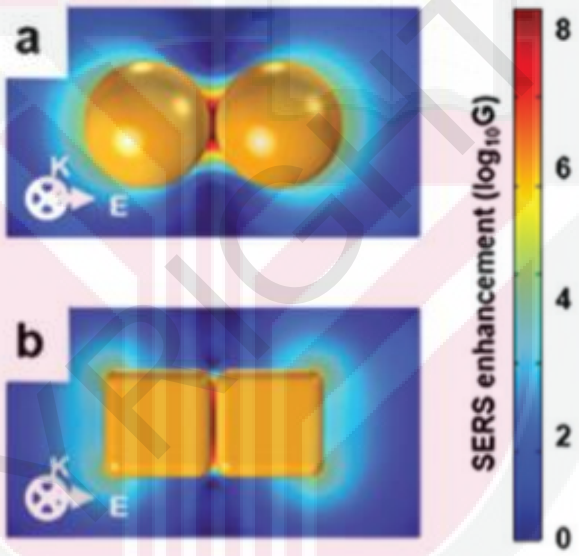

Figure 2.8: Simulation of SERS hot spots between nanospheres aggregate (a) and nanocubes aggregate (b).
(Ding et al., 2017)

One major drawback of SERS in colloidal system is the lack of reproducibility. The variation of nanoparticles between batches and the random formation of aggregates governed by the random Brownian motion of the molecules in the mixture. Moreover, different analytes require different optimised protocol for the optimum enhancement (Schneider et al., 1996). Incubation for the formation of aggregates also play a role in the reproducibility (Turzhitsky et al.,

2018). Several strategies were developed to improve the reproducibility of colloidal SERS such as improving the monodispersivity of the metallic nanoparticle colloid, filtration, sonication, vortexing and proper storage conditions of the metallic colloid (Tantra et al., 2007).

2.2.4 Surface-Enhanced Raman Spectroscopy for Bioanalysis

SERS is an emerging tool to perform diagnosis to inform prognosis and formulate treatment. In contrast to conventional omics methods for biopsy (Chen & Zhao, 2019; Chinello et al., 2019; B. Lee et al., 2020), SERS is cheap, fast and can be performed in a point-of-care setting. The methodologies employed in SERS is a diagnostic process are label-free SERS and indirect sensing using SERS tags as shown in Figure 2.9.

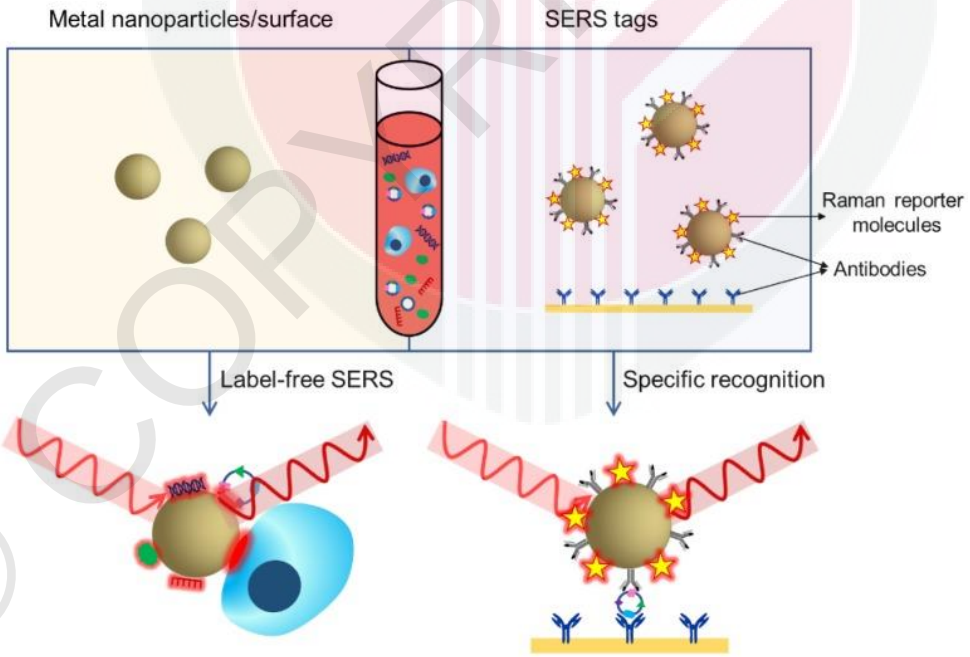

Figure 2.9: Label-free SERS and indirect sensing using SERS tags.
(Y. Zhang et al., 2019)

Label-free SERS analyses unique spectral fingerprint of the biomolecules, cells or microorganisms directly adsorbed on the metal surface. Due to the complexity of the spectra, statistical analysis such as PCA or LDA is often required to draw the necessary conclusion about the patient's health, discriminate biomolecules and cells or microorganisms of different species. Label-free SERS also has poor multiplexing capabilities due to the overlapping spectral fingerprints of the various biomolecules in the biofluid. Purification steps such as chromatography or assay are often necessary prior to SERS analysis (Y. Zhang et al., 2019).

SERS tags are created by conjugating molecules with strong Raman scattering, known as Raman reporters, on plasmonic nanoparticles surface, followed by conjugation with specific biorecognition molecules such as antibodies and aptamers. The SERS tags are used as labelling molecule for indirect sensing of target biomolecules (Gong et al., 2022). SERS tagging offers the unique advantages of being highly sensitive, extreme multiplexing ability and the short lifetime of Raman scattering reduces the risk of photobleaching and minimises the interference from fluorescence (Y. Wang et al., 2013). However, SERS tag labelling is extremely specific and does not give any qualitative information on the biomolecules detected (X.-S. Zheng et al., 2018).

Some disease biomarkers of interest are purines, proteins and carotenoids. The SERS protocols are tuned to be more specific to the different classes of biomarkers. Purine metabolites and proteins can be detected in liquid form

using colloidal SERS and dried on a solid SERS substrate; however, surface modification of the nanoparticles is necessary for protein detection. Surface-enhanced resonant Raman spectroscopy (SERRS) is used for the detection of carotenoids (Moisoiu et al., 2021)

Colloidal SERS is a relatively simple procedure where the analyte is simply mixed with a SERS active colloid with a certain ratio. However, simply mixing silver colloid with uric acid and albumin does not produce any signal as shown in Figure 2.10. The absence of the SERS signal from uric acid and albumin from unmodified silver nanoparticles in Figure 2.10 highlights the importance of the surface modification to promote the chemisorption of biomolecules to silver nanoparticles.

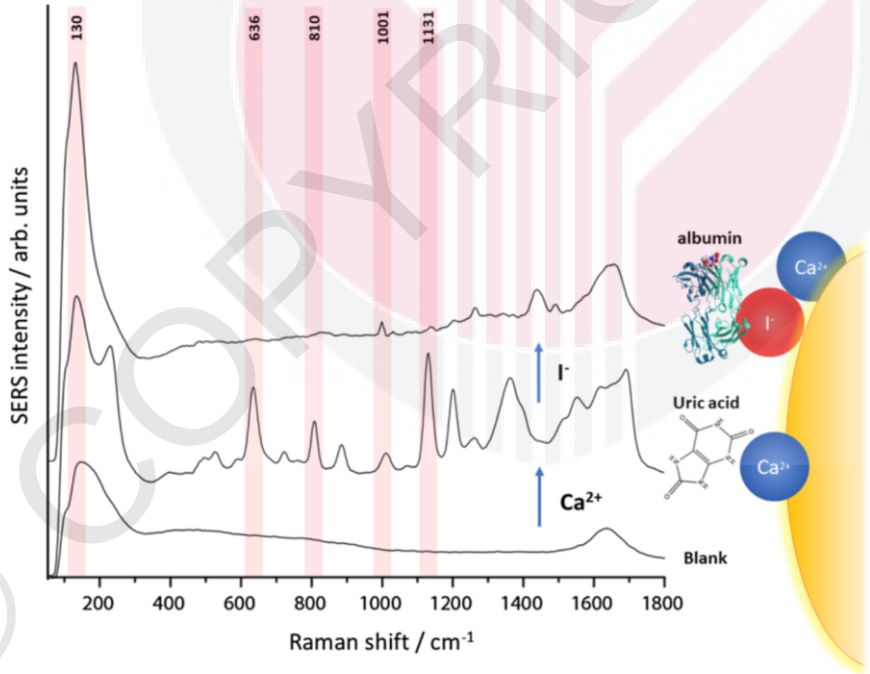

Figure 2.10: SERS spectra of uric acid and human serum albumin using silver nanoparticle colloid. The adsorption of specific adions "turns on" the SERS active sites for uric acid and albumin. Without the adions, uric acid and albumin do not produce any SERS signal.
(Moisoiu et al., 2021).

The adsorption of different species on the silver nanoparticles surface occurs competitively through electrostatic interactions. Therefore, the modification of the silver surface via adsorption of cationic or anionic species will select for a certain species of biomolecules based on their electrostatic interactions. Generally, surface modification with cationic species will detect anionic molecules while surface modification with anionic species will detect cationic molecules (Iancu et al., 2019). In addition, Xu et al (2014) demonstrated the adsorption of iodide on silver nanoparticles allowed for the detection of proteins. This method offers two distinct advantages for protein detection, namely, improved adsorption of proteins with positive charge and improved reproducibility by preventing conformational changes of proteins on the nanoparticle surface. The iodide layer serves as a buffer layer to prevent the strong chemical interaction between the silver surface and proteins.

SERRS is a combination of the surface-enhanced Raman scattering effect and the resonance of chromophore with electronic transition close to the excitation wavelength (W. E. Smith, 2008). Carotenoids have peak absorbance around 440 nm. Therefore, by utilising SERS techniques coupled with a blue and green laser, the detection of carotenoids using SERRS is possible. Most carotenoids are hydrophobic with limited affinity to silver nanoparticles. Therefore, some modifications to the SERS substrate or carotenoids are required. Thiol functionalisation of β-carotene leads to an amplification of the bands around 1005, 1155 and 1520 cm^{-1} via SERRS (Gühlke et al., 2016).

In dried SERS, the mixture of colloid and analyte is allowed to dry before spectra acquisition. This has two notable advantages: the signal from both purines and proteins is visible and the biomolecules are separated by their solubility through the coffee ring effect. However, the inhomogeneity of the dried film diminishes the repeatability and reproducibility of the SERS signal (Moisoiu et al., 2021). On the other hand, liquid SERS has been used to diagnose prostate cancer from urine sample using gold nanoparticles. Figure 2.11(a) shows the normalised spectra of urine from healthy patients and patients with prostate cancer. Using PCA and LDA, the selectivity and specificity is 100% and 89% respectively with diagnostic accuracy of 95%. The PCA plot and loading score are shown in Figure 2.11(b).

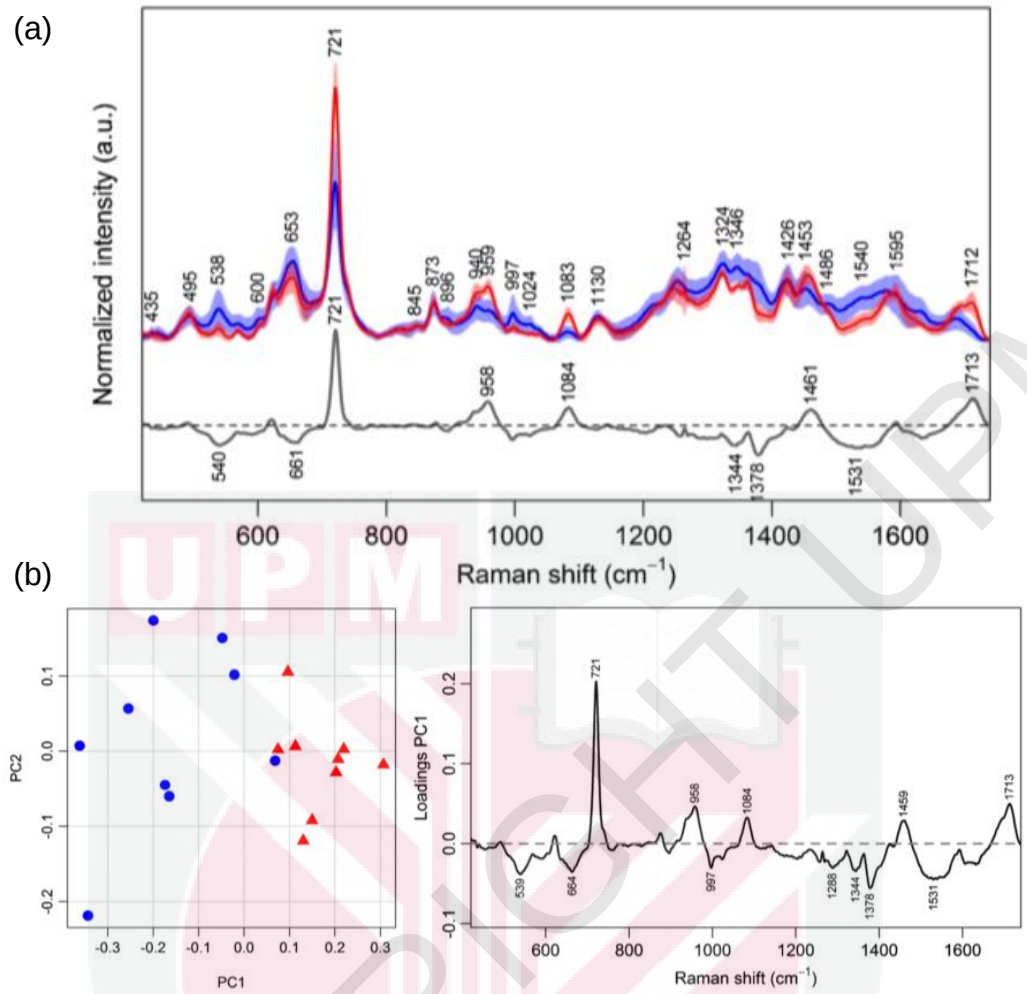

Figure 2.11: (a) Normalised average SERS spectra of urine from healthy patients (blue) and cancer patients (red). The Raman intensity difference is given at the bottom. (b) PCA plot of the SERS spectra from healthy patients (blue) and cancer patients (red). The loading scores of PC1 is given on the right.
(Mistro et al., 2015)

Label-free liquid SERS coupled with PCA and LDA has been demonstrated to determine histological grade of oral squamous cell carcinoma with 85% accuracy using a mixture of serum samples and gold nanoparticles (Xue et al., 2018) and Sjörgren's syndrome with 94% accuracy from saliva samples and 98% accuracy from serum samples using gold nanoparticles as the substrate (Stefancu et al., 2019). Iodide-modified silver nanoparticles are demonstrated to selectively amplify signal from proteins (L. J. Xu et al., 2014). Using iodide-

modified silver nanoparticles as the SERS substrate, (Bocsa et al., 2019) demonstrated the discrimination of knee osteoarthritis grade from synovial fluid samples.

Xiao et al (2016) conducted a large study of discriminating healthy patients from patients with hepatocellular carcinoma, breast cancer and lung cancer using silver coated gold nanorods as the SERS substrates. The SERS protocol employed is the dried SERS, where the mixture of serum sample and the nanorod colloid are mixed and dropped on a silicon wafer and dried. The diagnostic accuracy is above 75% for each group. Figure 2.12(a) shows the PCA plot of the SERS spectra from normal, hepatocellular carcinoma, lung, and breast cancer patients. The PCA plot shows good clustering between the groups. Figure 2.12(b) to (d) shows good separation between normal and cancer patients with PC1 being responsible for the separation of the groups.

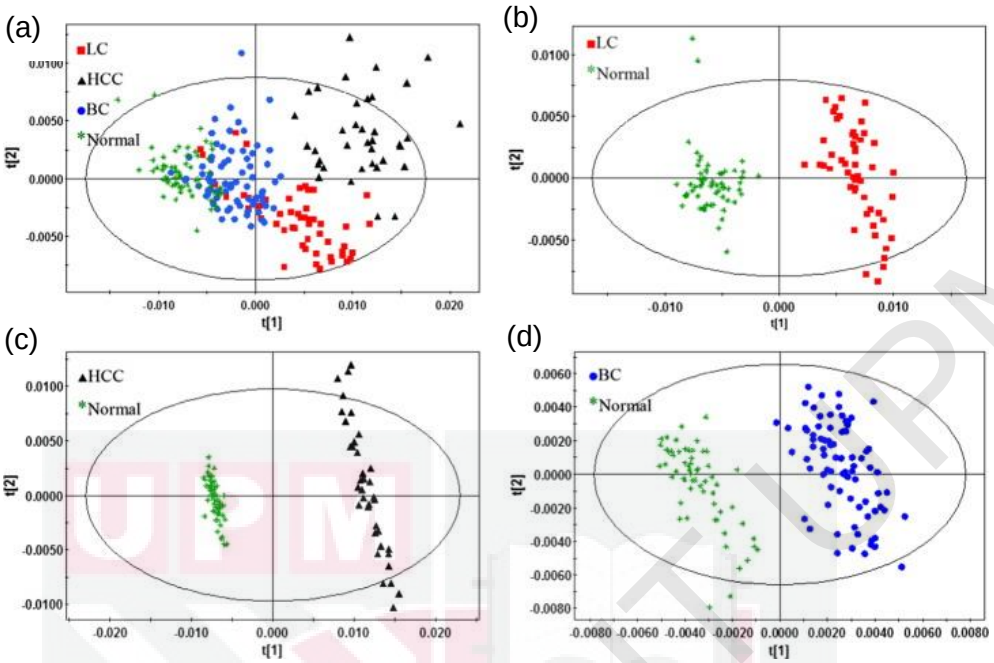

Figure 2.12: PCA plot of SERS spectra from (a) normal, lung cancer, breast cancer and hepatocellular carcinoma patients, (b) normal and lung cancer patients, (c) normal and lung cancer patients and (d) normal and breast cancer patients. LC: lung cancer, HCC: hepatocellular carcinoma and BC: breast cancer.
(Xiao et al., 2016)

Dried SERS of saliva on silver coated nanopillars substrate and oropharyngeal cell fixed on the SERS substrate has been used to diagnose oral squamous cell carcinoma with accuracy of 73% from saliva samples and 60% from oral cell samples (Connolly et al., 2016). Silver colloid deposited on a calcium fluoride (CaF_2) slide can also serve as a substrate for dried SERS. Using blood plasma dried on the silver deposited CaF_2 slide, breast cancer can be diagnosed with 89% accuracy (Știufiuc et al., 2020). Using a similar SERS substrate (Colceriu-Șimon et al., 2019) investigated the effect of low-dose irradiation from saliva samples dried on the SERS substrate. The increase in the intensity of the band related to salivary thiocyanate shows that this band is an indication of low-dose radiation exposure.

2.2.5 Surface-Enhanced Raman Spectroscopy in Aquaculture

Surface-enhanced Raman spectroscopy has a few notable advantages over conventional Raman spectroscopy, namely, very low limit of detection, down to a single molecule detection. Signal acquisition is quick, therefore, photodegradation and photobleaching can be avoided during the analysis process. Tuning the properties of the nanomaterial allows for better selectivity of biomolecule and SERS allows for multiplexing (Zong et al., 2018).

Utilising these advantages, SERS is used in aquaculture to detect trace amounts of illegal or harmful substances in fish products or the environment for monitoring purposes. Dyes like malachite green and crystal violet are used as a fungicide in aquaculture. Malachite green and crystal violet are quickly absorbed by fish and metabolised into leucomalachite green and leucocrystal violet (Hurtaud-Pessel et al., 2013). These compounds are toxic to humans, especially leucomalachite green which is shown to be a carcinogen (Curieux et al., 2021). Therefore, it is important to detect these compounds in aquaculture ponds and fish before they make it to the consumer. Another important molecule to monitor in aquaculture is nitrite. Nitrite in the environment is important for fish metabolism but excessive nitrite causes algal bloom (Z. Li et al., 2019).

Figure 2.13 and Figure 2.14 shows the TEM images of gold nanoparticles and the absorption spectrum of the gold nanoparticles. As seen in Figure 2.14, gold nanoparticles typically have absorption peak around 500 nm with the peak

being red-shifted with increasing particle size (Zhou et al., 2019). The absorption peak plays an important role in surface enhancement. The surface enhancement effect is greatest where there is an overlap between the excitation wavelength, absorption peak of the nanomaterial and the absorption of the analyte molecule.

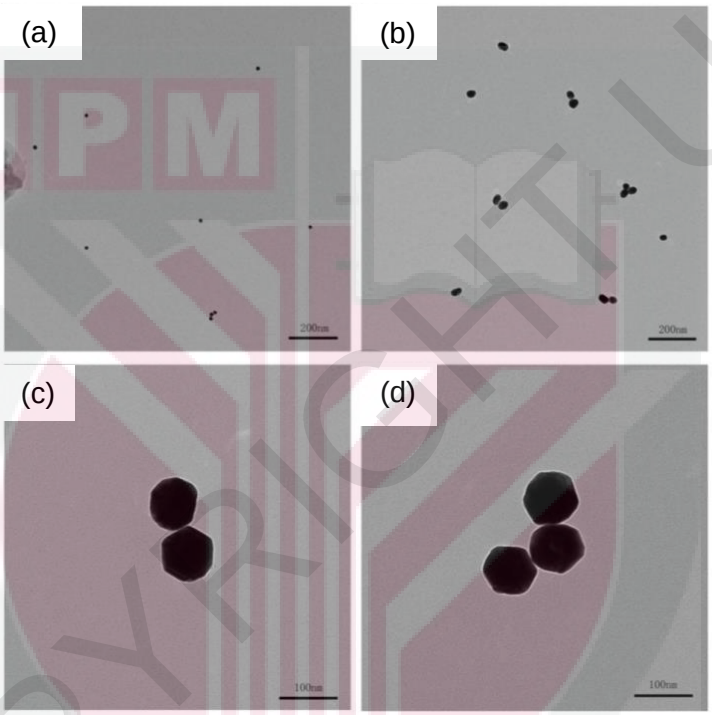

Figure 2.13: Transmission electron microscope (TEM) of (a) and (b) 16 nm gold nanoparticles, (c) 45 nm gold nanoparticles and (d) 100 nm gold nanoparticles.
(Zhou et al., 2019)

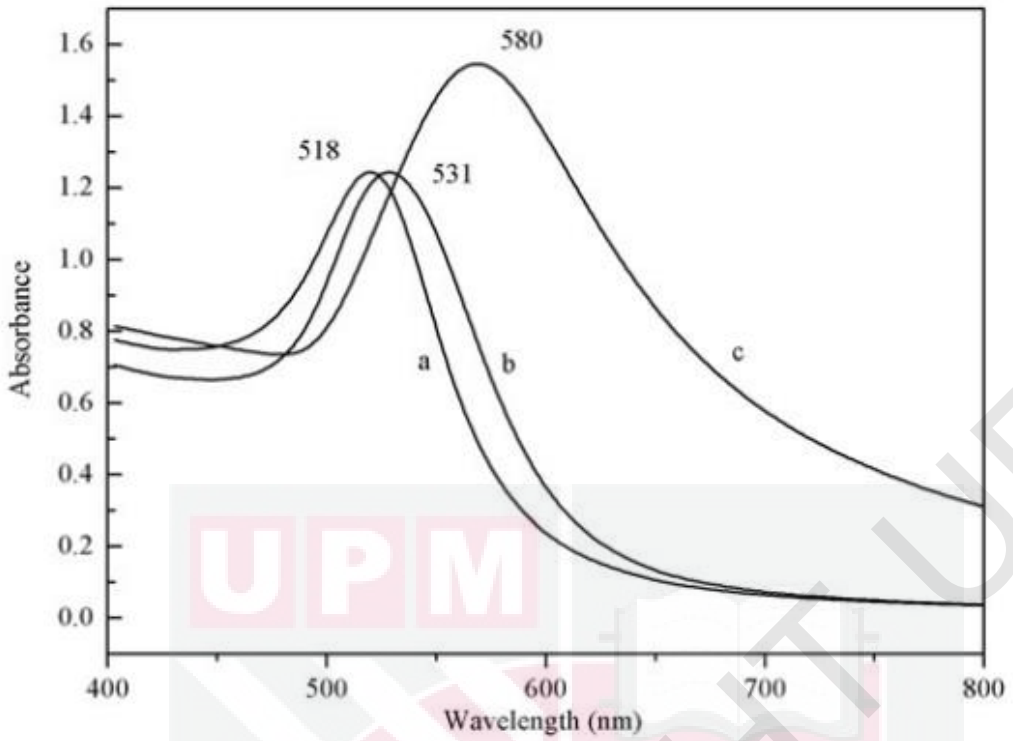

Figure 2.14: UV-visible absorption of gold nanoparticles of different sizes: (a) 16 nm, (b) 45 nm and (c) 100 nm.
(Zhou et al., 2019)

Figure 2.15 shows the Raman spectra of malachite green adsorbed on different gold nanoparticles and the Raman spectrum of malachite green without gold nanoparticles. The Raman peaks of malachite green is barely discernible. The Raman signal is greatly enhanced with the presence of gold nanoparticles. The characteristic peaks of malachite green in the 450 -1750 cm^{-1} can be clearly seen in all three spectra with the presence of gold nanoparticles.

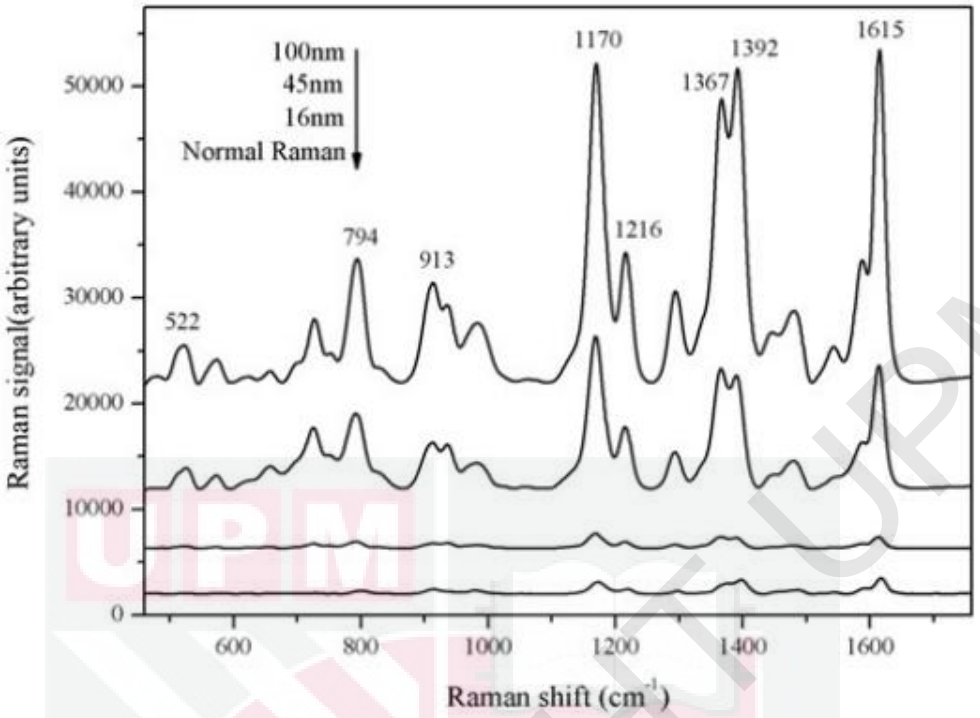

Figure 2.15. Raman spectra of 5 μM of malachite green on different gold nanoparticles and Raman spectrum of 0.5 M malachite green as a reference.
(Zhou et al., 2019)

The enhancement factor using 100 nm gold nanoparticles is the greatest. This is due to the higher surface area of the 100 nm gold nanoparticle, therefore, higher number of bumps on the particle surface leading to higher density of electromagnetic “hot spots”. The enhancement factor, EF is calculated as follows:

$$EF = \frac{I_{SERS} C_{Raman}}{I_{Raman} C_{SERS}} \quad (2)$$

where I_{SERS} and I_{Raman} are the peak intensities in the presence and absence of SERS substrate respectively. C_{SERS} and C_{Raman} are the analyte concentration in the presence and absence of SERS substrate respectively.

The EF at 1615 cm^{-1} is 2.06×10^6 for the 100 nm gold nanoparticles. There is a strong linear relationship between the peak intensity and concentration of malachite green in solution. Therefore, partial least square regression model can be used to predict the concentration of malachite green in aquaculture water with a limit of detection of 2.7 nM (Zhou et al., 2019).

In addition of detecting malachite green in aquaculture water, detection of malachite green and methylene blue in fish tissue using SERS with gold nanorods has been demonstrated by (T. Xu, Wang, Huang, Lai, & Fan, 2019). $AgNO_3$ is a shaping agent in the synthesis of gold nanorods. The aspect ratio of gold nanorods produced is determined by the amount of $AgNO_3$ solution used.

Figure 2.16 shows the TEM images of gold nanorods synthesized with different amount of $AgNO_3$ solution and their respective UV-Visible absorption spectrum is shown in Figure 2.17. The gold nanorods have two distinct absorption bands corresponding to the transverse and longitudinal plasmon resonance. The transverse plasmon band occurs at around 520 nm while the longitudinal plasmon band occurs at around 680 nm with the band being red-shifted with increasing aspect ratio. The intensity of the longitudinal plasmon band is due to the higher absorption in the longitudinal direction due to the higher electron density along the longitudinal direction.

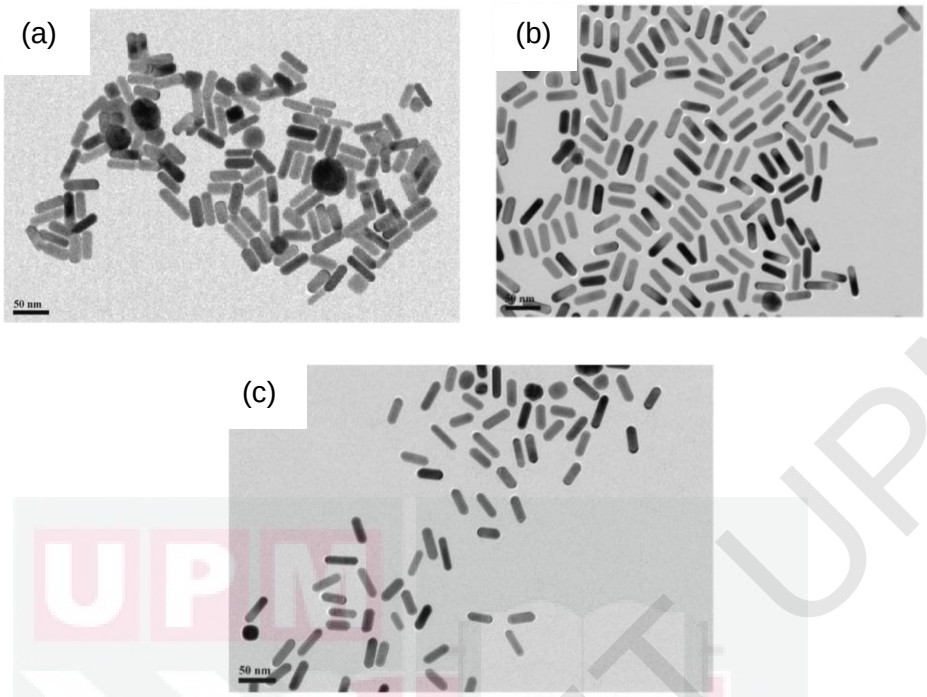

Figure 2.16: TEM images of gold nanorods synthesized with 50 µl (a), (b) 240 µl and 480 µl of $AgNO_3$ solution. The aspect ratio of (a), (b) and (c) are 2.2, 3.5 and 2 respectively.
(Xu et al., 2019)

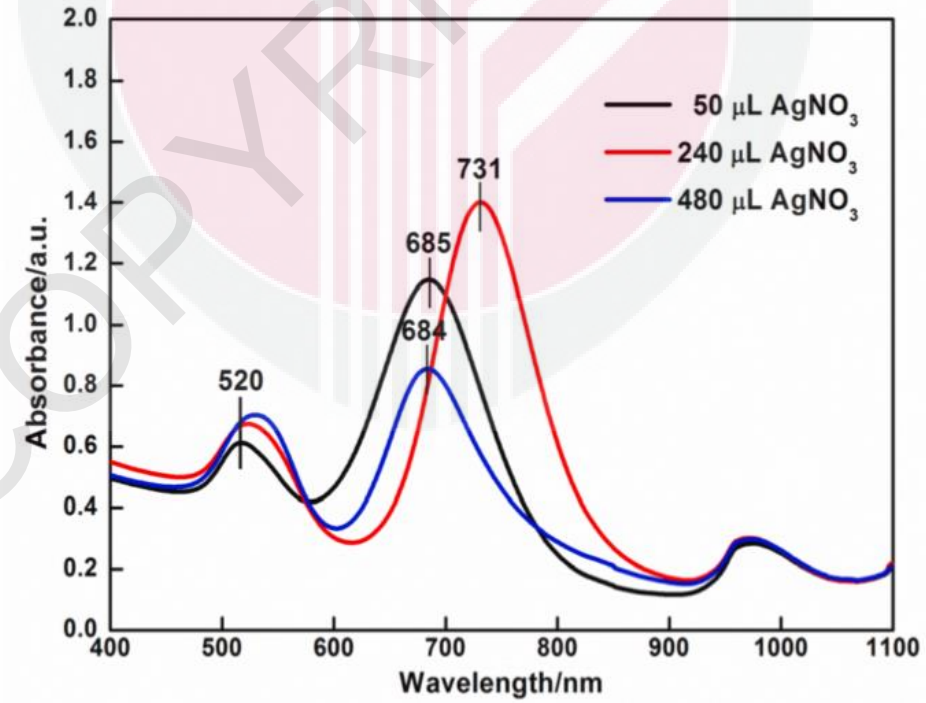

Figure 2.17: UV-Visible absorption spectrum of gold nanorods synthesized with different volume of $AgNO_3$ solution.
(T. Xu et al., 2019)

Figure 2.18 shows the Raman spectrum of methylene blue and malachite green. The fish tissue sample is spiked with malachite green and methylene blue and then homogenized and mixed with acetonitrile. Anhydrous magnesium and alumina were added to remove lipids and the mixture is centrifuged. The supernatant was dried under nitrogen gas at 50°C. This process converts most of the drugs into their reduced form in the fish tissue. An additional oxidation step is required for leucomalachite green as it is difficult to obtain the spectrum of leucomalachite green directly. The gold nanorods colloid is dropped onto a clean slide and dried at 50°C and the analyte solution is subsequently dropped and dried on the dried gold nanorods.

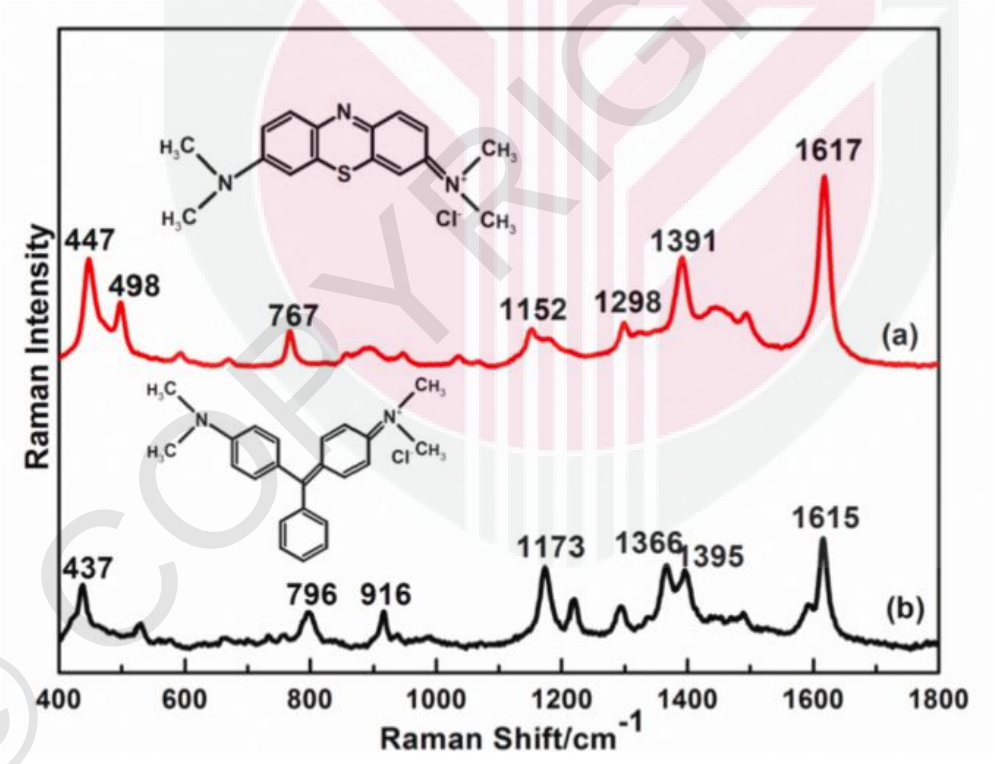

Figure 2.18: Raman spectrum of (a) methylene blue and (b) malachite green.
(T. Xu et al., 2019)

Four different fish species were analysed (snakehead fish, yellow catfish, tilapia fish and black carp) with the characteristic peaks of methylene blue and malachite green clearly identifiable. The limit of detection is 0.3 to 1 ng of dye per gram of fish tissue depending on fish species. The limit of detection in fish tissue is higher than the standard solution due to the interference from the fish matrix but this indicates that SERS is a possible route for analysing illicit drugs in fish tissue (T. Xu et al., 2019).

Traditional confocal Raman spectrometers are bulky and therefore, it has limited applications for in-situ monitoring in aquaculture. Optofluidics is the integration of microfluidics and photonics and is an emerging field and is promising for in-situ SERS analysis.

Figure 2.19 shows the pump free optofluidics device for SERS analysis developed by (Yazdi & White, 2013). The device is fabricated with polydimethylsiloxane (PDMS) using photolithography. Negative pressure is produced by the micropipette. The excitation laser is delivered using an optical fibre and the Raman scattered photons are collected with a multimode fibre. The analyte solution and the silver nanoparticles will be concentrated in the silica microspheres matrix. This device is able to detect three fungicides, namely, malachite green, methyl parathion and thiram, simultaneously. Utilizing optical fibres, the need for a microscope is eliminated, thus allowing for in-situ analysis of water in aquaculture ponds (Yazdi & White, 2013).

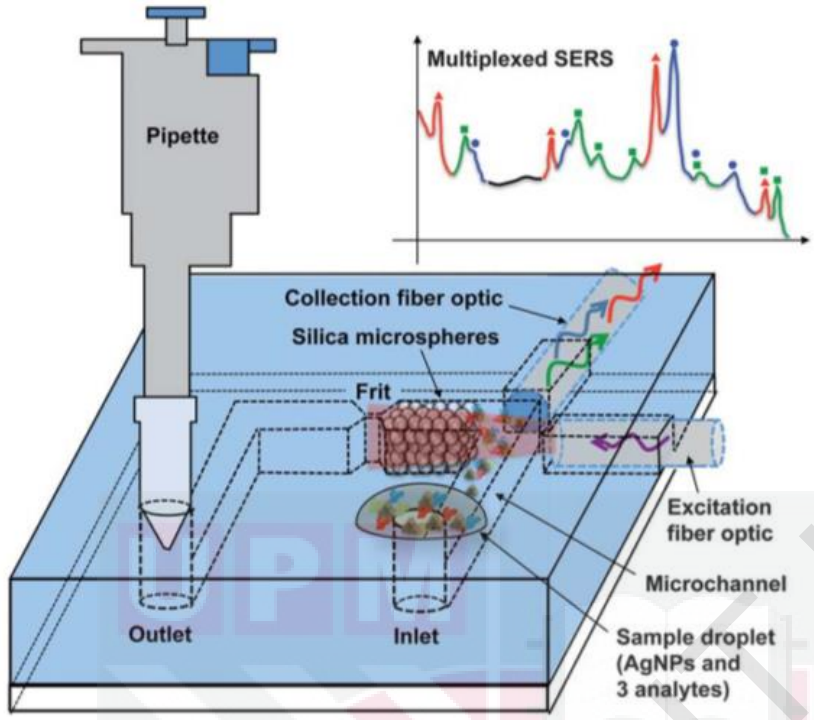

Figure 2.19: Pump free optofluidics device for SERS analysis.
(Yazdi & White, 2013).

In addition to optofluidics, modification of the nanoparticles can also improve the sensitivity of the SERS analysis. One such modification is the addition of halide salt into the metallic nanoparticle colloid. This is mainly due to the halide ions inducing aggregation of the nanoparticles, creating more "hot spots". Potassium bromide (KBr) modified silver nanoparticles has been shown to greatly improved the SERS signal of furazolidone (FUZD) and 3-amino-2-oxazolidinone (AOZ). Figure 2.20 shows the SERS spectrum of FUZD using silver nanoparticles and KBr modified silver nanoparticles. The characteristic peaks of FUZD are not observed when using silver nanoparticles alone. When compared to other halide ions, the enhancement from bromide ions is the greatest as shown in Figure 2.21 (Fan et al., 2021).

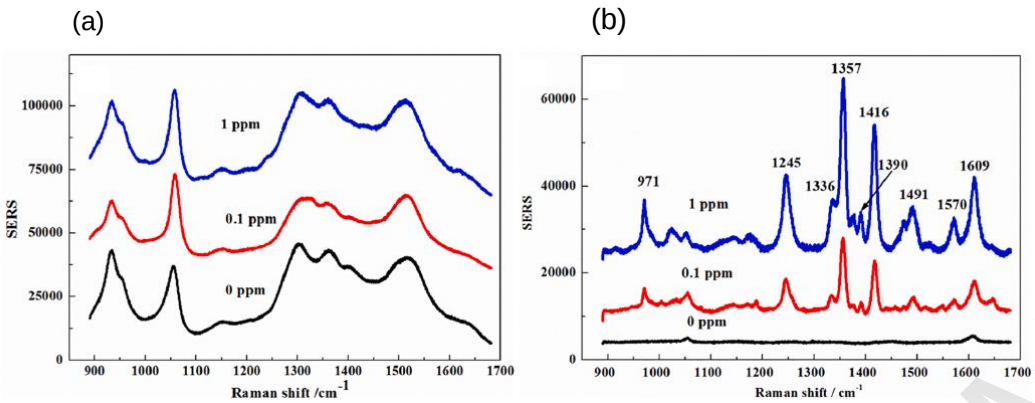

Figure 2.20: SERS of FUZD using silver nanoparticles (a) and SERS of FUZD using KBr modified silver nanoparticles (b).
(Fan et al., 2021)

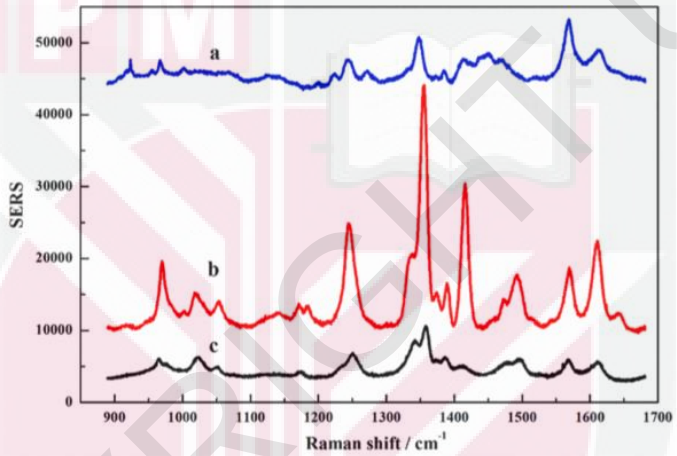

Figure 2.21: SERS spectrum of FUZD in the presence of iodide ions (a), bromide ions (b) and chloride ions (c).
(Fan et al., 2021).

Magnetic hybrid Fe_3O_4/Ag hybrid nanoparticles allows for self-assembled and tunable SERS substrate. Figure 2.22 shows the scanning electron microscopy (SEM) image of the hybrid nanoparticles. To attach the Fe_3O_4 nanoparticles to Ag nanoparticles, 3-Aminopropyltriethoxysilane is used as a linker. The surface plasmon resonance is tunable by adjusting the ratio of Fe_3O_4 and Ag nanoparticles. The nanoparticles colloid solution is dropped onto a slide on top of a magnet and dried under ambient condition. The magnetic field induces aggregation of the nanoparticles. Using the hybrid nanoparticles, the detection of FUZD is possible down to 500 ng per gram of fish feed

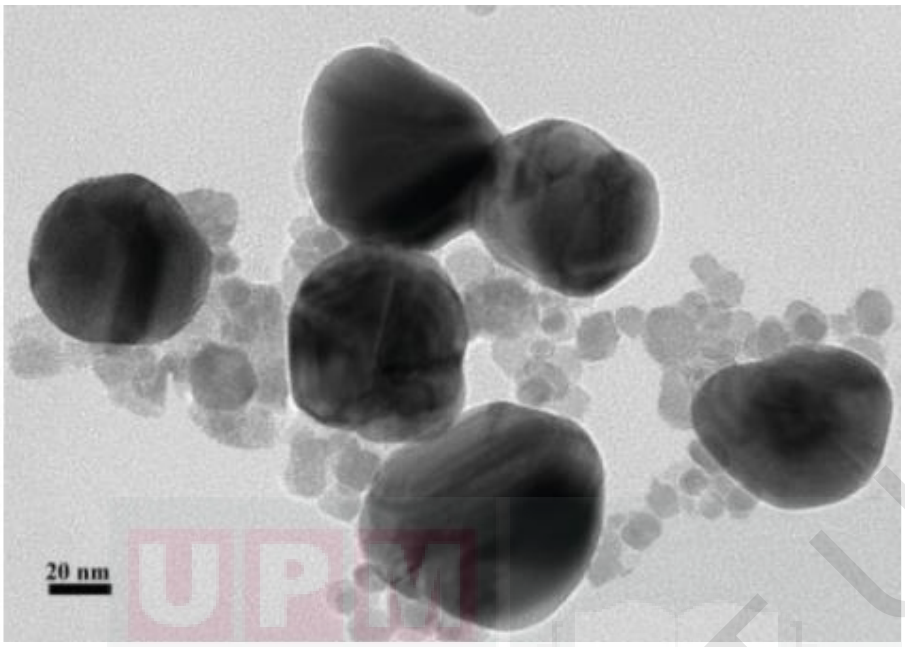

Figure 2.22: SEM image of Fe_3O_4/Ag hybrid nanoparticle.
(W. Yu et al., 2014)

In most cases SERS utilizes metallic nanoparticle colloid. However, this is not a necessity. Mechanical power-driven solid phase microextraction (MPD-SPME) onto a SERS active substrate allows for rapid and efficient SERS analysis without the need for organic solvent. Electrochemically etched silver wire can also serve as a SERS active substrate. Instead of nanoparticle colloid, the nanopores on the porous silver wire forms the electromagnetic hot spots.

Figure 2.23 shows the SEM images of the silver wire etched at different potential scan rates. The nanopores formed using 10 mVs^{-1} etch rate is the most uniform. The schematic diagram of the MPD-SPME-SERS process is showed in Figure 2.24. The stirring process is crucial in promoting the adsorption of analyte molecules on the wire. Using SERS trace amount of malachite green and crystal violet in water. The silver wire can be cleaned by immersing the wire in $NaBH_4$ solution for 5 minutes. Therefore, the porous silver wire is a recyclable SERS active and using MPE-SPME, the rapid detection of illegal substances in water.

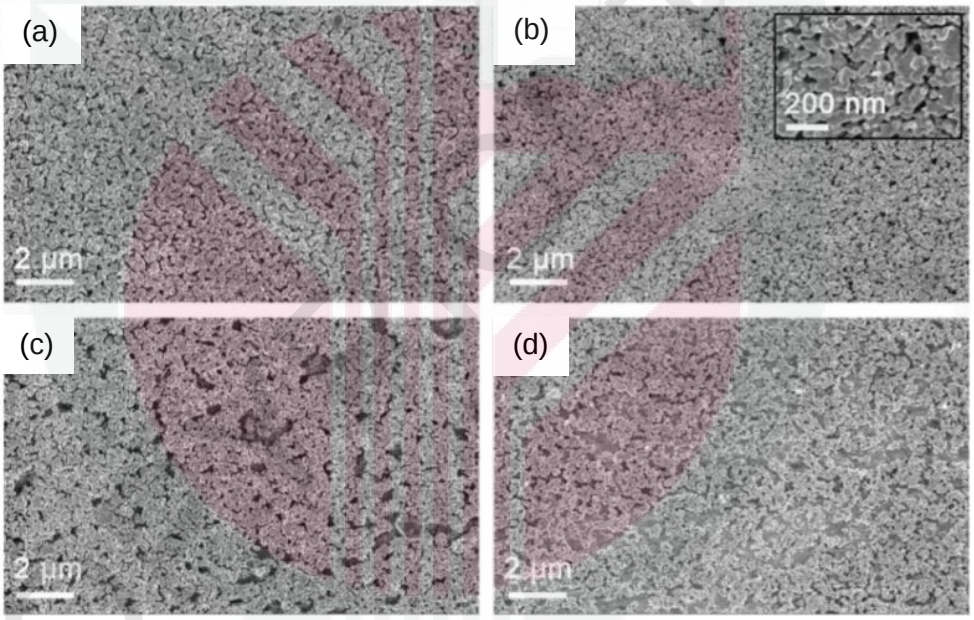

Figure 2.23: SEM image of the porous wire etched at different potential scan rates. (a) 5, (b) 10, (c) 15 and (d) 25 mVs^{-1}.
(Lv et al., 2021)

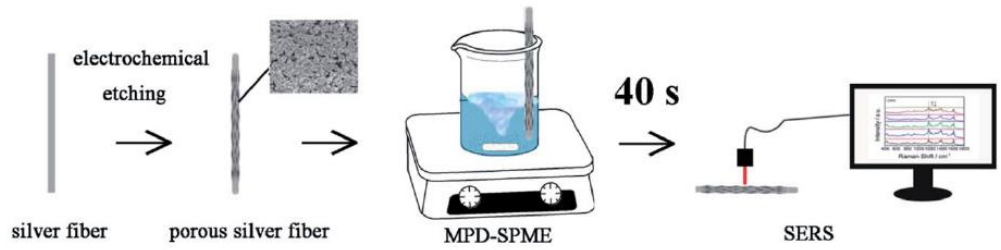

Figure 2.24: Schematic diagram of the MPD-SPME-SERS.
(Lv et al., 2021)

Direct detection is possible for molecules with characteristic peaks however, some molecules do not exhibit any characteristic peaks. One such molecule is nitrite. Figure 2.25 shows the SERS spectra of nitrite and nitrate in solution at different concentration. The nitrite peak is broad and therefore, quantification of nitrite is difficult from the spectral features. Thus, direct detection of nitrite is difficult.

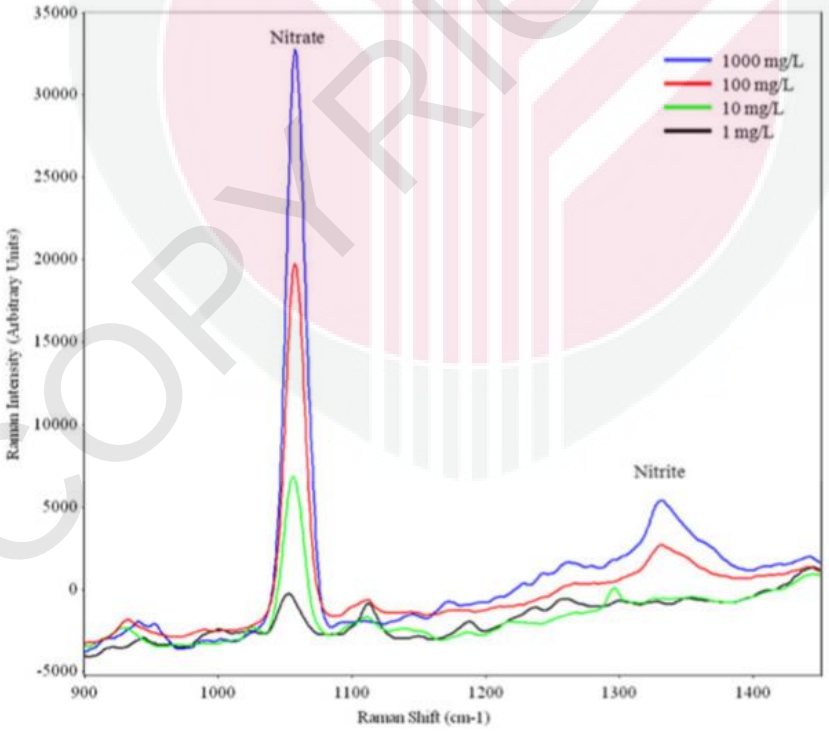

Figure 2.25: SERS spectra of nitrate and nitrite at different concentrations using gold nanoparticles as the SERS substrate.
(Gajaraj et al., 2013)

Figure 2.26 shows schematic of the detection of nitrite coupled with the diazo reaction. Under acidic condition, 4-aminothiophenol is added to the nitrite containing solution. This initiates the diazo reaction. Adding N-(1-naphthyl) ethylenediamine dihydrochloride (NED) to the mixture forms the azo dye and the solution turns carnation red. The reaction takes place in two minutes. The silver nanoparticle colloid is to the mixture and SERS is performed using a 532 nm laser. In this application, surface-enhanced resonance Raman scattering (SERRS) occurs due to the excitation laser energy is similar to the electronic transition of the azo dye. This leads to a higher sensitivity and selectivity of the detection to the azo dye.

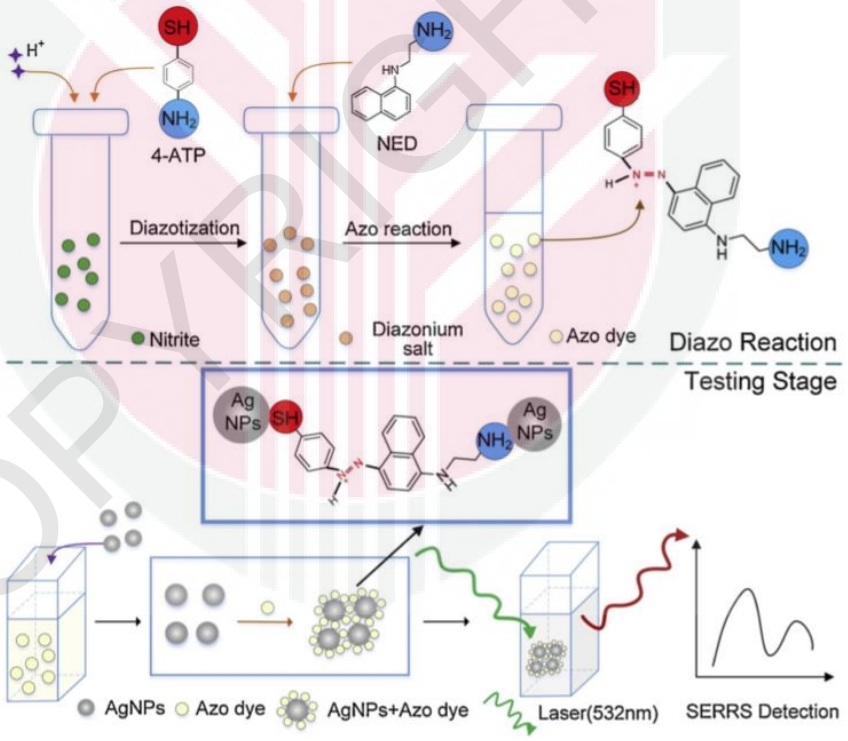

Figure 2.26: Schematic diagram of SERS detection of nitrite with diazo reaction to produce azo dye.
(Z. Li et al., 2019)

Figure 2.27 shows the SERRS spectra of azo dye with different concentration of silver nanoparticles. The characteristic peaks are highlighted. The limit of detection is as low as 9 nM for the peak at 1380

cm^{-1}. The intensity of the peaks increases with the concentration of silver nanoparticles and there is a linear relationship between the intensity of the Raman peaks and nitrite concentration. Therefore, the nitrite concentration in aquaculture water can be directly quantified using the intensity of the Raman peaks of the azo dye (Z. Li et al., 2019).

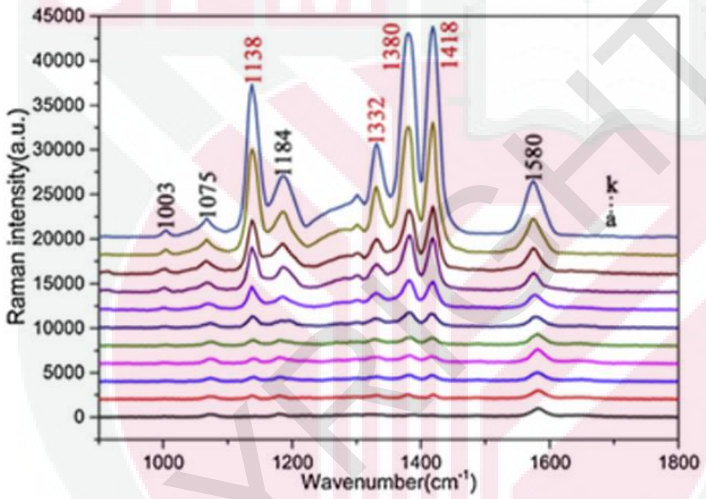

Figure 2.27: SERRS spectra of azo dye with different concentration of silver nanoparticles. (a-k): 0, 0.2, 0.4, 0.6, 0.8, 1.0, 2.0, 4.0, 6.0, 10.0 and 15.0 µM.
(Z. Li et al., 2019)

2.3 Conclusion and Outlook

Label-free SERS is a powerful and non-invasive tool for bioanalysis, with a remarkable diagnostic capability for a variety of diseases, including cancers. SERS of biofluid can be done in liquid and dried form. The SERS analysis in liquid form often requires tuning of the surface chemistry of the silver

nanoparticles for improved specificity to a class of biomolecules, however, this is not reported to be necessary for bioanalysis using gold nanoparticles. SERS efficiency in colloidal system highly depends on the aggregation of nanoparticles. The choice of aggregating agent, amount and concentration affects the SERS efficiency. By introducing forced convection to the colloid, the formation of aggregates will be less random, leading to a better reproducibility.

SERS applications in aquaculture are focused on detecting illicit substances and pollutants in fish tissue samples and aquaculture water. While fish epidermal mucus is a major component in fish immune defence and a reservoir of anti-microbial compounds, no reports on the SERS analysis of fish epidermal mucus has been reported.

Therefore, the SERS analysis of fish epidermal mucus is a promising area of research. A non-invasive, quick, and cost-effective in-situ analysis of fish epidermal mucus musing SERS may prove to be an indispensable tool for determining fish health status in fish farms. The breadth of diagnostic capabilities using label-free SERS and statistical analysis discussed in this section using biofluids can be extended to determine fish health status using SERS analysis of fish epidermal mucus samples. This work presents a new methodology to perform colloidal SERS of grouper epidermal mucus.

CHAPTER 3

MATERIALS AND METHODOLGY

3.1 Introduction

Gold nanoparticles were synthesised using the standard citrate reduction method outlined by (Turkevich, Stevenson, & Hillier, 1951). Sodium citrate acts as the reducing agent to reduce the Au^{3+} ions in the gold salt and the capping agent to shape the gold atoms into spherical nanoparticles. In addition, the citrate layer also acts as a stabilising agent for the gold nanoparticles colloid. The prepared gold nanoparticles were characterised using UV-Visible spectroscopy, dynamic light scattering (DLS) and transmission electron microscopy (TEM).

Both sodium sulphate (Na_2SO_4) and sodium chloride (NaCl) were tested as the aggregating agent. The appropriate aggregating agent was chosen based on its tendency to competitively bind with analyte molecules on the gold nanoparticle surface and the background SERS spectrum generated upon the addition of the aggregating agent, which should be featureless.

The colloidal SERS efficacy using the synthesised gold nanoparticles and the chosen aggregating agent were tested using two test molecules with a fixed concentration, namely, 0.1 mM Rhodamine 6G (R6G) and 300 µg/ml lysozyme. The SERS enhancement for R6G and lysozyme was observed at

different concentrations of the aggregating agent to obtain the ideal concentration of the aggregating agent to produce the best SERS spectrum. Subsequently, the gold nanoparticles and aggregating agent were used to conduct colloidal SERS analysis of grouper epidermal mucus and the ideal concentration of the aggregating agent to obtain the best spectrum SERS spectrum of grouper epidermal mucus was determined. Savitsky-Golay algorithm was used to remove noise from the spectra and asymmetric least square smoothing algorithm was used to calculate the baseline and its removal.

3.2 Chemicals and Reagents

Gold (III) chloride solution ($HAuCl_4$, 99.99% trace metal basis, 30% wt in dilute HCl), sodium citrate dihydrate ($Na_3Ct.2H_2O$, USP testing specifications), sodium sulphate (Na_2SO_4, ACS reagent grade), lysozyme from hen egg white and Rhodamine 6G (R6G, 99% pure) were purchased from Sigma-Aldrich. Sodium chloride (NaCl, 99.5% assay basis) was purchased from R&M chemicals. All syntheses were carried out in deionised water. The lysozyme and R6G solution were prepared by dissolving an appropriate amount in deionised water. The concentration of the lysozyme and R6G solution were 300 µg/mL and 0.1 mM respectively.

3.3 Instrumentation

Gold nanoparticles were characterised using UV-Visible spectroscopy (Lambda 35, Perkin Elmer), dynamic light scattering (DLS, Zetasizer Nano-S, 633 nm, Malvern Panalytical) and transmission electron microscopy (TEM, JEOL JEM 2100F Field Emission TEM). The Raman spectroscopy setup consisted of a 785 nm narrow linewidth source (XIM-6206-785-500-2, Yixi Intelligent Technology), high sensitivity spectrometer (YIM-6703-01-S03L01F05G02, Yixi Intelligent Technology), a 785 nm Raman probe (Wasatch Photonics) and a Raman immersion probe with a sapphire ball lens (MarqMetrix). Baseline correction and spectral pre-processing were conducted using OriginLab Pro (ver. 2018, OriginLab Corporation).

3.4 Synthesis of Gold Nanoparticles

Gold nanoparticles were synthesised using the standard citrate reduction proposed by Turkevich (Daruich De Souza et al., 2019) with some modifications to the duration of synthesis. 50 mL of 0.25 mM $HAuCl_4$ solution (pH ~3) is prepared in an Erlenmeyer flask. The solution was placed on a hotplate and stirred rapidly (500 rpm) and heated until boiling (100oC). When the solution was boiling, 367.6 µL of 38.25 mM Na3Ct solution (1:12 molar ratio for $HAuCl_4$ to Na_3Ct) was quickly injected into the solution. The diameter of the gold nanoparticles was controlled by adjusting the molar ratio of $HAuCl_4$ to Na3Ct and the target diameter was 50 nm since 50 nm gold nanoparticles exhibited optimal SERS enhancement (Hong & Li, 2013). The mixture was kept

at 100°C for an hour with constant stirring. The flask was covered with aluminium foil with a beaker of ice placed on top to minimise solvent loss by condensing the steam. After an hour, the heat was shut off and the gold colloid was allowed to cool down to room temperature with constant stirring. When the colloid was cooled to room temperature, deionised water was added until the final volume was 50 mL. The colloid was stored in a brown bottle in the refrigerator (4°C) until it was used for analysis. The schematic of the gold nanoparticles synthesis is shown in Figure 3.1.

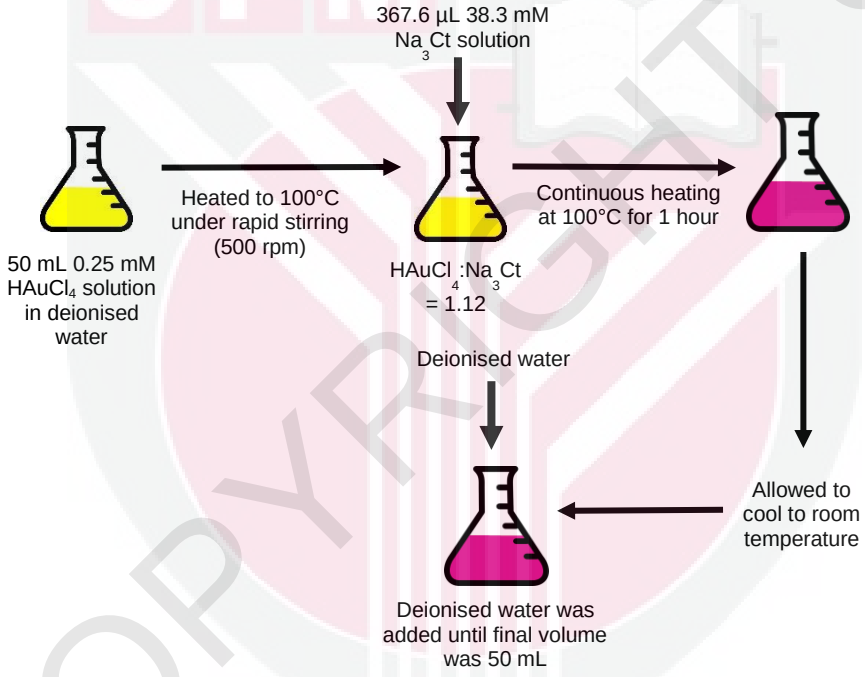

Figure 3.1: Schematic of the gold nanoparticles synthesis.

The colour change of the reagent during the gold nanoparticles synthesis is shown in Figure 3.2. The $HAuCl_4$ solution is initially light yellow as depicted in Figure 3.2(a). Upon reaching 100°C, sodium citrate was added to the solution. The colour immediately changed to dark purple (refer to Figure 3.2(b)) which indicates nucleation of the gold atoms have been initiated. Finally, the colour changed to purplish red as the gold nanoparticles are formed as portrayed in Figure 3.2(c). The colour change from dark purple (refer to Figure 3.2(b)) to purplish-red (refer to Figure 3.2(c)) occurred within 15 minutes.

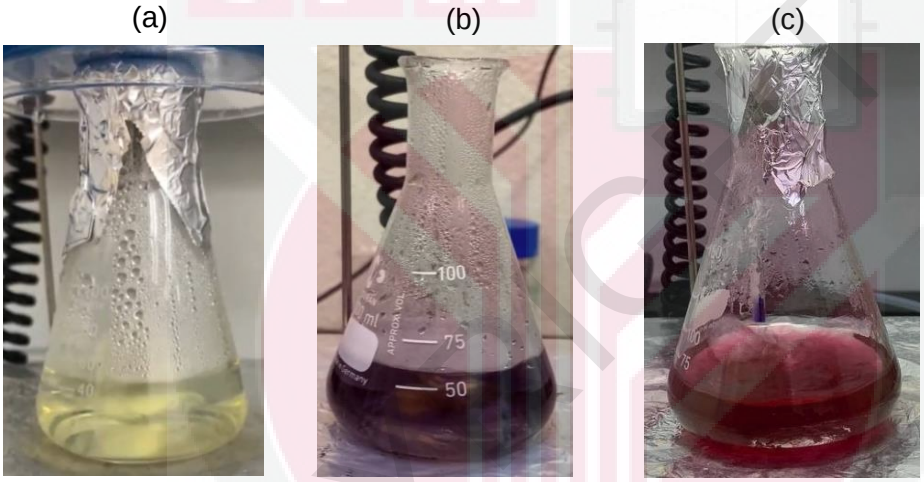

Figure 3.2: Colour change of the reagent during the gold nanoparticles synthesis. (a) shows the initial colour of the $HAuCl_4$ solution, (b) shows the colour of the solution upon the addition of sodium citrate and (c) shows the colour of the solution when the gold nanoparticles are formed.

3.5 Characterisation of Gold Nanoparticles

UV-Visible spectroscopy was performed to obtain the absorption spectrum of the gold colloid and TEM was used to obtain the diameter of the synthesised gold nanoparticles. Dynamic light scattering was conducted on the colloid to measure the hydrodynamic diameter and to obtain the size distribution of the gold nanoparticles. About 10 µL of the colloid was dropped and dried on a

copper mesh grid for TEM. In addition to UV-Visible spectroscopy and TEM, dynamic light scattering was performed to validate the particle size measurements and to investigate the polydispersity of the gold nanoparticles. For UV-Visible spectroscopy and dynamic light scattering, the gold colloid was diluted 5 times using deionised water.

3.6 Mucus Sampling

Hybrid groupers (*Epinephelus fuscoguttatus* x *Epinephelus lanceolatus*) were used in this experiment. Institutional Animal Care and Use Committee, UPM has reviewed and approved the utilisation of grouper fish in this research work. The ethics approval number was UPM/IACUC/AUP-R054/2022.

Prior to the mucus sampling three 5-litre tanks were washed and filled with seawater. In one tank, tricaine methanesulfonate (100 ppm) was added. One grouper (~15 cm in length) was transferred to one tank from the main tank. Silicon scrappers were used for scraping the mucus into a microcentrifuge tube. Prior to scraping, all tools were sanitised with 70% isopropanol. The mucus sampling flow is shown in Figure 3.3 (a). The fish was transferred to the anaesthesia tank and left in the tank for a few minutes until the movement of the fish was minimal. The fish was scraped from head to tail on both sides to collect the epidermal mucus as shown in Figure 3.3 (b). The mucus was stored in a freezer at -20^{o}C until it was analysed. The fish was transferred to the recovery tank after sampling and returned to the main tank after the effects of the anaesthesia had worn off.

(a)

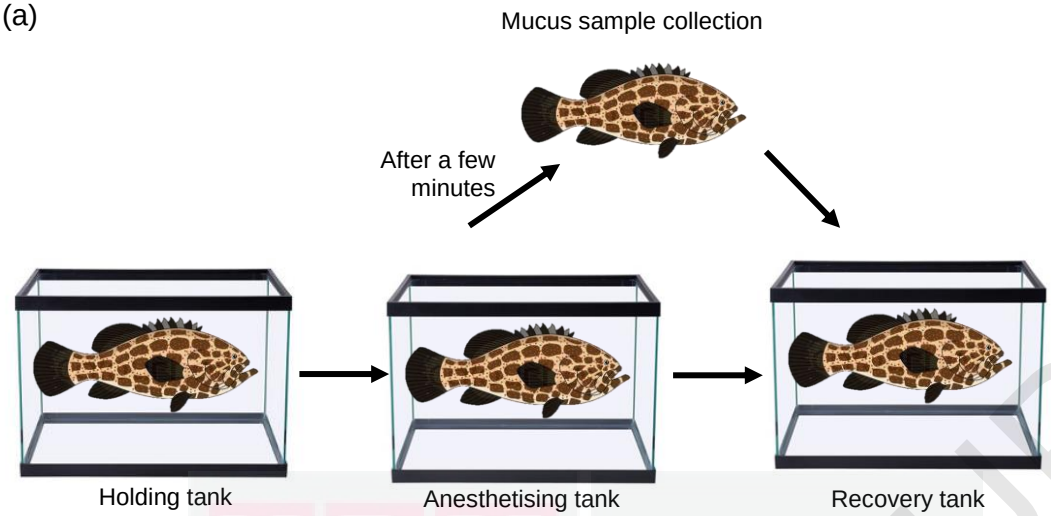

(b)

Figure 3.3: (a) Sampling flow to collect grouper epidermal mucus and the sampling method is shown in (b).

3.7 Sample Preparation

The sample preparation for Raman measurement was based on the protocol proposed by Turzhitsky et al (2018) with some modifications. Initially, the gold nanoparticles were washed by centrifuging (4000 rpm, 30 minutes) and redispersed in deionised water for three cycles to remove excess citrate and unreacted reactants. After the washing process, the gold colloid had a pH of ~7. Prior to the SERS analysis, 4.5 mL of the gold colloid was concentrated to 50 µL by centrifuging (4000 rpm, 30 minutes) and the appropriate amount of the supernatant was removed. Subsequently, 9.5 µL of gold nanoparticles were mixed with 10 µL of the analyte, followed by adding 0.5 µL of the aggregating agent or deionised water (for control) into the mixture. The mixture was vortexed (1000 rpm) for one minute and allowed to further incubate for another minute before being dropped on the aluminium foil for SERS analysis. The vortexing step introduces forced convection to promote a more uniform formation of aggregates instead of relying on the random Brownian motion of the molecules to form the aggregates (Tantra et al., 2007). Figure 3.4 shows the schematic of the sample preparation.

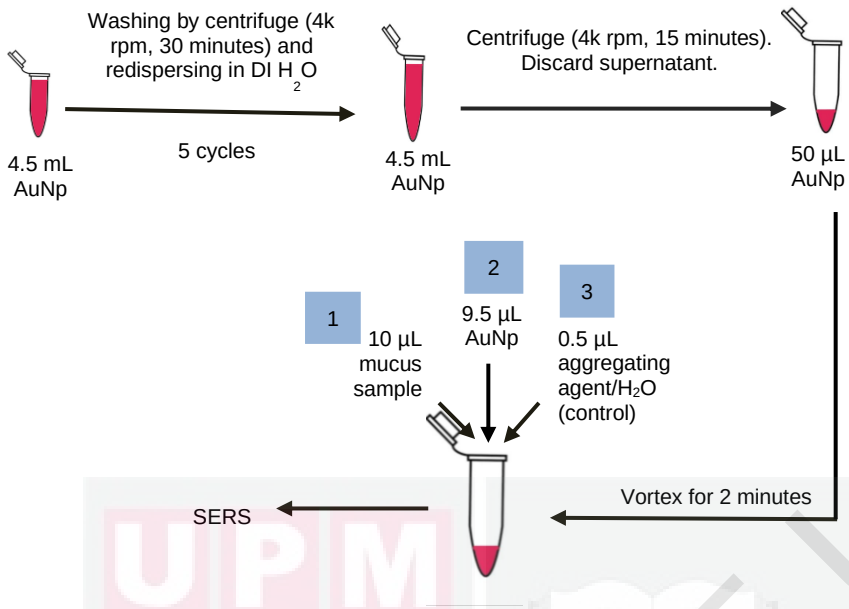

Figure 3.4: Schematic of the sample preparation.

3.8 Surface-Enhanced Raman Spectroscopy

3.8.1 Experimental Setup

Figure 3.5 (a) shows the schematic of experimental setup for SERS of grouper mucus with the individual components labelled. The liquid sample was dropped onto a concave glass slide lined with aluminium foil. The aluminium foil blocks the fluorescent emission from the glass slide, reducing the substrate interference in the SERS spectra acquired (Cui et al., 2016). The aluminium foil covered slide was wiped thoroughly with isopropanol prior to spectra acquisition. The ball lens of the immersion probe was lowered until it was in contact with the liquid droplet. The position of the sample was further adjusted using the translation stage until the signal intensity was optimal. The experimental setup is shown in Figure 3.5 (b).

(a)

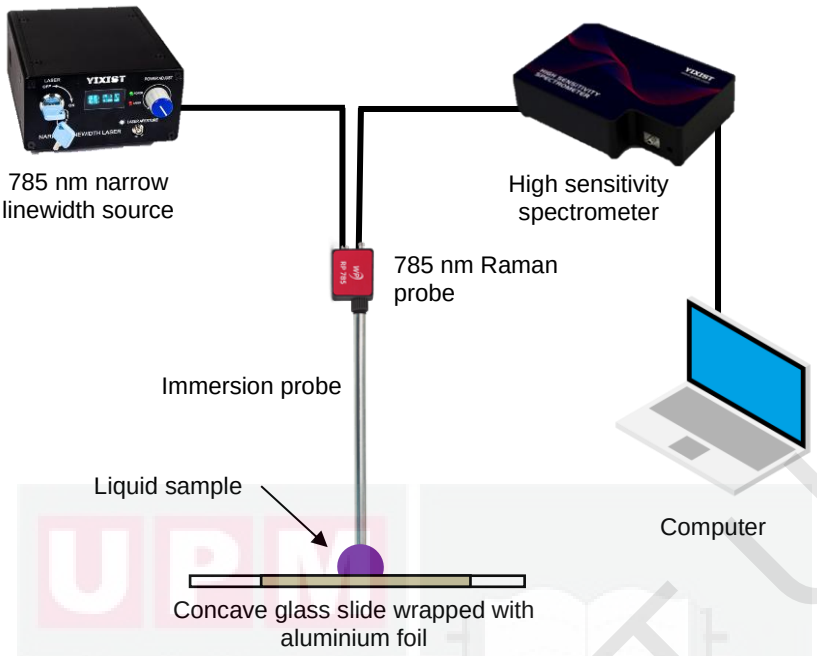

(b)

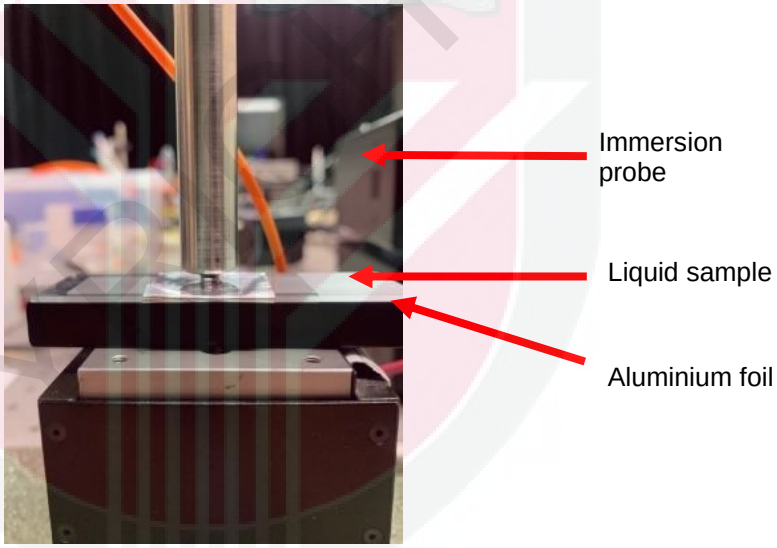

Figure 3.5: The SERS experimental set up; (a) schematic diagram and (b) the ball lens of the immersion probe in contact with the liquid sample.

3.8.2 Aggregating Agent

The aggregating agent used in the SERS experiment was acidified sodium sulphate (Na_2SO_4) and sodium chloride (NaCl). The concentrations were prepared in the range of 2 M, 1 M, 0.5 M, 0.25 M and 0.1 M. During the preparation of the sodium sulphate solutions, the pH was adjusted to 3 using dilute sulphuric acid. The sodium chloride was used without any pH adjustments.

The selection of aggregating agent plays a crucial role in the formation of aggregates. Certain ionic species exhibit a strong binding affinity to the gold nanoparticle surface. This is detrimental to the enhancement of the Raman scattering of the analyte molecules as the ionic species will competitively bind to the gold nanoparticle surface, leading to a diminished SERS intensity. Ideally, the aggregates formed trap the analyte molecules in the hot spots formed by the nanogaps between the nanoparticles but not large enough to shield the hot spots from the laser radiation (Turzhitsky et al., 2018). Han et al (2009) successfully obtained the SERS spectra from proteins without chromophore using silver nanoparticles colloid and acidified Na_2SO_4 as the aggregating agent due to its poor binding affinity to silver nanoparticles. The acidic condition ensures that the solution is below the isoelectric point of proteins where proteins exhibit a positive charge and are effectively attracted to the negatively charged citrate ions capping the silver nanoparticles. Sodium chloride is a typical aggregating agent used in colloidal SERS (Cyrankiewicz et al., 2007). Both acidified sodium sulphate and sodium sulphate will be

compared as the aggregating agent for colloidal SERS.

3.8.3 Spectral Acquisition, Pre-processing and Data Analysis

The laser power (measured at the fibre ferrule) was 50 mW. The integration time was 10 s. The spectra were smoothed using the Savitzky-Golay algorithm with 13 points window and cubic polynomial to remove shot noise. These parameters were chosen because they were found to preserve most of the spectral characteristics with the best signal-to-noise ratio (Radzol et al., 2014). Baseline correction was done using the asymmetric least square smoothing algorithm in OriginLab Pro (asymmetric factor of 0.001, threshold of 0.1, smoothing factor of 4 and using 10 iterations). After the baseline correction, the spectra were smoothed again using the Savitzky-Golay algorithm using the same parameters for further denoising followed by a constant subtraction to set the baseline at zero.

3.8.4 Flowchart of SERS Experiment

Figure 3.6 (next page) shows the flowchart of the SERS experiments. First, the suitable choice of aggregating agent was determined based on the background spectra obtained when the aggregating agent is added and the tendency to competitively bind with the analyte molecules. Next, the efficacy of the prepared gold nanoparticles and the chosen aggregating agent was evaluated using 0.1 mM R6G solution and lysozyme solution. Once good results were obtained with R6G and lysozyme, the SERS of grouper epidermal mucus was studied.

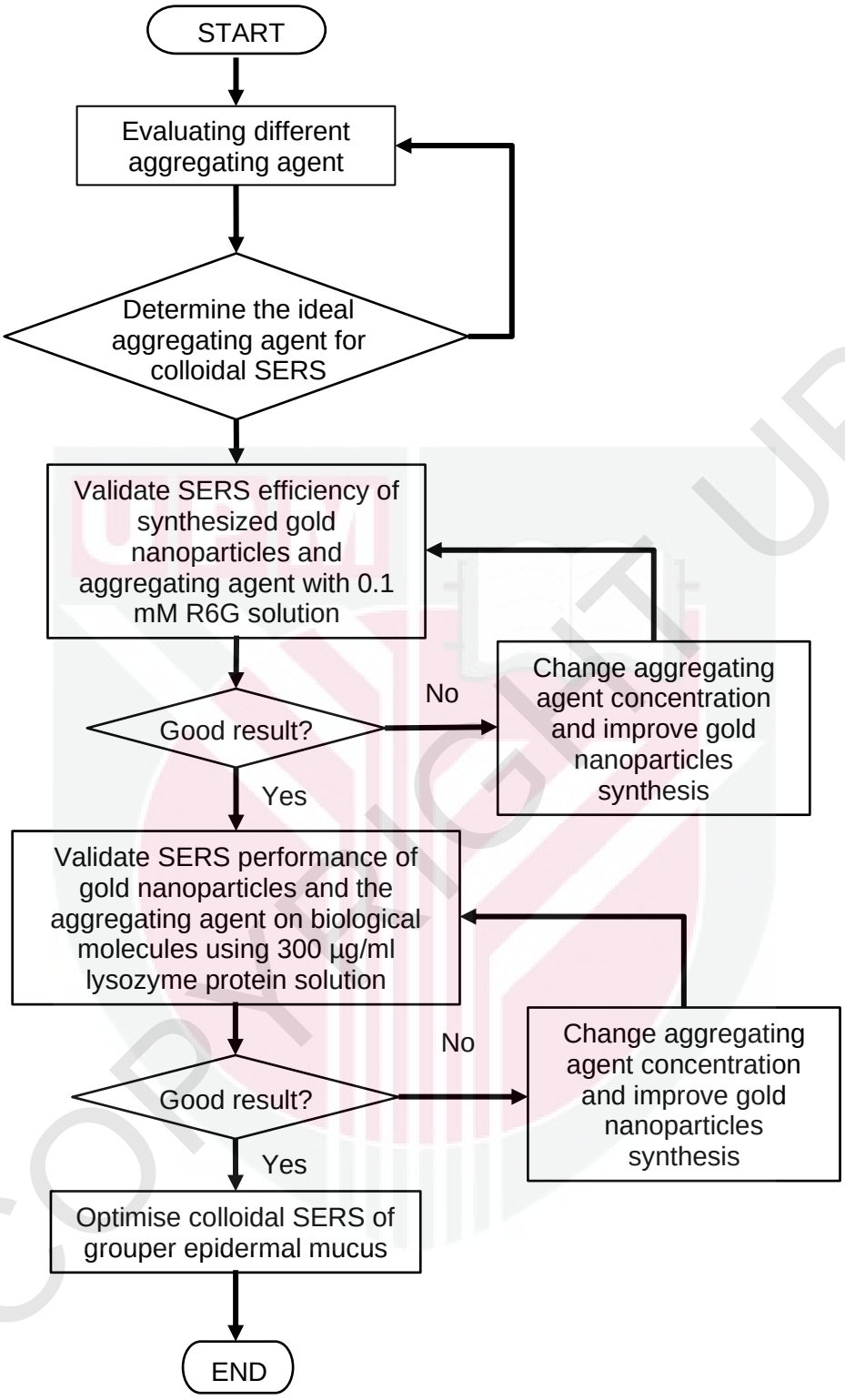

Figure 3.6: Flowchart of the SERS experiment.

CHAPTER 4

RESULTS AND DIDCUSSION

4.1 Introduction

The synthesised gold nanoparticles were characterised using UV-Visible spectroscopy, dynamic light scattering to measure the hydrodynamic diameter and transmission electron microscopy to measure the actual diameter which was measured to be 44 nm. The measured diameter of the gold nanoparticles was used to estimate the concentration of the gold nanoparticles.

The efficacy of the acidified Na_2SO_4 and NaCl solution as the aggregating agent was evaluated based on the background spectrum obtained upon the addition of the aggregating agent. Acidified sodium sulphate was chosen as the appropriate aggregating agent in subsequent SERS experiment due to its low affinity to bind to the gold nanoparticle surface and the featureless background spectrum.

The colloidal SERS performance synthesised gold nanoparticles and acidified sodium sulphate was tested with two test molecules, namely, 0.1 mM R6G solution and 300 µg/mL. The addition of gold nanoparticles and Na_2SO_4 greatly enhanced the peaks of both analytes. The optimal concentration of Na_2SO_4 for the best enhancement of the SERS spectrum of R6G and lysozyme was 1 M and 0.1 M respectively. This result indicates that lysozyme induces a higher

degree of aggregation compared to R6G.

The optimal concentration of Na_2SO_4 for the enhancement for the peaks corresponding to protein in grouper mucus was 1 M. The enhancement was not uniform across all peaks because grouper mucus is a complex matrix containing a wide range of biomolecules that have different affinities to gold nanoparticles surface. There were some overlapping peaks in the SERS spectrum of lysozyme and grouper mucus. This shows that it is possible to detect lysozyme in grouper mucus.

4.2 Characterisation of Gold Nanoparticles

4.2.1 UV-Visible Absorption Spectroscopy

The absorption of the gold nanoparticles was scanned from 400 nm to 800 nm. As shown in Figure 4.1, the surface plasmon resonance (SPR) peak of the synthesised gold nanoparticles was located at 537 nm. Using the SPR peak, the diameter of the gold nanoparticles can be estimated using the equation:

$$d\ (nm) = \frac{1}{L_2}\left(\frac{\ln(\lambda_{SPR}-\lambda_o)}{L_1}\right) \quad (3)$$

where λ_0 = 512, L_1= 6.53 and L_2= 0.0216 (Haiss et al., 2007). The diameter of the gold nanoparticles estimated using Equation (3) is 62.2 nm.

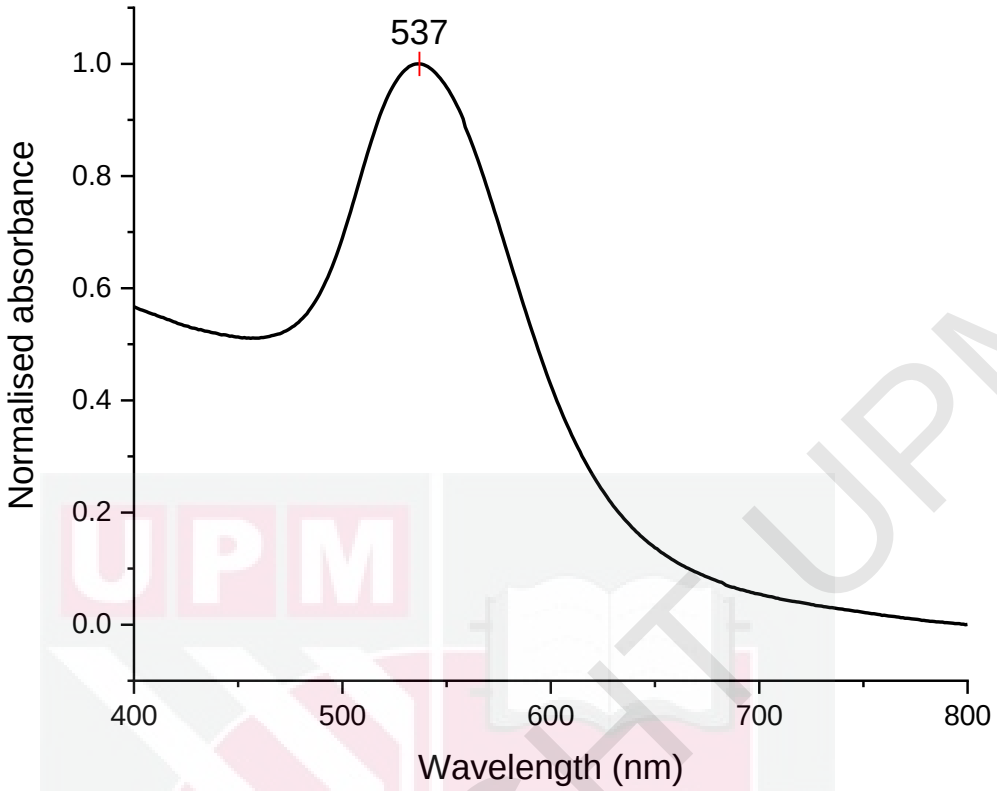

Figure 4.1: UV-Visible absorption spectroscopy of the synthesised gold nanoparticles.

4.2.2 Dynamic Light Scattering

Dynamic light scattering measures the intensity of the scattered light caused by the gold nanoparticles. The fluctuation of the light intensity is analysed using an autocorrelation function to determine the diffusion constant and the hydrodynamic diameter (T. Zheng, Bott, et al., 2016). The hydrodynamic diameter is the sum of the diameter of the gold nanoparticles and the contribution of the ligand (T. Zheng, Cherubin, et al., 2016). Figure 4.2 shows the hydrodynamic measurement of citrate-capped gold nanoparticles.

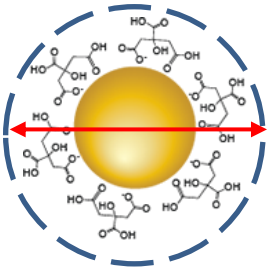

Figure 4.2: Illustration of hydrodynamic diameter of a citrate capped gold nanoparticle.

Three measurements were conducted on the colloid for dynamic light scattering. The nominal diameter of the gold nanoparticles obtained from dynamic light scattering was 68.1 nm as depicted in Figure 4.3. Average polydispersity index was 0.356 which indicates that the nanoparticles were fairly polydisperse. The polydispersity index value ranges from 0 for highly monodisperse sample to 1 to for heterogenous sample. The fairly polydisperse nature of the colloid was reflected in the standard deviation of the nominal peaks of the three measurements which have the values of 37.14 nm, 24.54 nm and 29.78 nm. The peaks at the sub 10 nm range were due to the multiple scattering effects. This effect occurs when a photon of light is scattered more than once by a particle in the scattering volume before reaching the detector, altering the time scale of light fluctuations, causing error in performing the autocorrelation function in the instrument. The multiple scattering effect is directly proportional to the mean free path of the photon in the colloid. Both the concentration and nanoparticle size influence the mean free path of the photons in the colloid (T. Zheng, Bott, et al., 2016). The presence of the multiple scattering effect in Figure 4.3 shows the colloid needs to be further diluted. However, this does not influence the hydrodynamic diameter and size distribution measurement as the peak in the sub 10 nm region can be ignored.

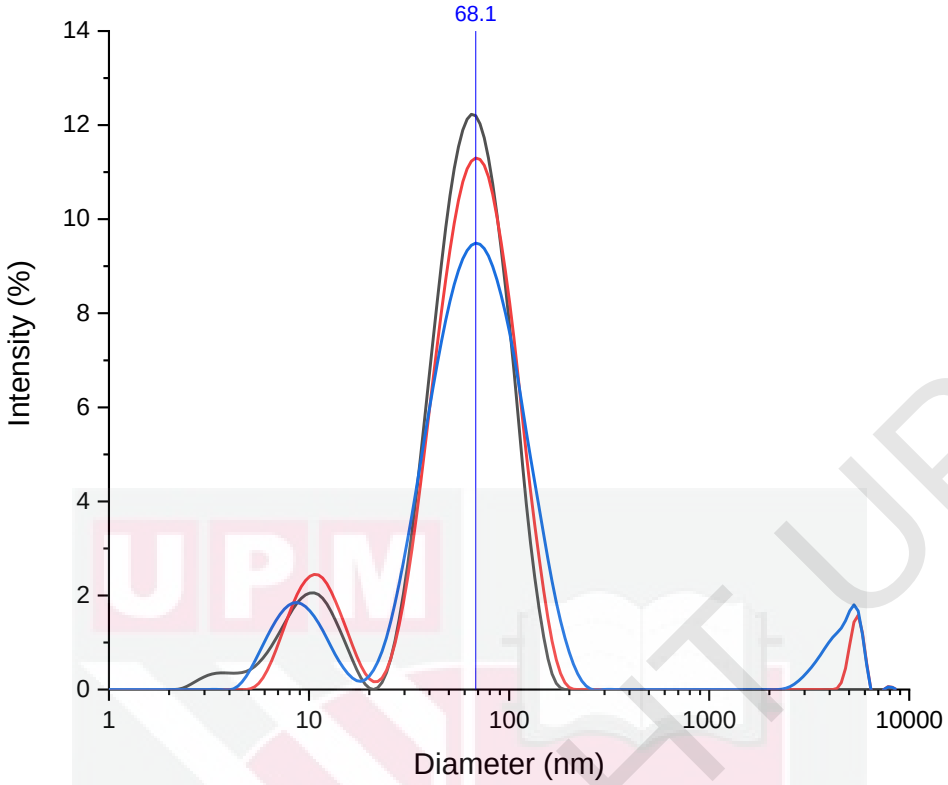

Figure 4.3. Size distribution measured by dynamic light scattering.

4.2.3 Transmission Electron Microscopy

The actual diameter of the gold nanoparticles can be determined from the TEM image as shown in Figure 4.4. The size distribution was obtained by measuring the size of the 86 particles in the TEM image using an image processing software (ImageJ 1.53K). From Figure 4.4(a), the mean diameter was 44 nm. Naturally, diameter of the gold nanoparticles obtained using UV-Visible absorbance spectra and dynamic light scattering will be larger than the actual diameter due to the influence of the citrate ligand.

The number of gold atom per nanoparticle is given by Equation (4), assuming the gold nanoparticles have a face-centred cubic structure.

$$\mathrm{N} = \frac{\pi(19.3\ \mathrm{D}^3)}{6(197)} \tag{4}$$

where D is the diameter of the gold nanoparticle in nm. The density of gold is 19.3 g/cm^3 and the molecular mass is 197 g/mol. The concentration of the gold colloid is given by Equation (5).

$$C = \frac{N_{Au}}{N \times N_A \times V} \tag{5}$$

where N_{Au} is the total number of gold atoms used in the synthesis and V is the volume of the solution.

(a)

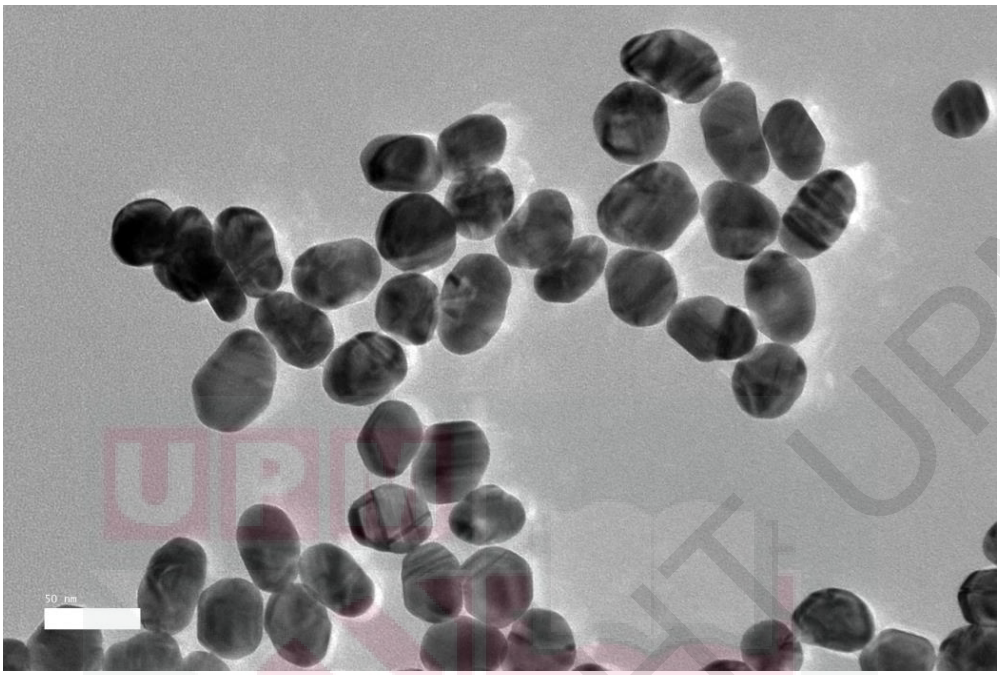

(b)

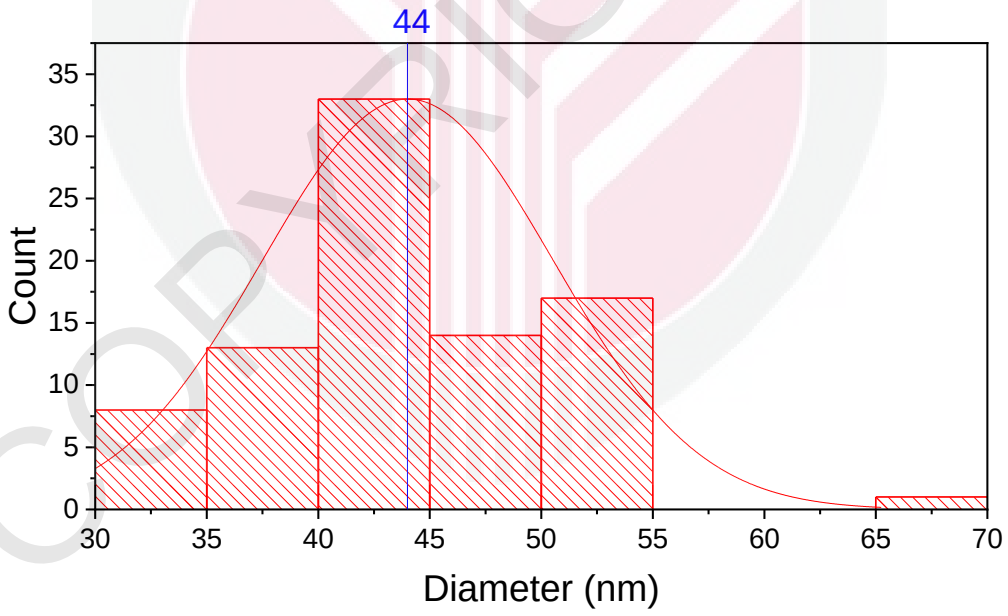

Figure 4.4: (a) TEM image of the synthesised gold nanoparticles and (b) size distribution of the gold nanoparticles measured from the TEM image.

Using the mean diameter of 44 nm and Equations (4) and (5), the concentration of gold nanoparticles was 5.72×10^{13} particles/mL. After concentrating from 4.5 mL to 50 µL, the concentration of the gold colloid used in the SERS analysis was 5.15×10^{15} particles/mL, assuming no particles were lost during the centrifugation process. The concentrating process increases the concentration of SERS hot-spots that will be formed when aggregation is induced.

4.3 Surface-enhanced Raman Spectroscopy

4.3.1 Evaluation of Na_2SO_4 as the Aggregating Agent

Figure 4.5 illustrates the interaction between citrate-capped gold nanoparticles and analyte molecules and the formation of aggregates in the presence of sulphate ions. Citrate ions are weakly-bonded ligands that can be easily displaced by the analyte molecules. The displacement of citrate ions allows the analyte molecules to be adsorbed onto the surface of the gold nanoparticles, reducing the surface charge of the gold nanoparticles. As a result, aggregates are formed due to the Van der Waals attraction overcoming the weaker electromagnetic repulsion. The addition of salt further depletes the surface charge and form larger aggregates.

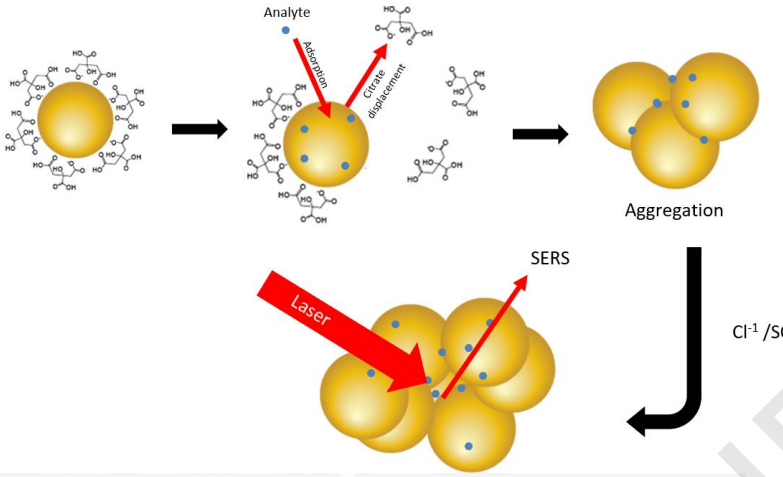

Figure 4.5: Schematic of the interaction between the analyte molecules and citrate-capped gold nanoparticles and formation of aggregates in saline media.

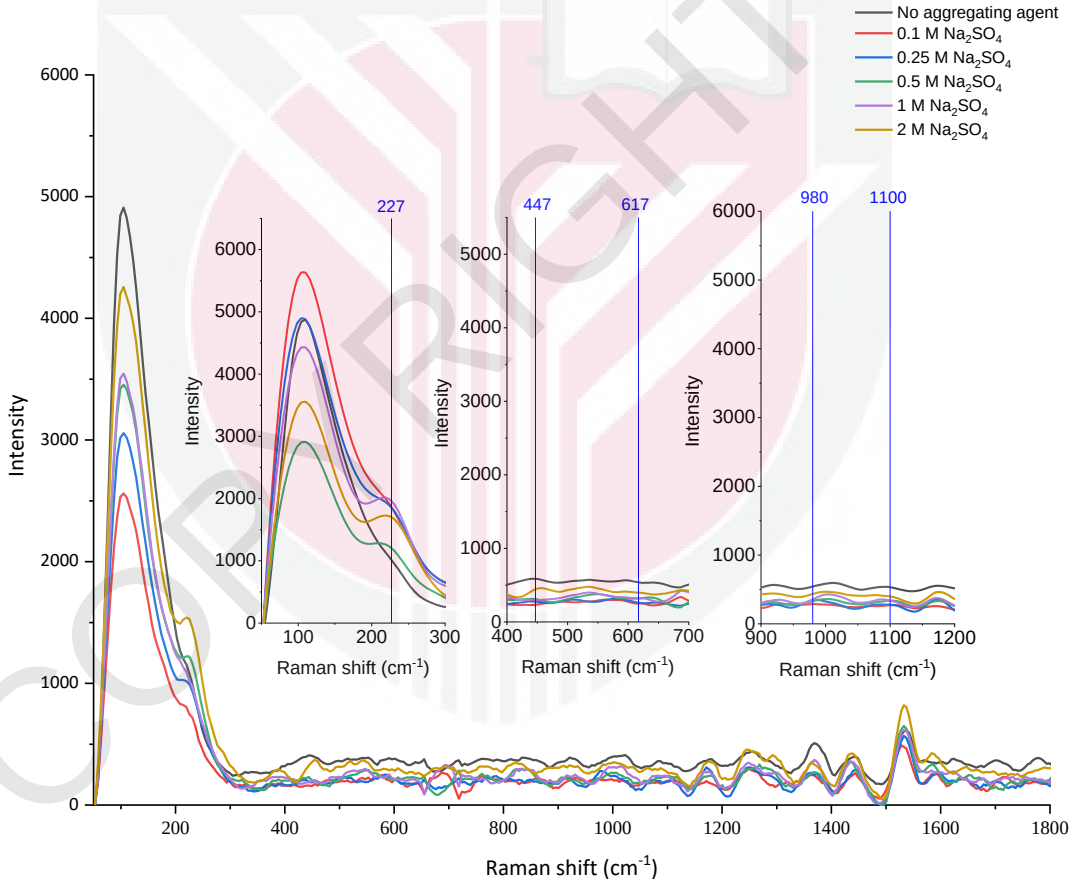

Figure 4.6: SERS spectra of gold nanoparticles with different concentration of Na_2SO_4 without the presence of analyte. The insets show the region between 50 to 300 cm^{-1} (left), 400 to 700 cm^{-1} (centre) and 900 to 1100 cm^{-1} (right). The Au-Cl peak was located at 227 cm^{-1} while the SO_4^{2-} peaks were located at 447, 617, 980 and 1100 cm^{-1}.

The efficacy of acidified Na_2SO_4 as aggregating agent for SERS analysis using gold nanoparticles was evaluated by adding acidified Na_2SO_4 solution with concentrations ranging from 0.1 M to 2 M to gold nanoparticles colloid and acquiring the Raman spectra as shown in Figure 4.6. The peaks corresponding to sulphate ions at 447, 617, 980 and 1100 cm^{-1} were not visible in the SERS spectra, giving a relatively featureless background. The peak located at 227 cm^{-1} can be attributed to the Au-Cl bond (Liu et al., 2018) was contributed by the residual chloride ions from the gold precursor used in the synthesis. This peak is not detectable prior to aggregation, thus, showing that the addition of sulphate ion to the colloid can induce aggregation which traps molecules in the nanogaps between the gold nanoparticles, leading to the enhancement of the SERS signal of that molecule. Therefore, these observations showed that acidified Na_2SO_4 is a good candidate for colloidal SERS due to its ability to generate SERS hot-spots via aggregation by the enhancement of the Au-Cl peak at 227 cm^{-1} and the low affinity to the gold nanoparticle surface indicated by the relatively clean background spectrum as shown in Figure 4.6.

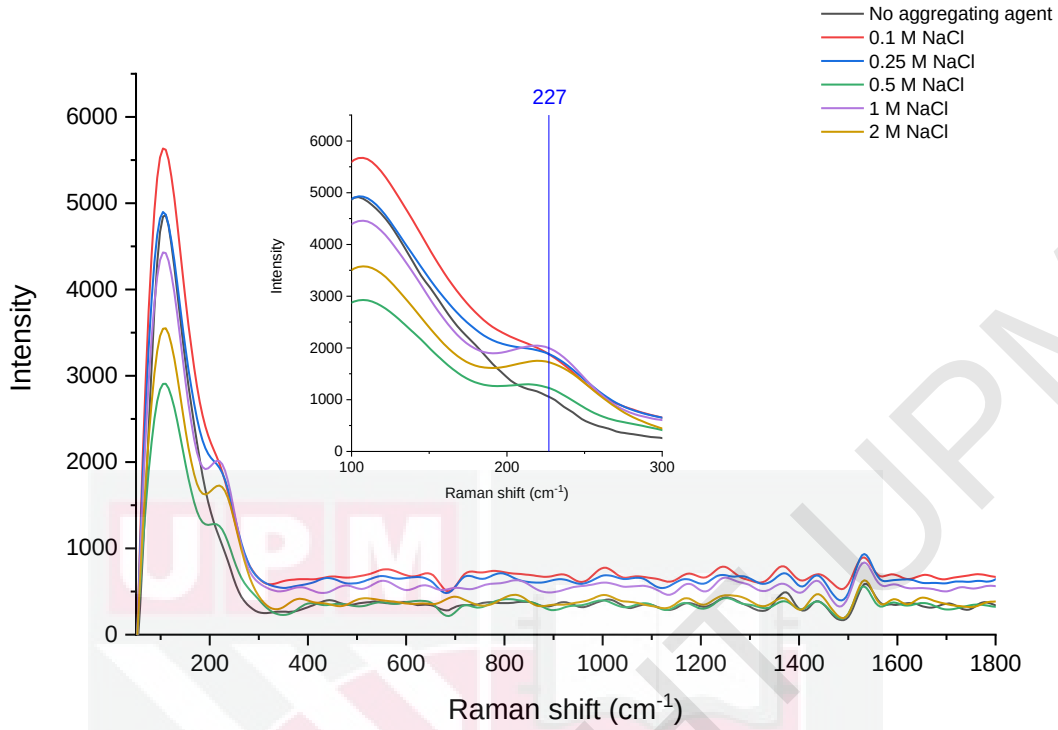

Figure 4.7: SERS spectra of gold nanoparticles with the addition of different concentrations of NaCl. The inset shows the region between 100 to 300 cm^{-1}.

As shown in Figure 4.7, the background spectra obtained using NaCl and acidified Na_2SO_4 (refer to Figure 4.6) as the aggregating agent were similar. Similar to Na_2SO_4, NaCl was able to induce the aggregation of gold nanoparticles to generate the SERS hot-spots, indicated by the enhancement of the Au-Cl peak at 227 cm^{-1} (Liu et al., 2018). The background spectra obtained using both aggregating agents were relatively featureless.

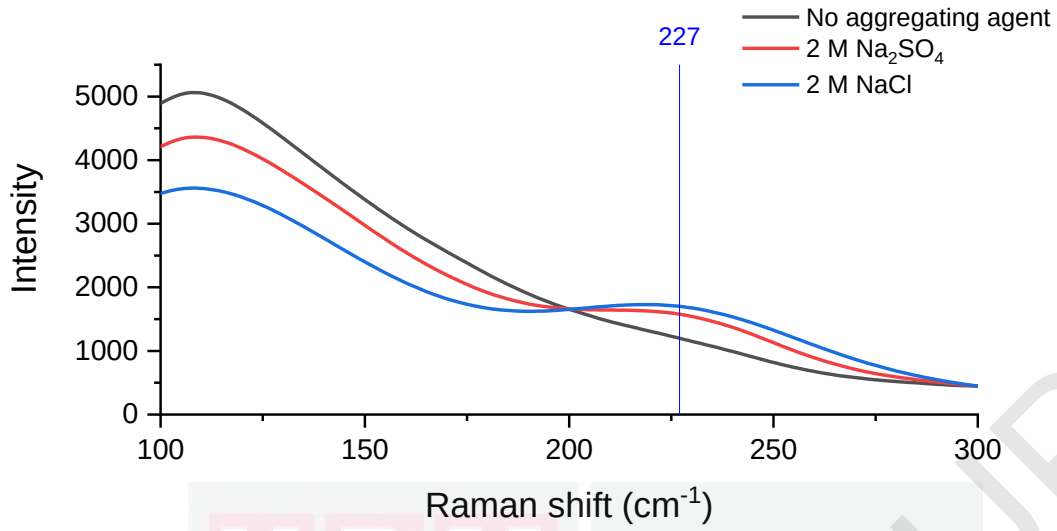

Figure 4.8: SERS spectra of gold nanoparticles in the region between 100 to 300 cm^{-1} upon the addition of 2 M NaCl and 2 M Na_2SO_4.

Figure 4.8 shows the comparison between NaCl and Na_2SO_4 as the aggregating agent. The addition of 2 M NaCl showed a higher intensity of the Au-Cl peak at 227 cm^{-1} which can be explained by the adsorption of additional Cl^- ions onto the surface of the gold nanoparticles. This result shows that NaCl can potentially competitively bind with the analyte molecules which may impair the SERS efficiency.

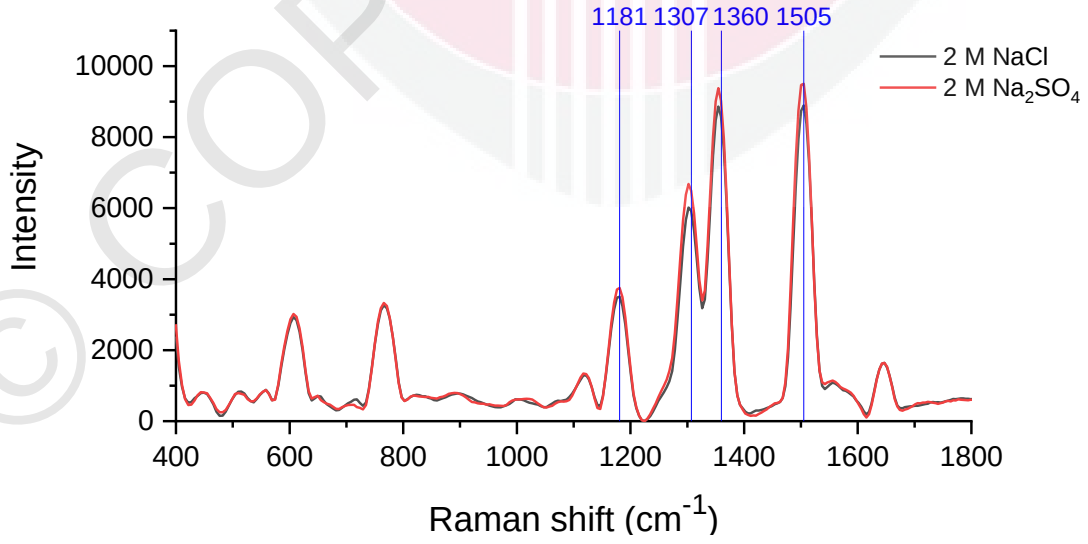

Figure 4.9: SERS spectra of R6G obtained using 2 M NaCl and 2 M Na_2SO_4.

Using R6G as a test molecule, the SERS efficiency of NaCl and Na_2SO_4 was evaluated. As shown in Figure 4.9, the peak intensity at 1181, 1307, 1360 and 1505 cm^{-1} were higher using Na_2SO_4 as the aggregating agent. This shows that Cl^- ions will competitively bind with the analyte molecules on the surface of gold nanoparticles. Therefore, as shown in Figure 4.8 and Figure 4.9, the performance of Na_2SO_4 as the aggregating agent was better due to the low affinity of SO_4^{2-} ions to bind to gold nanoparticles, thus, competitive binding is less likely. These observations indicate that Na_2SO_4 was an appropriate aggregating agent to perform colloidal SERS. Consequently, acidified Na_2SO_4 will be used as the aggregating agent in the subsequent experimental works.

Given that different molecules interact with the surface charge on the gold nanoparticle surface differently, the formation of the initial aggregate is highly dependent on the analyte solution added to the gold nanoparticles colloid. Thus, the impact of adding acidified Na_2SO_4 to colloid was investigated in the presence of three different analyte solutions as follows:

a) R6G to investigate the SERS performance of the protocol proposed on an analyte molecule known to have strong bonding affinity to anionic gold nanoparticles (Ganbold et al., 2011),
b) Lysozyme to test the SERS efficacy on a protein molecule.
c) Grouper epidermal mucus which is a complex matrix containing a wide range of biomolecules.

4.3.2 Surface-Enhanced Raman Spectroscopy of R6G Using Acidified Sodium Sulphate as the Aggregating Agent

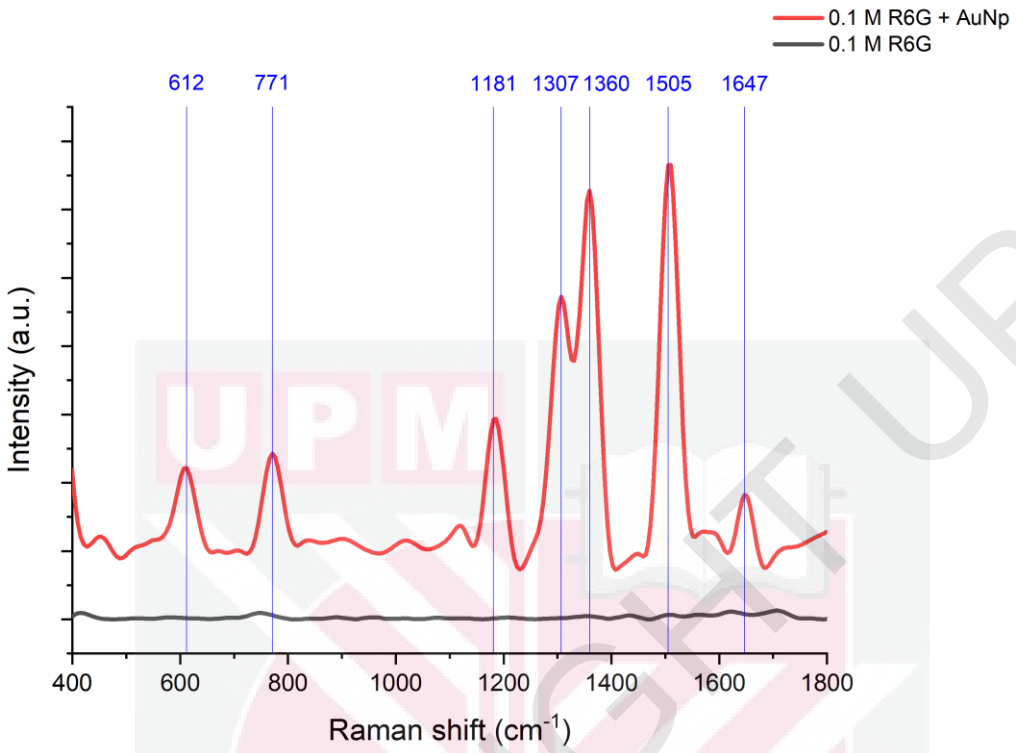

Figure 4.10: SERS spectrum of 0.1 mM R6G (red) and Raman spectrum of R6G (black). Both spectra were obtained using laser power of 50 mW and 10 s integration time. The graphs were shifted for clarity.

R6G is a fluorescent dye with characteristic peaks in the region between 600 to 1700 cm^{-1}. The SERS spectrum and Raman spectrum of R6G is shown in Figure 4.10. The characteristic peaks of R6G were not visible in the Raman spectrum. However, the addition of gold nanoparticles greatly increases the Raman peaks of R6G. This shows that the synthesised gold nanoparticles were able to perform colloidal SERS.

As shown in Figure 4.11 (a) and (b), the optimal concentration of Na_2SO_4 for the highest SERS signal of R6G is 1 M. The peak assignment for R6G is summarised in Table 4.1. As shown in Figure 4.11 (b), the intensity of the

peaks initially decreases upon the addition of 0.1 M Na_2SO_4. This is possibly due to the displacement of R6G molecules by the sulphate ions and at a low concentration, insufficient aggregation is induced. This observation is consistent with the findings by Hu et al (2020) where aggregation of gold nanoparticles was observed when salt concentration is above 0.1 M. As the concentration of Na_2SO_4 increases, larger aggregates are formed, forming more SERS hot-spots which resulted in the increasing intensity of the peaks as evident in Figure 4.11 (b). At 2 M, the intensity reduces due to the shielding of the SERS hot-spots (Turzhitsky et al., 2018). Therefore, this result shows that the synthesised gold nanoparticles and the chosen aggregating agent were able to perform colloidal SERS using a typical Raman reporter molecule, R6G.

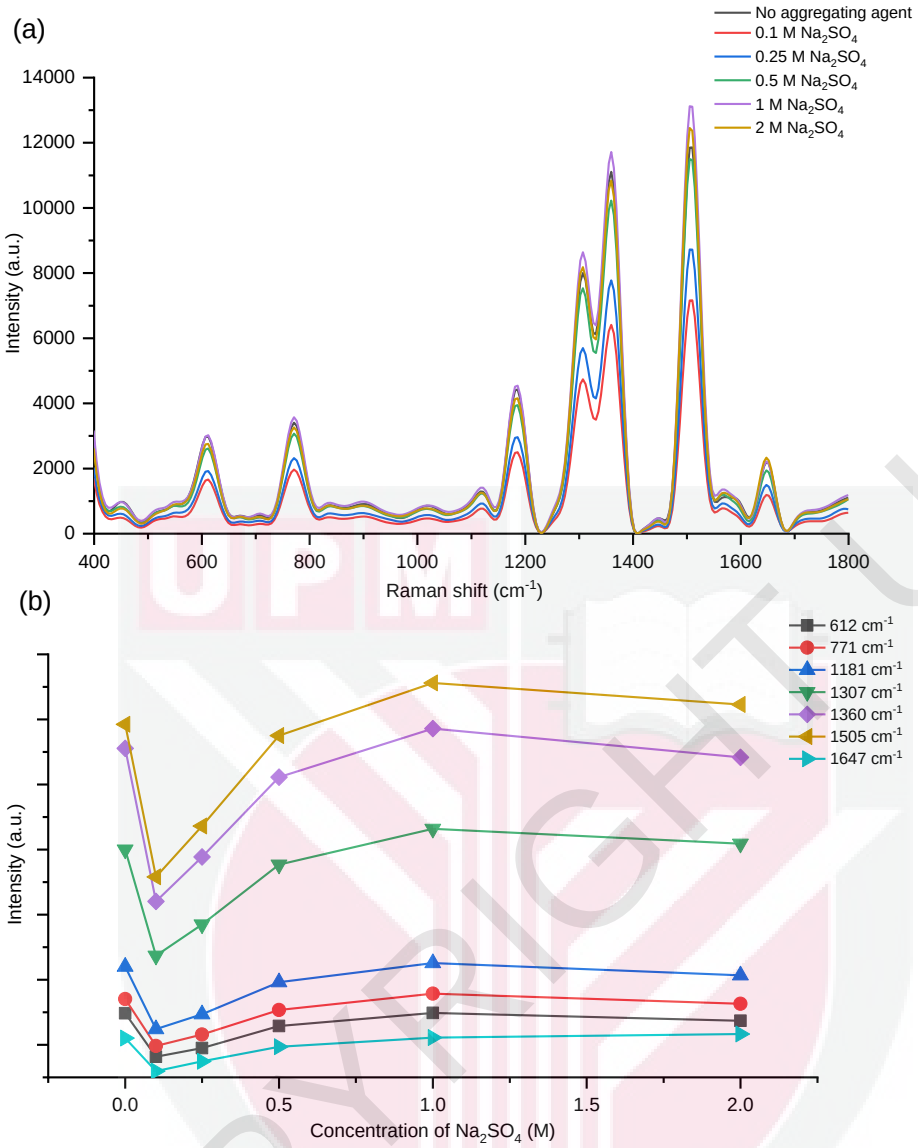

Figure 4.11: (a) The SERS spectra of R6G obtained using different concentrations of Na_2SO_4. The peaks identified in Figure 4.10 were plotted against the concentration of Na_2SO_4 in (b). The graphs were shifted for clarity.

Table 4.1. Peak assignment for the SERS spectrum of R6G.

Peak center (cm^{-1})	Peak assignment
606	C-C-C ring in plane vibration
711	C-H out of plane vibration
1181	C-H in plane vibration
1307	N-H in plane bend
1360	C-C stretching
1505	C-C stretching
1647	C-C stretching

4.3.3 Surface-Enhanced Raman Spectroscopy of Lysozyme Using Acidified Sodium Sulphate as the Aggregating Agent

Subsequently, SERS of lysozyme using the synthesised gold nanoparticles and chosen aggregating agent was performed to test its efficacy in detection of biological molecules which have complex surface charge compared to the uncharged R6G molecules. Proteins have three characteristic vibrations resulting from the polypeptide backbone. Namely, the amide I region (1600 to 1700 cm^{-1}) which is associated with the C=O stretch of the carbonyl group in the amide backbone (Sadat & Joye, 2020), the amide III region (1200 to 1300 cm^{-1}) is the combination of the N-H in plane vibration and the C-N stretch with some overlap with the C=O in plane bend and C-C stetch and finally, the amide II region (1480 to 1580 cm^{-1}) is the combination of N-H bend, C-N stretch with significant overlap from the C-C stretch and C=O bend (Kuhar et al., 2021). The SERS spectrum of proteins will be comprised of these three amide vibrations and the peaks from the amino acid side chains.

As evident in Figure 4.12 (a), the Raman spectrum of lysozyme was relatively poor. Only the amide I vibration and minor peaks from S-S and C-S stretch at 416 and 750 cm^{-1} respectively. In contrast, the SERS spectrum of lysozyme exhibited all the characteristic peaks of protein and peaks from the amino acid side chains. Both the Raman spectrum and SERS spectrum were obtained using laser power of 50 mW and 10 s integration time. The peaks assignment of lysozyme is summarised in Table 4.2. The peaks were assigned within $\pm$ 10 cm^{-1} of the literature values to account for instrumentation differences (J. Hu et al., 1995; Szekeres & Kneipp, 2019; Yvon, 2017).

The difference between the Raman spectrum and SERS spectrum in the amide I region depicted Figure 4.12 (b). Due to the nature of the localised surface plasmon resonance of nanoparticles, the electromagnetic field quickly diminishes with distance from the surface of the nanoparticle. The bulky amino acid side chains will shield the polypeptide backbone from the plasmonic nanostructure, resulting in the suppression of the amide I band. This effect prominent for SERS of globular proteins such lysozyme (Kurouski et al., 2013). In addition, the blue-shift of the amide I band in the SERS spectrum in comparison with the Raman spectrum from 1629 cm^{-1} to 1611 cm^{-1} indicates a structural change from α-helical structure to β-sheets and random coils (Sethuraman & Belfort, 2005).

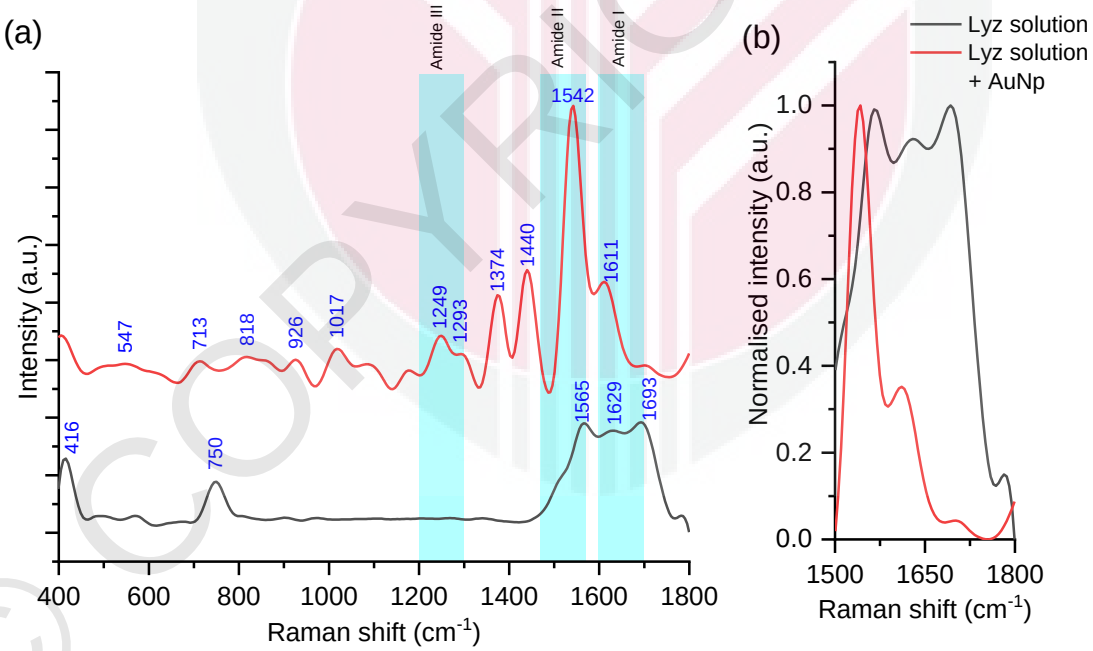

Figure 4.12. (a) SERS spectrum (red) and Raman spectrum (black) of 300 µg/ml lysozyme solution. The graphs were shifted for clarity. The normalised SERS and Raman spectrum in the amide I region is shown in (b).

Table 4.2: Peak assignment of lysozyme.

Peak (cm^{-1})	Raman	SERS	Peak assignment
406		✓	S-S stretch
416	✓		
713		✓	C-S stretch (aliphatic)
750	✓		
818		✓	Tyr
926		✓	C-C-N deformation
1017		✓	Phe
1249		✓	Amide III
1293		✓	
1374		✓	CH_3 deformation
1440		✓	CH_2 deformation
1542		✓	Trp, amide II
1565	✓		Amide II
1611		✓	Amide I
1629	✓		
1693	✓		

This structural change and protein unfolding on the gold nanoparticle surface plays a crucial role in aggregation of gold nanoparticles (D. Zhang et al., 2009). Due to the coalescing of protein-gold nanoparticles complex, the higher degree of aggregation induced by lysozyme is evident in Figure 4.12(a) and (b) as only 0.1 M of Na_2SO_4 was required for the optimal aggregation of gold nanoparticles to obtain the highest peak intensities across most peaks compared to the 1 M required for R6G. However, the enhancement factor at 0.1 M is not consistent across all peaks, namely the peak associated with CH_3 at 1374 cm^{-1}. Due to the three-dimensional structure of lysozyme, certain peaks may be selectively enhanced due to the orientation of lysozyme on the gold nanoparticle surface as the aggregates are formed.

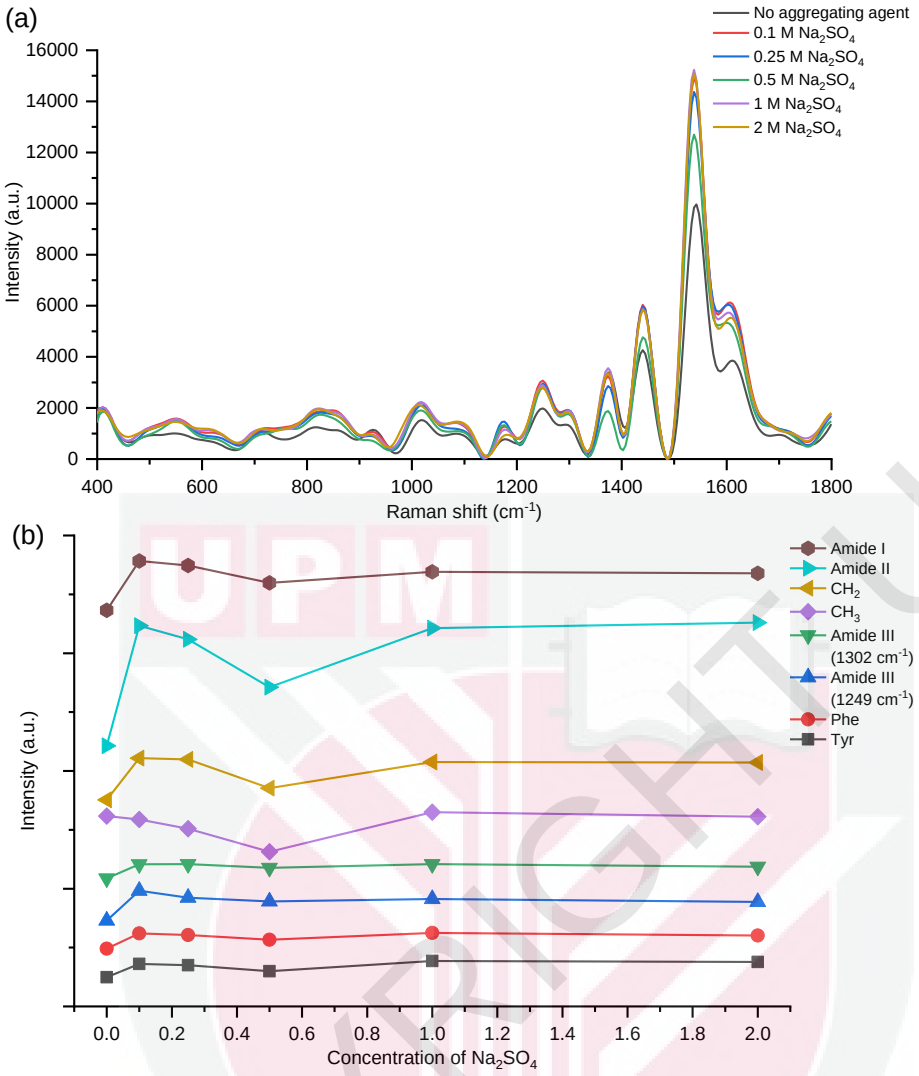

Figure 4.13: (a) The SERS spectra of 300 µg/ml lysozyme solution obtained using different concentrations of Na_2SO_4. The peaks identified in Figure 4.12 were plotted against the concentration of Na_2SO_4 in (b).

The increase in intensity of the peaks of the SERS spectrum of lysozyme beyond 0.5 M of Na_2SO_4 may be contributed by the adsorption of lysozyme on the outer layers of the aggregates as larger aggregates have higher surface area for adsorption of lysozyme and at 2 M, no more gold nanoparticles were available to form the aggregates. The number of lysozyme molecules in 10 µl of a 300 µg/ml solution was 1.254×10^{14} while the calculated number of gold nanoparticles was 4.89×10^{13} in 9.5 µl.

4.3.4 Surface-enhanced Raman Spectroscopy of Grouper Mucus Using Acidified Sodium Sulphate as the Aggregating Agent

Grouper mucus is a complex matrix composed of saccharides, lipids, proteins and a wide range of small metabolites. The SERS spectra will show the multiplexing of multiple peaks contributed by the various biomolecules present in the mucus, thus, making the identification of the constituents challenging without accompanying metabolomics and proteomics study. (Nurhikmah et al., 2022) identified potential biomarkers in mucus for *Vibrio*-resistant juvenile hybrid groupers (*Epinephelus fuscoguttatus* × *Epinephelus lanceolatus*) using proteomic study, however, the identified proteins were not available off-the-shelf, rendering SERS characterisation of the identified proteins difficult. Some metabolomics studies were conducted on grouper. For example, the published work focused on metabolomic profiling of volatile compounds constituting to the flavour of grouper fish (*Epinephelus coioides*) using muscle tissue extract (Chu et al., 2023) and identifying metabolome changes in intestinal tissue caused by castor-meal induced enteritis in juvenile hybrid groupers (*Epinephelus fuscoguttatus* × *Epinephelus lanceolatus)*. At present, there is a lack of published metabolomic and proteomic profiling of grouper mucus that is applicable to this study. Nevertheless, the SERS spectra of grouper mucus can serve as a rapid and cost-effective method to characterise grouper epidermal mucus.

Figure 4.14 (a) shows the SERS spectra of grouper epidermal mucus obtained using different concentrations of Na_2SO_4. The significant peaks were labelled, however, only the functional groups and the probable biomolecules were able

to be assigned to the peaks based on the literature (J. Hu et al., 1995; Szekeres & Kneipp, 2019; Yvon, 2017). The peak assignment of grouper epidermal mucus is summarised in Table 4.3. The values were assigned within $\pm$ 10 cm^{-1} of the literature values to account for instrumentation differences.

Table 4.3. Tentative peak assignment of grouper epidermal mucus.

Peak (cm^{-1})	Tentative peak assignment
542	S-S stretch
729	C-S stretch
839	Tyr, C-O-C, saccharides
997	Phe, aromatic ring
1171	Tyr, C-N stretch
1254 1298	Amide III
1454	CH_2 stretch, CH_3 stretch
1547	Amide II

As shown in Figure 4.14(b), the optimal concentration of Na_2SO_4 to obtain the highest peak intensity across most peaks was 1 M. However, the enhancement was not uniform across all peaks at 542 and 839 cm^{-1} being diminished upon the addition of 1 M Na_2SO_4. While the peak at 997 cm^{-1} associated with aromatic ring which may be indicative of phenylalanine residue recorded the highest intensity at 2 M Na_2SO_4. This is indicative of complex interactions between the biomolecules present in grouper epidermal mucus and gold nanoparticles where different biomolecules have different binding affinity towards gold nanoparticles based on the nature of their bond with the gold nanoparticle surface (covalent or electrostatic attraction). Despite this, majority of the peaks and the peaks associated with protein were shown to have the highest intensity at 1 M Na_2SO_4.

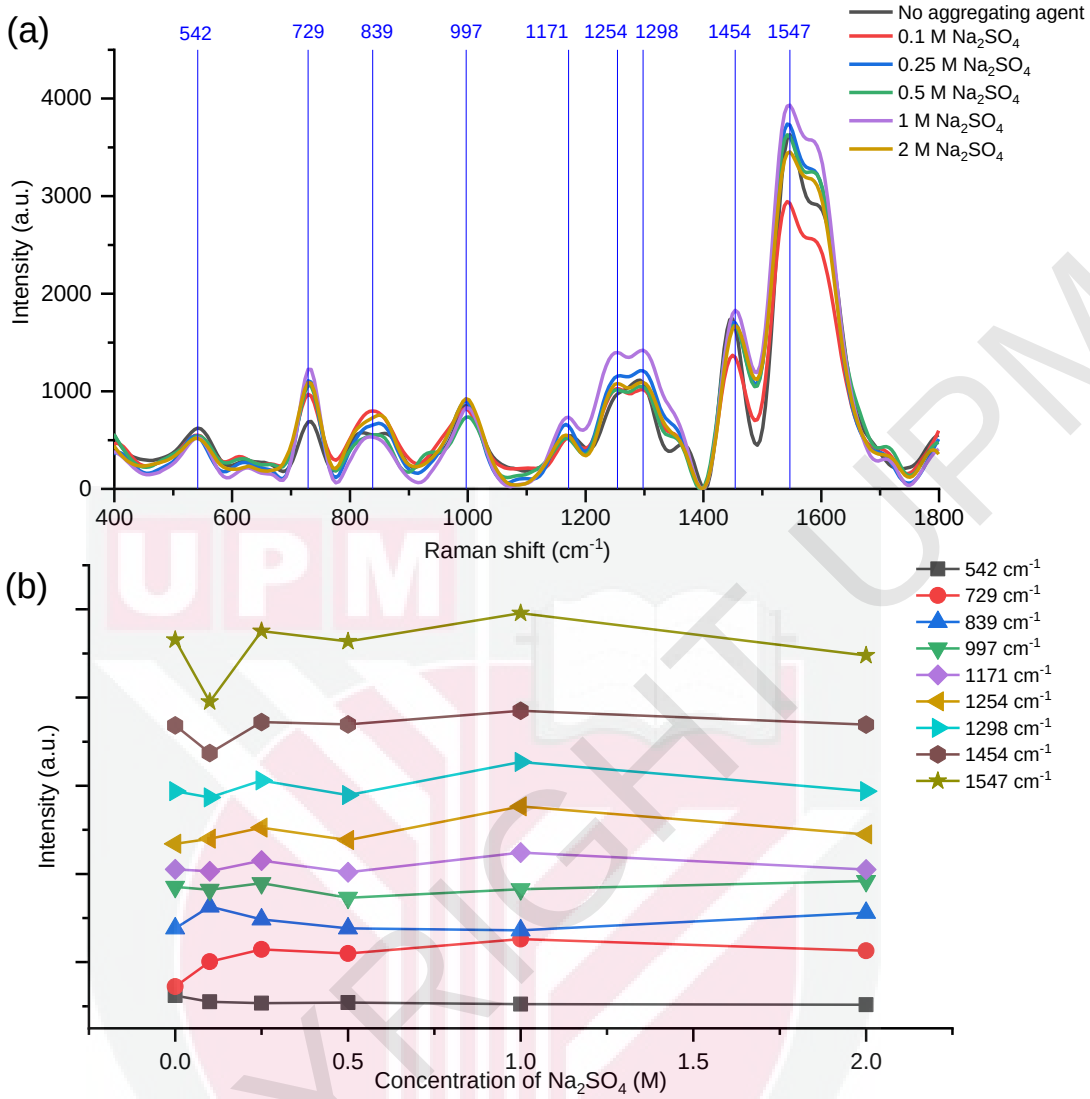

Figure 4.14: (a) The SERS spectra of grouper epidermal mucus obtained using different concentrations of Na_2SO_4. The intensities of the peaks identified in (a) were plotted in (b). The graphs were shifted for clarity.

Due to the fact that lysozyme is an important antipathogenic protein found in fish epidermal mucus (Dash et al., 2018), the normalised SERS spectra of lysozyme and grouper mucus were compared in Figure 4.15. The spectra were normalised using standard normal variate followed by baseline correction to set the baseline of each spectrum at zero. Several overlapping peaks were found, namely at 818, 1283, 1454 and 1542 cm^{-1}. Both spectra were obtained using 50 mW laser power and 10 s integration time. The concentration of

Na_2SO_4 used was the optimal concentration for lysozyme and grouper mucus as identified in Figure 4.13(a) and (b) and Figure 4.14(a) and (b) which were 0.1 M and 1 M for lysozyme and grouper mucus respectively.

The peak located at 1454 cm^{-1} is associated with CH_2 and CH_3 stretch which is universal for all organic molecules, therefore, this peak may not be a good candidate for the detection of lysozyme in grouper epidermal mucus. The other peaks at 818, 1283, and 1542 cm^{-1} may be good candidates for the detection of lysozyme in grouper mucus if multiplexing with other proteins can be ruled out using specific ligands to select for lysozyme or lysozyme extraction from grouper mucus. However, due to the limited availability of off-the-shelf ligand to target fish biomolecules, difficulties in synthesising specific ligands to select for lysozyme in fish and in the interest of performing in-situ analysis, steps to extract lysozyme or functionalisation of gold nanoparticles with ligands to target the lysozyme in grouper epidermal mucus is beyond the scope of this work.

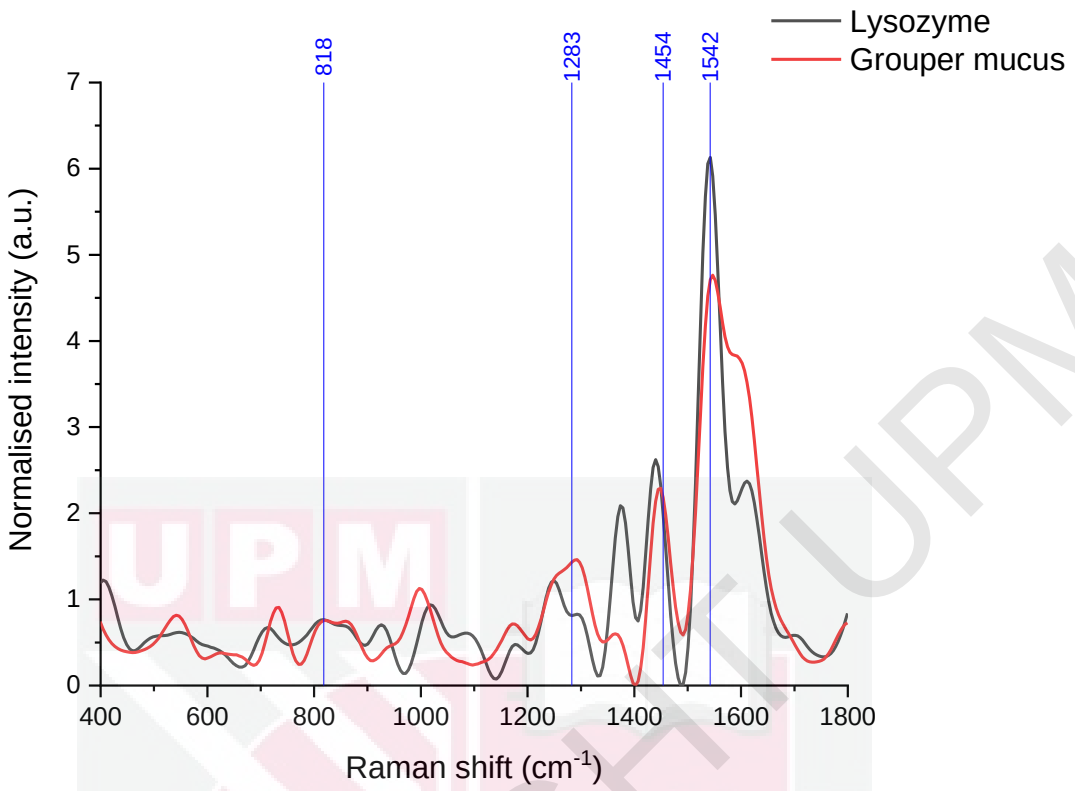

Figure 4.15: Normalised SERS spectrum of lysozyme and grouper mucus. The spectra were normalised using standard normal variate followed by baseline correction to set the baseline to zero.

4.4 Summary

To summarise, Na_2SO_4 was determined to be the suitable aggregating agent due to the clean background spectrum generated and the higher intensity of the SERS of R6G as compared to NaCl. The efficacy of the synthesised gold nanoparticles and Na_2SO_4 was tested with 0.1 mM R6G and 300 µg/mL lysozyme solution. The ideal concentration of Na_2SO_4 for the SERS of R6G and lysozyme was 1 M and 0.1 M, respectively. For grouper epidermal mucus, the enhancement was not uniform across all peaks, but 1 M Na_2SO_4 was determined to be the ideal concentration to obtain the highest enhancement for the peaks corresponding to proteins. The peaks at 818, 1283, and 1542 cm^{-1} were found to be overlapped in the SERS spectra of lysozyme and grouper epidermal mucus. This result shows that lysozyme may be detected in the grouper epidermal mucus using the aforementioned overlapping peaks.

CHAPTER 5

CONCLUSION AND RECCOMENDATIONS

5.1 Conclusion

Label-free SERS analysis for human biofluids have been well studied with many available published works on methodology to obtain SERS spectra various biofluids such as blood, saliva, urine, and synovial fluid. However, grouper epidermal mucus is significantly different compared to human biofluids and the SERS techniques used in analysis of human biofluids may not be applicable to grouper mucus. Therefore, this work addresses the gap in research in colloidal label-free SERS of grouper epidermal mucus.

This work presents a methodology for the colloidal SERS of grouper mucus. Aggregation plays an important role for SERS in colloidal system. Acidified Na_2SO_4 was chosen as the aggregating agent due to its ability to induce the aggregation of gold nanoparticles while having low affinity to form bonds on the surface of the gold nanoparticles. The sulphate ions do not competitively bind with the analyte molecules on the surface of the gold nanoparticles; thus, the SERS efficiency was not impaired upon the addition of aggregating agent. When using 2 M NaCl and Na_2SO_4, as the aggregating agent, the SERS spectrum of R6G obtained using NaCl exhibited a lower intensity compared to the spectrum obtained using Na_2SO_4 as the aggregating agent, which showed that NaCl has the tendency to competitively bind with analyte molecule on the

gold nanoparticle surface.

The gold nanoparticles were synthesised using the standard citrate reduction. The prepared gold nanoparticles and acidified Na_2SO_4 were used to perform colloidal SERS. Using TEM, the gold nanoparticles had a mean diameter of 44 nm. The SPR peak of the synthesised gold nanoparticles was located at 537 nm and the hydrodynamic diameter was measured to be 68.1 nm using DLS with a good monodispersivity. The diameter measured from DLS and obtained using the calculation based on the SPR peak was larger than the TEM measurements due to the presence of the citrate ligand.

Using R6G and lysozyme as the test molecules, the results showed that the prepared gold nanoparticles and the acidified Na_2SO_4 can be used to perform colloidal SERS. However, due to protein structural change on the surface of gold nanoparticles, lysozyme was able to induce a greater degree of aggregation. The concentration of aggregating agent required to obtain the highest overall enhancement of the peaks of lysozyme was 0.1 M which was 10 times lower than that of R6G which was found to be 1 M. Thus, the concentration of aggregating agent required to obtain the best enhancement highly depends on the nature of the analyte.

The lower pH of aggregating agent ensures that the pH of the overall mixture is acidic. The acidic environment ensures that most proteins in grouper epidermal mucus exhibit a positive charge and will be electrostatically attracted to the negatively charged citrate capping on the gold nanoparticles surface.

The optimal concentration of Na_2SO_4 for the enhancement across most peaks in the SERS spectrum of grouper mucus was 1 M. However, the enhancement was not uniform across all peaks due to the various biomolecules present having different affinities to the gold nanoparticle surface.

From the SERS spectrum of grouper epidermal mucus, the peaks located at 542 and 729 cm^{-1} corresponds to S-S stretch and C-S stretch which were indicative of amino acids. The peaks corresponding to amino acid residues were also identified at 839 and 1171 cm^{-1} which corresponds to tyrosine and 997 cm^{-1} which corresponds to phenylalanine. Additionally, the peak at 839 cm^{-1} can also be attributed to the C-O-C group found in saccharides. The polypeptide backbone vibration from proteins can also be identified by the peaks at 1254, 1298 and 1547 cm^{-1}. The SERS spectrum of grouper epidermal mucus offers a rapid, minimally invasive, and cost-effective method to profile grouper mucus, however, without additional profiling data, the individual biomolecules present in the mucus was difficult to elucidate due to the multiplexing of the peaks contributed from a wide range of biomolecules.

Nevertheless, there were several overlapping peaks between the SERS spectrum of lysozyme and grouper epidermal mucus, namely, 818, 1283, 1454 and 1542 cm^{-1}. However, peak at 1454 cm^{-1} corresponds to C-H group, which is universal to all organic compounds, thus, this peak is not indicative of lysozyme. Therefore, the peaks at 818, 1283, and 1542 cm^{-1} are good candidates for the detection of lysozyme in grouper epidermal mucus using SERS analysis.

5.2 Recommendations

This work addresses the gap in the available research on the methodology for the SERS of fish epidermal mucus and establishes a baseline for future research of grouper epidermal mucus profiling for various fish health conditions using SERS. The constituent biomolecules in grouper epidermal mucus can be identified using SERS spectral data accompanied with metabolomics or proteomics profiling of grouper epidermal mucus. Consequently, the selectivity and specificity of the SERS detection of biomolecules of interest can be improved once they were identified using metabolomics or proteomics data. As previously mentioned in section 5.1, (Nurhikmah et al., 2022) identified 13 proteins in grouper epidermal mucus that are significantly perturbed upon infection with *Vibrio alginolyticus* bacteria with immune related proteins being upregulated for resistant fish. Antibodies, specifically monoclonal antibodies which are highly specific, or aptamers need to be synthesised to target the proteins of interest found in grouper epidermal mucus. SERS immunoassay can be utilised to detect specific proteins as shown in Figure 5.1. SERS tags can be designed by functionalising gold nanoparticles with ligands (antibody is shown in Figure 5.1) and Raman reporter molecules. Raman reporters are molecules with characteristic Raman spectrum. If multiplexing is desired, Raman reporters with minimal overlapping peaks must be selected. The antibodies are immobilised on a substrate. Upon the addition of samples, the biomolecules will be captured by the immobilised antibodies. Subsequently, the SERS tags are added. After washing away unbonded biomolecules and free SERS tags, the SERS spectrum of the

Raman reporter can be measured and the intensity of the SERS signal is directly correlated to the amount of captured biomolecules (Y. Wang et al., 2013). Therefore, specificity and selectivity can be improved significantly by designing SERS tags that can target biomolecules of interest. However, SERS immunoassay is limited by the availability of the ligands that target specific biomolecules as the design and production of new ligands is a laborious process.

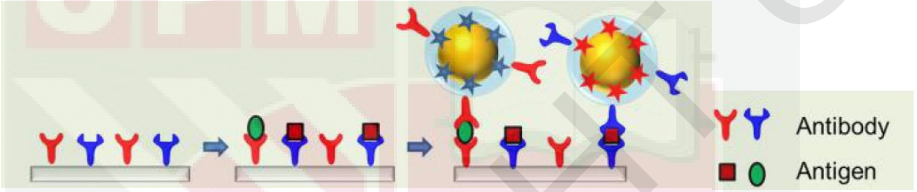

Figure 5.1: Schematic of SERS immunoassay.
(Y. Wang et al., 2013).

Protein precipitation is a simple method to minimise the multiplexing of the peaks of the amino acid residue in the protein chain and free amino acid molecules. Subsequently, the protein fraction and the protein-free mucus can be analysed separately using SERS. Several protein precipitation methods can be used. For example, precipitation using trichloroacetic acid, ammonium sulphate, acetone and a mixture of methanol and chloroform and ultrafiltration (Jiang et al., 2004). However, the peaks from the reagents used to precipitate the proteins can contribute to interference in the SERS spectrum. Therefore, ultrafiltration is the most suitable method to precipitate proteins.

A reusable SERS substrate can also be fabricated to reduce the long-term cost of performing SERS analysis of grouper mucus. Typically, reusable SERS

substrates are fabricated using plasmonic nanostructures immobilised on a substrate such as gold nanoparticles deposited on a zinc nanorod array on a quartz substrate (Pal et al., 2019). Additionally, gold nanoparticles can be immobilised on flexible substrate to fabricate a flexible and reusable SERS substrate. For example, gold nanoparticles can ne immobilised on a cotton fabric coated with reduced graphene oxide (Yang et al., 2021).

REFERENCES

Almehmadi, L. M., Curley, S. M., Tokranova, N. A., Tenenbaum, S. A., & Lednev, I. K. (2019). Surface Enhanced Raman Spectroscopy for Single Molecule Protein Detection. *Scientific Reports*, *9*(1), 12356. https://doi.org/10.1038/s41598-019-48650-y

Baena, J. R., & Lendl, B. (2004). Raman spectroscopy in chemical bioanalysis. *Current Opinion in Chemical Biology*, *8*(5), 534–539. https://doi.org/10.1016/j.cbpa.2004.08.014

Bell, S. E. J., & McCourt, M. R. (2009). SERS enhancement by aggregated Au colloids: effect of particle size. *Physical Chemistry Chemical Physics*, *11*(34), 7455–7462. https://doi.org/10.1039/B906049A

Betz, J. F., Yu, W. W., Cheng, Y., White, I. M., & Rubloff, G. W. (2014). Simple SERS substrates: powerful, portable, and full of potential. *Physical Chemistry Chemical Physics*, *16*(6), 2224–2239. https://doi.org/10.1039/C3CP53560F

Bocsa, C. D., Moisoiu, V., Stefancu, A., Leopold, L. F., Leopold, N., & Fodor, D. (2019). Knee osteoarthritis grading by resonant Raman and surface-enhanced Raman scattering (SERS) analysis of synovial fluid. *Nanomedicine: Nanotechnology, Biology and Medicine*, *20*, 102012. https://doi.org/https://doi.org/10.1016/j.nano.2019.04.015

Bratchenko, I. A., Bratchenko, L. A., Moryatov, A. A., Khristoforova, Y. A., Artemyev, D. N., Myakinin, O. O., Orlov, A. E., Kozlov, S. V., & Zakharov, V. P. (2021). In vivo diagnosis of skin cancer with a portable Raman spectroscopic device. *Experimental Dermatology*, *30*(5), 652–663. https://doi.org/10.1111/EXD.14301

Campanella, B., Palleschi, V., & Legnaioli, S. (2021). Introduction to vibrational spectroscopies. *ChemTexts*, *7*(1). https://doi.org/10.1007/S40828-020-00129-4

Chamuah, N., Saikia, A., Joseph, A. M., & Nath, P. (2019). Blu-ray DVD as SERS substrate for reliable detection of albumin, creatinine and urea in urine. *Sensors and Actuators B: Chemical*, *285*, 108–115. https://doi.org/https://doi.org/10.1016/j.snb.2019.01.031

Chen, M., & Zhao, H. (2019). Next-generation sequencing in liquid biopsy: cancer screening and early detection. *Human Genomics*, *13*(1), 34. https://doi.org/10.1186/s40246-019-0220-8

Chinello, C., Stella, M., Piga, I., Smith, A. J., Bovo, G., Varallo, M., Ivanova, M., Denti, V., Grasso, M., & Grasso, A. (2019). Proteomics of liquid biopsies: Depicting RCC infiltration into the renal vein by MS analysis of urine and plasma. *Journal of Proteomics*, *191*, 29–37.

Chu, Y., Mei, J., & Xie, J. (2023). Integrated volatile compounds and non-targeted metabolomics analysis reveal the characteristic flavor formation of proteins in grouper (Epinephelus coioides) during cold storage. *Food Research International*, *172*, 113145. https://doi.org/https://doi.org/10.1016/j.foodres.2023.113145

Colceriu-Șimon, I. M., Hedeșiu, M., Toma, V., Armencea, G., Moldovan, A., Știufiuc, G., Culic, B., Țărmure, V., Dinu, C., Berindan-Neagoe, I., Știufiuc, R. I., & Băciuț, M. (2019). The Effects of Low-Dose Irradiation on Human Saliva: A Surface-Enhanced Raman Spectroscopy Study. In *Diagnostics* (Vol. 9, Issue 3). https://doi.org/10.3390/diagnostics9030101

Connolly, J. M., Davies, K., Kazakeviciute, A., Wheatley, A. M., Dockery, P., Keogh, I., & Olivo, M. (2016). Non-invasive and label-free detection of oral squamous cell carcinoma using saliva surface-enhanced Raman spectroscopy and multivariate analysis. *Nanomedicine: Nanotechnology, Biology and Medicine*, *12*(6), 1593–1601. https://doi.org/https://doi.org/10.1016/j.nano.2016.02.021

Crocombe, R. A. (2018). Portable Spectroscopy. *Applied Spectroscopy*, *72*(12), 1701–1751. https://doi.org/10.1177/0003702818809719/ASSET/IMAGES/LARGE/10.1177_0003702818809719-FIG17.JPEG

Cui, L., Butler, H. J., Martin-Hirsch, P. L., & Martin, F. L. (2016). Aluminium foil as a potential substrate for ATR-FTIR{,} transflection FTIR or Raman spectrochemical analysis of biological specimens. *Anal. Methods*, *8*(3), 481–487. https://doi.org/10.1039/C5AY02638E

Curieux, F. Le, Gohlke, J. M., Pronk, A., Andersen, W. C., Chen, G., Fang, J.-L., Mitrowska, K., Sanders, P. J., Sun, M., Umbuzeiro, G. A., Umemura, T., Benbrahim-Tallaa, L., Ghissassi, F. El, Grosse, Y., Gwinn, W., Middleton, D., Suonio, E., Chung, F., Miranda-Filho, A., … Schubauer-Berigan, M. K. (2021). Carcinogenicity of gentian violet, leucogentian violet, malachite green, leucomalachite green, and CI Direct Blue 218. *The Lancet. Oncology*, *22*(5), 585–586. https://doi.org/10.1016/S1470-2045(21)00178-9

Cyrankiewicz, M., Wybranowski, T., & Kruszewski, S. (2007). Study of SERS efficiency of metallic colloidal systems. *Journal of Physics: Conference Series*, *79*(1), 2–8. https://doi.org/10.1088/1742-6596/79/1/012013

Daruich De Souza, C., Ribeiro Nogueira, B., & Rostelato, M. E. C. M. (2019). Review of the methodologies used in the synthesis gold nanoparticles by chemical reduction. *Journal of Alloys and Compounds*, *798*, 714–740. https://doi.org/10.1016/J.JALLCOM.2019.05.153

Dash, S., Das, S. K., Samal, J., & Thatoi, H. N. (2018). Epidermal mucus, a major determinant in fish health: A review. *Iranian Journal of Veterinary Research*, *19*(2), 72–81. https://doi.org/10.22099/ijvr.2018.4849

Ding, S. Y., You, E. M., Tian, Z. Q., & Moskovits, M. (2017). Electromagnetic theories of surface-enhanced Raman spectroscopy. *Chemical Society Reviews*, *46*(13), 4042–4076. https://doi.org/10.1039/c7cs00238f

Dou, X., Jung, Y. M., Cao, Z.-Q., & Ozaki, Y. (1999). Surface-Enhanced Raman Scattering of Biological Molecules on Metal Colloid II: Effects of Aggregation of Gold Colloid and Comparison of Effects of pH of Glycine Solutions between Gold and Silver Colloids. *Applied Spectroscopy*, *53*(11), 1440–1447. https://doi.org/10.1366/0003702991945803

Elumalai, S., Managó, S., & De Luca, A. C. (2020). Raman Microscopy: Progress in Research on Cancer Cell Sensing. *Sensors 2020, Vol. 20, Page 5525*, *20*(19), 5525. https://doi.org/10.3390/S20195525

Exline, D. (2013). *Comparison of Raman and FTIR Spectroscopy: Advantages and Limitations*. Gateway Analytical. https://gatewayanalytical.com/resources/publications/comparison-raman-and-ftir-spectroscopy-advantages-and-limitations/

Fan, W., Yang, S., Gao, W., Wang, D., & Fan, M. (2021). Highly sensitive bromide aided SERS detection of furazolidone and 3-amino-2-oxazolidinone residual in aquaculture products. *Microchemical Journal*, *169*(April), 106532. https://doi.org/10.1016/j.microc.2021.106532

Fang, C., Agarwal, A., Ji, H., Karen, W. Y., & Yobas, L. (2009). Preparation of a SERS substrate and its sample-loading method for point-of-use application. *Nanotechnology*, *20*(40), 405604. https://doi.org/10.1088/0957-4484/20/40/405604

Fleischmann, M., Hendra, P. J., & McQuillan, A. J. (1974). Raman spectra of pyridine adsorbed at a silver electrode. *Chemical Physics Letters*, *26*(2), 163–166. https://doi.org/https://doi.org/10.1016/0009-2614(74)85388-1

Fujiwara, S., Kawasaki, D., Sueyoshi, K., Hisamoto, H., & Endo, T. (2022). Gold Nanocone Array with Extensive Electromagnetic Fields for Highly Reproducible Surface-Enhanced Raman Scattering Measurements. In *Micromachines* (Vol. 13, Issue 8). https://doi.org/10.3390/mi13081182

Gajaraj, S., Fan, C., Lin, M., & Hu, Z. (2013). Quantitative detection of nitrate in water and wastewater by surface-enhanced Raman spectroscopy. *Environmental Monitoring and Assessment*, *185*(7), 5673–5681. https://doi.org/10.1007/s10661-012-2975-4

Ganbold, E.-O., Park, J.-H., Dembereldorj, U., Ock, K.-S., & Joo, S.-W. (2011). Charge-dependent adsorption of rhodamine 6G on gold nanoparticle surfaces: fluorescence and Raman study. *Journal of Raman Spectroscopy*, *42*(8), 1614–1619. https://doi.org/https://doi.org/10.1002/jrs.2907

Gong, T., Das, C. M., Yin, M. J., Lv, T. R., Singh, N. M., Soehartono, A. M., Singh, G., An, Q. F., & Yong, K. T. (2022). Development of SERS tags for human diseases screening and detection. *Coordination Chemistry Reviews*, *470*, 214711. https://doi.org/10.1016/J.CCR.2022.214711

Gühlke, M., Heiner, Z., & Kneipp, J. (2016). Surface-Enhanced Raman and Surface-Enhanced Hyper-Raman Scattering of Thiol-Functionalized Carotene. *The Journal of Physical Chemistry C*, *120*(37), 20702–20709. https://doi.org/10.1021/acs.jpcc.6b01895

Haiss, W., Thanh, N. T. K., Aveyard, J., & Fernig, D. G. (2007). Determination of Size and Concentration of Gold Nanoparticles from UV−Vis Spectra. *Analytical Chemistry*, *79*(11), 4215–4221. https://doi.org/10.1021/ac0702084

Han, X. X., Huang, G. G., Zhao, B., & Ozaki, Y. (2009). Label-Free Highly Sensitive Detection of Proteins in Aqueous Solutions Using Surface-Enhanced Raman Scattering. *Analytical Chemistry*, *81*(9), 3329–3333. https://doi.org/10.1021/ac900395x

Han, Y., Lan, X., Wei, T., Tsai, H.-L., & Xiao, H. (2009). Surface enhanced Raman scattering silica substrate fast fabrication by femtosecond laser pulses. *Applied Physics A*, *97*(3), 721–724. https://doi.org/10.1007/s00339-009-5306-z

Hanna, K., Krzoska, E., Shaaban, A. M., Muirhead, D., Abu-Eid, R., & Speirs, V. (2021). Raman spectroscopy: current applications in breast cancer diagnosis, challenges and future prospects. *British Journal of Cancer 2021 126:8*, *126*(8), 1125–1139. https://doi.org/10.1038/s41416-021-01659-5

Hong, S., & Li, X. (2013). Optimal size of gold nanoparticles for surface-enhanced Raman spectroscopy under different conditions. *Journal of Nanomaterials*, *2013*. https://doi.org/10.1155/2013/790323

Hu, J., Sheng, R. S., Xu, Z. S., & Zeng, Y. (1995). Surface enhanced Raman spectroscopy of lysozyme. *Spectrochimica Acta Part A: Molecular and Biomolecular Spectroscopy*, *51*(6), 1087–1096. https://doi.org/https://doi.org/10.1016/0584-8539(94)00225-Z

Hu, S., Huang, P. J. J., Wang, J., & Liu, J. (2020). Dissecting the Effect of Salt for More Sensitive Label-Free Colorimetric Detection of DNA Using Gold Nanoparticles. *Analytical Chemistry*, *92*(19), 13354–13360. https://doi.org/10.1021/ACS.ANALCHEM.0C02688/SUPPL_FILE/AC0C02688_SI_001.PDF

Hurtaud-Pessel, D., Couëdor, P., Verdon, E., & Dowell, D. (2013). Determination of residues of three triphenylmethane dyes and their metabolites (Malachite green, leuco malachite green, crystal violet, leuco crystal violet, and brilliant green) in aquaculture products by LC/MS/MS: First action 2012.25. *Journal of AOAC International*, *96*(5), 1152–1157. https://doi.org/10.5740/jaoacint.13-142

Iancu, S. D., Stefancu, A., Moisoiu, V., Leopold, L. F., & Leopold, N. (2019). The role of Ag+, Ca2+, Pb2+ and Al3+ adions in the SERS turn-on effect of anionic analytes. *Beilstein Journal of Nanotechnology*, *10*, 2338–2345.

Israelsen, N. D., Hanson, C., & Vargis, E. (2015). Nanoparticle Properties and Synthesis Effects on Surface-Enhanced Raman Scattering Enhancement Factor: An Introduction. *The Scientific World Journal*, *2015*, 124582. https://doi.org/10.1155/2015/124582

Jiang, L., He, L., & Fountoulakis, M. (2004). Comparison of protein precipitation methods for sample preparation prior to proteomic analysis. *Journal of Chromatography A*, *1023*(2), 317–320. https://doi.org/https://doi.org/10.1016/j.chroma.2003.10.029

Kalasinsky, K. S., & Kalasinsky, V. F. (2005). Infrared and Raman microspectroscopy of foreign materials in tissue specimens. *Spectrochimica Acta. Part A, Molecular and Biomolecular Spectroscopy*, *61*(7), 1707–1713. https://doi.org/10.1016/j.saa.2004.12.048

Ke, Q., Chen, L., Fang, B., Chen, Y., & Zhang, W. (2021). Simulating electric field intensity distribution of LSPR based on gold nanobipyramids. *Materials Today Communications*, *26*, 101953. https://doi.org/10.1016/J.MTCOMM.2020.101953

Kuhar, N., Sil, S., & Umapathy, S. (2021). Potential of Raman spectroscopic techniques to study proteins. *Spectrochimica Acta Part A: Molecular and Biomolecular Spectroscopy*, *258*, 119712. https://doi.org/10.1016/J.SAA.2021.119712

Kurouski, D., Postiglione, T., Deckert-Gaudig, T., Deckert, V., & Lednev, I. K. (2013). Amide I vibrational mode suppression in surface (SERS) and tip (TERS) enhanced Raman spectra of protein specimens. *Analyst*, *138*(6), 1665–1673. https://doi.org/10.1039/C2AN36478F

Lee, B., Mahmud, I., Marchica, J., Dereziński, P., Qi, F., Wang, F., Joshi, P., Valerio, F., Rivera, I., & Patel, V. (2020). Integrated RNA and metabolite profiling of urine liquid biopsies for prostate cancer biomarker discovery. *Scientific Reports*, *10*(1), 1–17.

Lee, P. C., & Meisel, D. (1982). Adsorption and surface-enhanced Raman of dyes on silver and gold sols. *The Journal of Physical Chemistry*, *86*(17), 3391–3395. https://doi.org/10.1021/j100214a025

Li, C., Hu, J., Jiang, L., Xu, C., Li, X., Gao, Y., & Qu, L. (2020). Shaped femtosecond laser induced photoreduction for highly controllable Au nanoparticles based on localized field enhancement and their SERS applications. *Nanophotonics*, *9*(3), 691–702. https://doi.org/10.1515/NANOPH-2019-0460/ASSET/GRAPHIC/J_NANOPH-2019-0460_FIG_007.JPG

Li, H., Merkl, P., Sommertune, J., Thersleff, T., Sotiriou, G. A., Li, H., Merkl, P., Sotiriou, G. A., Sommertune, J., & Thersleff, T. (2022). SERS Hotspot Engineering by Aerosol Self-Assembly of Plasmonic Ag Nanoaggregates with Tunable Interparticle Distance. *Advanced Science*, *9*(22), 2201133. https://doi.org/10.1002/ADVS.202201133

Li, Z., Li, M., Wang, C., Zhou, X., Li, J., & Li, D. (2019). Highly sensitive and selective method for detection of trace amounts of nitrite in aquaculture water by SERRS coupled with diazo reaction. *Sensors and Actuators, B: Chemical*, *297*(July), 126757. https://doi.org/10.1016/j.snb.2019.126757

Lin, C.-H., Jiang, L., Chai, Y.-H., Xiao, H., Chen, S.-J., & Tsai, H.-L. (2009). One-step fabrication of nanostructures by femtosecond laser for surface-enhanced Raman scattering. *Optics Express*, *17*(24), 21581–21589. https://doi.org/10.1364/OE.17.021581

Liu, X., Li, X., Xu, W., Zhang, X., Huang, Z., Wang, F., & Liu, J. (2018). Sub-Angstrom Gold Nanoparticle/Liposome Interfaces Controlled by Halides. *Langmuir*, *34*(22), 6628–6635. https://doi.org/10.1021/acs.langmuir.8b01138

Lv, H., Guan, Q., Wang, Y., & Zhang, X. (2021). Mechanical power driven SPME-SERS ultra-fast detection of illegal additives in aquaculture water. *RSC Advances*, *11*(21), 12893–12901. https://doi.org/10.1039/d0ra10227j

Magalhães, S., Goodfellow, B. J., & Nunes, A. (2021). FTIR spectroscopy in biomedical research: how to get the most out of its potential. *Applied Spectroscopy Reviews*, *56*(8–10), 869–907. https://doi.org/10.1080/05704928.2021.1946822

Mahmoud, A. Y. F., Rusin, C. J., & McDermott, M. T. (2020). Gold nanostars as a colloidal substrate for in-solution SERS measurements using a handheld Raman spectrometer. *The Analyst*, *145*(4), 1396–1407. https://doi.org/10.1039/c9an02439e

Mistro, G. Del, Cervo, S., Mansutti, E., Spizzo, R., Colombatti, A., Belmonte, P., Zucconelli, R., Steffan, A., Sergo, V., & Bonifacio, A. (2015). Surface–enhanced raman spectroscopy of urine for prostate cancer detection: A preliminary study. *Analytical and Bioanalytical Chemistry*, *407*(12), 3271–3275. https://doi.org/10.1007/s00216-015-8610-9

Moisoiu, V., Iancu, S. D., Stefancu, A., Moisoiu, T., Pardini, B., Dragomir, M. P., Crisan, N., Avram, L., Crisan, D., Andras, I., Fodor, D., Leopold, L. F., Socaciu, C., Bálint, Z., Tomuleasa, C., Elec, F., & Leopold, N. (2021). SERS liquid biopsy: An emerging tool for medical diagnosis. *Colloids and Surfaces B: Biointerfaces*, *208*(August). https://doi.org/10.1016/j.colsurfb.2021.112064

Moram, S. S. B., Byram, C., Shibu, S. N., Chilukamarri, B. M., & Soma, V. R. (2018). Ag/Au Nanoparticle-Loaded Paper-Based Versatile Surface-Enhanced Raman Spectroscopy Substrates for Multiple Explosives Detection. *ACS Omega*, *3*(7), 8190–8201. https://doi.org/10.1021/acsomega.8b01318

Mosier-Boss, P. A. (2017). Review of SERS Substrates for Chemical Sensing. In *Nanomaterials* (Vol. 7, Issue 6). https://doi.org/10.3390/nano7060142

Natnan, M. E., Low, C. F., Chong, C. M., Bunawan, H., & Baharum, S. N. (2021). Integration of Omics Tools for Understanding the Fish Immune Response Due to Microbial Challenge. *Frontiers in Marine Science*, *8*, 668771. https://doi.org/10.3389/FMARS.2021.668771/BIBTEX

Nurhikmah, Christianus, A., Wan Solahudin, W. M., Lau, B. Y., Ismail, I. S., & Fei, L. C. (2022). Skin Mucus Proteome Analysis Reveals Disease-Resistant Biomarker Signatures in Hybrid Grouper (Epinephelus fuscoguttatus ♀ × Epinephelus lanceolatus ♂) against Vibrio alginolyticus. In *Fishes* (Vol. 7, Issue 5). https://doi.org/10.3390/fishes7050278

Pal, A. K., Pagal, S., Prashanth, K., Chandra, G. K., Umapathy, S., & D., B. M. (2019). Ag/ZnO/Au 3D hybrid structured reusable SERS substrate as highly sensitive platform for DNA detection. *Sensors and Actuators B: Chemical*, *279*, 157–169. https://doi.org/https://doi.org/10.1016/j.snb.2018.09.085

Péron, O., Rinnert, E., Lehaitre, M., Crassous, P., & Compère, C. (2009). Detection of polycyclic aromatic hydrocarbon (PAH) compounds in artificial sea-water using surface-enhanced Raman scattering (SERS). *Talanta*, *79*(2), 199–204. https://doi.org/https://doi.org/10.1016/j.talanta.2009.03.043

Prestrelski, S. J., Tedeschi, N., Arakawa, T., & Carpenter, J. F. (1993). Dehydration-induced conformational transitions in proteins and their inhibition by stabilizers. *Biophysical Journal*, *65*(2), 661–671. https://doi.org/10.1016/S0006-3495(93)81120-2

Radzol, A. R. M., Lee, K. Y., Mansor, W., & Azman, A. (2014). Optimization of Savitzky-Golay smoothing filter for salivary surface enhanced Raman spectra of non structural protein 1. *TENCON 2014 - 2014 IEEE Region 10 Conference*, 1–6. https://doi.org/10.1109/TENCON.2014.7022409

Sadat, A., & Joye, I. J. (2020). Peak fitting applied to fourier transform infrared and raman spectroscopic analysis of proteins. *Applied Sciences (Switzerland)*, *10*(17). https://doi.org/10.3390/app10175918

Sauer, G., Nickel, U., & Schneider, S. (2000). Preparation of SERS-active silver film electrodes via electrocrystallization of silver. *Journal of Raman Spectroscopy*, *31*(5), 359–363. https://doi.org/https://doi.org/10.1002/1097-4555(200005)31:5<359::AID-JRS482>3.0.CO;2-I

Schneider, S., Grau, H., Halbig, P., Freunscht, P., & Nickel, U. (1996). Stabilization of Silver Colloids by Various Types of Anions and Their Effect on the Surface-Enhanced Raman Spectra of Organic Dyes. *Journal of Raman Spectroscopy*, *27*(1), 57–68. https://doi.org/https://doi.org/10.1002/(SICI)1097-4555(199601)27:1<57::AID-JRS926>3.0.CO;2-J

Sethuraman, A., & Belfort, G. (2005). Protein structural perturbation and aggregation on homogeneous surfaces. *Biophysical Journal*, *88*(2), 1322–1333. https://doi.org/10.1529/biophysj.104.051797

Shan, F., Zhang, X.-Y., Fu, X.-C., Zhang, L.-J., Su, D., Wang, S.-J., Wu, J.-Y., & Zhang, T. (2017). Investigation of simultaneously existed Raman scattering enhancement and inhibiting fluorescence using surface modified gold nanostars as SERS probes. *Scientific Reports*, *7*(1), 6813. https://doi.org/10.1038/s41598-017-07311-8

Shi, D., Sheng, F., Zhang, X., & Wang, G. (2018). Gold nanoparticle aggregation: Colorimetric detection of the interactions between avidin and biotin. *Talanta*, *185*, 106–112. https://doi.org/https://doi.org/10.1016/j.talanta.2018.02.102

Siiman, O., & Feilchenfeld, H. (1988). Internal fractal structure of aggregates of silver particles and its consequences on surface-enhanced Raman scattering intensities. *The Journal of Physical Chemistry*, *92*(2), 453–464. https://doi.org/10.1021/j100313a042

Singh, R. (2002). C. V. Raman and the Discovery of the Raman Effect. *Physics in Perspective*, *4*(4), 399–420. https://doi.org/10.1007/s000160200002

Smith, E., & Dent, G. (2005). Modern Raman spectroscopy—a practical approach. In *Journal of Raman Spectroscopy*. John Wiley & Sons Ltd.

Smith, W. E. (2008). Practical understanding and use of surface enhanced Raman scattering/surface enhanced resonance Raman scattering in chemical and biological analysis. *Chem. Soc. Rev.*, *37*(5), 955–964. https://doi.org/10.1039/B708841H

Stefancu, A., Badarinza, M., Moisoiu, V., Iancu, S. D., Serban, O., Leopold, N., & Fodor, D. (2019). SERS-based liquid biopsy of saliva and serum from patients with Sjögren's syndrome. *Analytical and Bioanalytical Chemistry*, *411*(22), 5877–5883. https://doi.org/10.1007/s00216-019-01969-x

Știufiuc, G. F., Toma, V., Buse, M., Mărginean, R., Morar-Bolba, G., Culic, B., Tetean, R., Leopold, N., Pavel, I., Lucaciu, C. M., & Știufiuc, R. I. (2020). Solid Plasmonic Substrates for Breast Cancer Detection by Means of SERS Analysis of Blood Plasma. In *Nanomaterials* (Vol. 10, Issue 6). https://doi.org/10.3390/nano10061212

Szekeres, G. P., & Kneipp, J. (2019). SERS probing of proteins in gold nanoparticle agglomerates. *Frontiers in Chemistry*, *7*(JAN), 1–10. https://doi.org/10.3389/fchem.2019.00030

Tantra, R., Brown, R. J. C., & Milton, M. J. T. (2007). Strategy to improve the reproducibility of colloidal SERS. *Journal of Raman Spectroscopy*, *38*(11), 1469–1479. https://doi.org/https://doi.org/10.1002/jrs.1797

Tay, L.-L., Hulse, J., Kennedy, D., & Pezacki, J. P. (2010). Surface-Enhanced Raman and Resonant Rayleigh Scatterings From Adsorbate Saturated Nanoparticles. *The Journal of Physical Chemistry C*, *114*(16), 7356–7363. https://doi.org/10.1021/jp9093222

Turkevich, J., Stevenson, P. C., & Hillier, J. (1951). A study of the nucleation and growth processes in the synthesis of colloidal gold. *Discuss. Faraday Soc.*, *11*(0), 55–75. https://doi.org/10.1039/DF9511100055

Turzhitsky, V., Zhang, L., Horowitz, G. L., Vitkin, E., Khan, U., Zakharov, Y., Qiu, L., Itzkan, I., & Perelman, L. T. (2018a). Picoanalysis of Drugs in Biofluids with Quantitative Label-Free Surface-Enhanced Raman Spectroscopy. *Small*, *14*(47), 1802392. https://doi.org/10.1002/SMLL.201802392

Tuschel, D. D., Pemberton, J. E., & Cook, J. E. (1986). SERS and SEM of roughened silver electrode surfaces formed by controlled oxidation-reduction in aqueous chloride media. *Langmuir*, *2*(4), 380–388. https://doi.org/10.1021/la00070a002

van de Poll, S. W. E., Römer, T. J., Volger, O. L., Delsing, D. J. M., Schut, T. C. B., Princen, H. M. G., Havekes, L. M., Jukema, J. W., van der Laarse, A., & Puppels, G. J. (2001). Raman Spectroscopic Evaluation of the Effects of Diet and Lipid-Lowering Therapy on Atherosclerotic Plaque Development in Mice. *Arteriosclerosis, Thrombosis, and Vascular Biology*, *21*(10), 1630–1635. https://doi.org/10.1161/hq1001.096651

Wan, F., Du, L., Chen, W., Wang, P., Wang, J., & Shi, H. (2017). A Novel Method to Directly Analyze Dissolved Acetic Acid in Transformer Oil without Extraction Using Raman Spectroscopy. *Energies 2017, Vol. 10, Page 967*, *10*(7), 967. https://doi.org/10.3390/EN10070967

Wang, Q., Wu, G., Pian, F., Shan, P., Li, Z., & Ma, Z. (2021). Simultaneous detection of glucose, triglycerides, and total cholesterol in whole blood by Fourier-Transform Raman spectroscopy. *Spectrochimica Acta Part A: Molecular and Biomolecular Spectroscopy*, *260*, 119906. https://doi.org/10.1016/J.SAA.2021.119906

Wang, Y., Yan, B., & Chen, L. (2013). SERS Tags: Novel Optical Nanoprobes for Bioanalysis. *Chemical Reviews*, *113*(3), 1391–1428. https://doi.org/10.1021/cr300120g

Wijesuriya, S., Burugapalli, K., Mackay, R., Ajaezi, G. C., & Balachandran, W. (2016). Chemically Roughened Solid Silver: A Simple, Robust and Broadband SERS Substrate. In *Sensors* (Vol. 16, Issue 10). https://doi.org/10.3390/s16101742

Wu, D.-Y., Li, J.-F., Ren, B., & Tian, Z.-Q. (2008). Electrochemical surface-enhanced Raman spectroscopy of nanostructures. *Chemical Society Reviews*, *37*(5), 1025–1041. https://doi.org/10.1039/B707872M

Xiao, R., Zhang, X., Rong, Z., Xiu, B., Yang, X., Wang, C., Hao, W., Zhang, Q., Liu, Z., Duan, C., Zhao, K., Guo, X., Fan, Y., Zhao, Y., Johnson, H., Huang, Y., Feng, X., Xu, X., Zhang, H., & Wang, S. (2016). Non-invasive detection of hepatocellular carcinoma serum metabolic profile through surface-enhanced Raman spectroscopy. *Nanomedicine: Nanotechnology, Biology and Medicine*, *12*(8), 2475–2484. https://doi.org/https://doi.org/10.1016/j.nano.2016.07.014

Xie, L., Lu, J., Liu, T., Chen, G., Liu, G., Ren, B., & Tian, Z. (2020). Key Role of Direct Adsorption on SERS Sensitivity: Synergistic Effect among Target, Aggregating Agent, and Surface with Au or Ag Colloid as Surface-Enhanced Raman Spectroscopy Substrate. *Journal of Physical Chemistry Letters*, *11*(3), 1022–1029. https://doi.org/10.1021/ACS.JPCLETT.9B03724/SUPPL_FILE/JZ9B03724_SI_001.PDF

Xu, L. J., Zong, C., Zheng, X. S., Hu, P., Feng, J. M., & Ren, B. (2014). Label-free detection of native proteins by surface-enhanced Raman spectroscopy using iodide-modified nanoparticles. *Analytical Chemistry*, *86*(4), 2238–2245. https://doi.org/10.1021/ac403974n

Xu, T., Wang, X., Huang, Y., Lai, K., & Fan, Y. (2019). Rapid detection of trace methylene blue and malachite green in four fish tissues by ultra-sensitive surface-enhanced Raman spectroscopy coated with gold nanorods. *Food Control*, *106*(March), 106720. https://doi.org/10.1016/j.foodcont.2019.106720

Xue, L., Yan, B., Li, Y., Tan, Y., Luo, X., & Wang, M. (2018). Surface-enhanced raman spectroscopy of blood serum based on gold nanoparticles for tumor stages detection and histologic grades classification of oral squamous cell carcinoma. *International Journal of Nanomedicine*, *13*, 4977–4986. https://doi.org/10.2147/IJN.S167996

Yang, J., Xu, J., Bian, X., Pu, Y., Chiu, K. lam, Miao, D., & Jiang, S. (2021). Flexible and reusable SERS substrate for rapid conformal detection of residue on irregular surface. *Cellulose*, *28*(2), 921–936. https://doi.org/10.1007/s10570-020-03568-x

Yazdi, S. H., & White, I. M. (2013). Multiplexed detection of aquaculture fungicides using a pump-free optofluidic sers microsystem. *Analyst*, *138*(1), 100–103. https://doi.org/10.1039/c2an36232e

Ye, Z. hao, Chen, X. tong, Zhu, H. yan, Liu, X. qian, Deng, W. hui, Song, W., Li, D. xiang, Hou, R. yan, Cai, H. mei, & Peng, C. yi. (2023). Aggregating-agent-assisted surface-enhanced Raman spectroscopy–based detection of acrylamide in fried foods: A case study with potato chips. *Food Chemistry*, *403*, 134377. https://doi.org/10.1016/J.FOODCHEM.2022.134377

Yu, W., Huang, Y., Pei, L., Fan, Y., Wang, X., & Lai, K. (2014). Magnetic FeAg hybrid nanoparticles as surface-enhanced raman scattering substrate for trace analysis of furazolidone in fish feeds. *Journal of Nanomaterials*, *2014*. https://doi.org/10.1155/2014/796575

Yu, X., Li, W., Liang, O., Bai, Y., & Xie, Y. (2020). Molecular orientation and specificity in the identification of biomolecules via surface enhanced Raman spectroscopy. *Analytical Biochemistry*, *599*, 113709. https://doi.org/10.1016/j.ab.2020.113709

Yue, W., Wang, Z., Yang, Y., Chen, L., Syed, A., Wong, K., & Wang, X. (2012). Electron-beam lithography of gold nanostructures for surface-enhanced Raman scattering. *Journal of Micromechanics and Microengineering*, *22*(12), 125007. https://doi.org/10.1088/0960-1317/22/12/125007

Yvon, H. J. (2017). Raman Spectroscopy for Analysis and Monitoring. *Horiba Jobin Yvon, Raman Application Note*, 1–2.

Zeiri, L., Rechav, K., Porat, Z., & Zeiri, Y. (2012). Silver Nanoparticles Deposited on Porous Silicon as a Surface-Enhanced Raman Scattering (SERS) Active Substrate. *Applied Spectroscopy*, *66*(3), 294–299.

Zhang, D., Neumann, O., Wang, H., Yuwono, V. M., Barhoumi, A., Perham, M., Hartgerink, J. D., Wittung-Stafshede, P., & Halas, N. J. (2009). Gold nanoparticles can induce the formation of protein-based aggregates at physiological pH. *Nano Letters*, *9*(2), 666–671. https://doi.org/10.1021/n1803054h

Zhang, Y., Mi, X., Tan, X., & Xiang, R. (2019). Recent Progress on Liquid Biopsy Analysis using Surface-Enhanced Raman Spectroscopy. *Theranostics*, *9*(2), 491–525. https://doi.org/10.7150/thno.29875

Zheng, T., Bott, S., & Huo, Q. (2016). Techniques for Accurate Sizing of Gold Nanoparticles Using Dynamic Light Scattering with Particular Application to Chemical and Biological Sensing Based on Aggregate Formation. *ACS Applied Materials & Interfaces*, *8*(33), 21585–21594. https://doi.org/10.1021/acsami.6b06903

Zheng, T., Cherubin, P., Cilenti, L., Teter, K., & Huo, Q. (2016). A simple and fast method to study the hydrodynamic size difference of protein disulfide isomerase in oxidized and reduced form using gold nanoparticles and dynamic light scattering. *Analyst*, *141*(3), 934–938. https://doi.org/10.1039/C5AN02248G

Zheng, X.-S., Jahn, I. J., Weber, K., Cialla-May, D., & Popp, J. (2018). Label-free SERS in biological and biomedical applications: Recent progress, current challenges and opportunities. *Spectrochimica Acta Part A: Molecular and Biomolecular Spectroscopy*, *197*, 56–77. https://doi.org/https://doi.org/10.1016/j.saa.2018.01.063

Zhou, X., Li, Z., Hao, Y., Duan, Q., Wang, C., Wang, T., & Li, D. (2019). Surface-enhanced Raman spectroscopy with partial least squares regression for rapid and accurate detection of malachite green in aquaculture water using large-size gold nanoparticles. *Spectroscopy Letters*, *53*(1), 63–75. https://doi.org/10.1080/00387010.2019.1696366

APPENDICES

Appendix A: Dynamic Light Scattering

Size Distribution Report by Intensity

v2.2

Malvern

Sample Details

Sample Name:	AuNp 1.25 MR 1
SOP Name:	Nathaniel.sop
General Notes:	

File Name:	Nathinel.dts	**Dispersant Name:**	Water
Record Number:	142	**Dispersant RI:**	1.330
Material RI:	0.20	**Viscosity (cP):**	0.8872
Material Absorbtion:	3.320	**Measurement Date and Time:**	Monday, January 01, 2007 11...

System

Temperature (°C):	25.0	**Duration Used (s):**	60
Count Rate (kcps):	305.9	**Measurement Position (mm):**	4.65
Cell Description:	Disposable sizing cuvette	**Attenuator:**	7

Results

		Size (d.nm):	**% Intensity:**	**St Dev (d.n...**
Z-Average (d.nm):	60.96	**Peak 1:**	69.24	86.8	26.48
PdI:	0.190	**Peak 2:**	10.00	12.0	3.206
Intercept:	0.795	**Peak 3:**	3.499	1.2	0.5463

Result quality : Refer to quality report

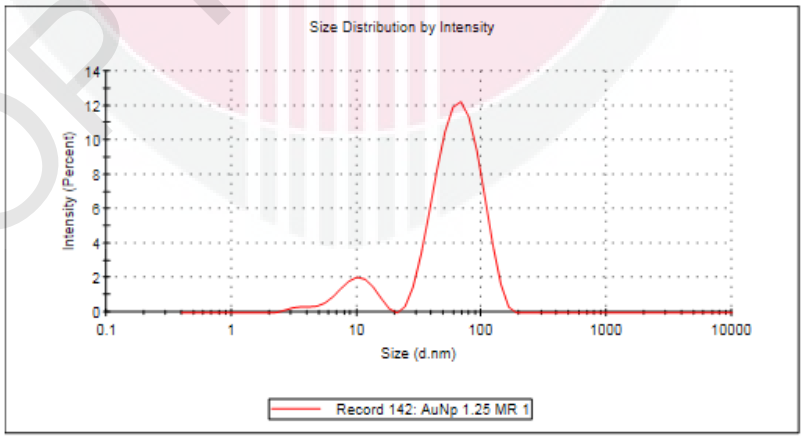

Malvern Instruments Ltd
www.malvern.com

Zetasizer Ver. 7.11
Serial Number : MAL1027945

File name: Nathinel
Record Number: 142
01 Jan 2007 11:28:26 PM

Size Distribution Report by Intensity

v2.2

Malvern

Sample Details

Sample Name: AuNp 1.25 MR 2

SOP Name: Nathaniel.sop

General Notes:

File Name:	Nathinel.dts	**Dispersant Name:**	Water
Record Number:	143	**Dispersant RI:**	1.330
Material RI:	0.20	**Viscosity (cP):**	0.8872
Material Absorbtion:	3.320	**Measurement Date and Time:**	Monday, January 01, 2007 11...

System

Temperature (°C):	25.0	**Duration Used (s):**	60
Count Rate (kcps):	308.0	**Measurement Position (mm):**	4.65
Cell Description:	Disposable sizing cuvette	**Attenuator:**	7

Results

			Size (d.nm):	% Intensity:	St Dev (d.n...
Z-Average (d.nm):	57.69	**Peak 1:**	73.07	85.4	29.78
PdI:	0.303	**Peak 2:**	11.20	12.6	3.162
Intercept:	0.800	**Peak 3:**	5392	2.0	314.9

Result quality : Refer to quality report

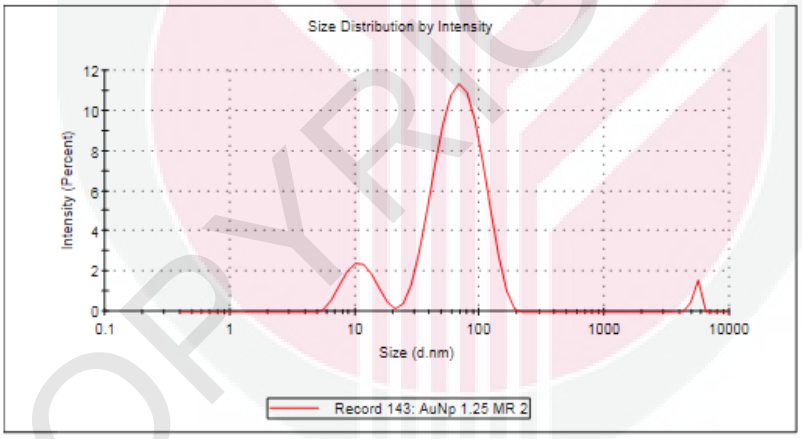

Size Distribution Report by Intensity

v2.2

Malvern

Sample Details

Sample Name: AuNp 1.25 MR 2

SOP Name: Nathaniel.sop

General Notes:

File Name:	Nathinel.dts	**Dispersant Name:**	Water
Record Number:	143	**Dispersant RI:**	1.330
Material RI:	0.20	**Viscosity (cP):**	0.8872
Material Absorbtion:	3.320	**Measurement Date and Time:**	Monday, January 01, 2007 11...

System

Temperature (°C):	25.0	**Duration Used (s):**	60
Count Rate (kcps):	308.0	**Measurement Position (mm):**	4.65
Cell Description:	Disposable sizing cuvette	**Attenuator:**	7

Results

			Size (d.nm):	% Intensity:	St Dev (d.n...
Z-Average (d.nm):	57.69	**Peak 1:**	73.07	85.4	29.78
PdI:	0.303	**Peak 2:**	11.20	12.6	3.162
Intercept:	0.800	**Peak 3:**	5392	2.0	314.9

Result quality : Refer to quality report

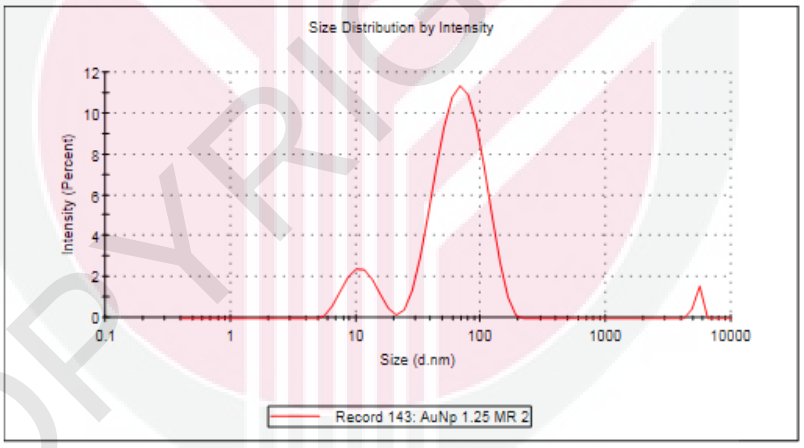

PUBLICATION

Leong, N., Yaacob, M. H., Zain, A. R. M., Aziz, T. H. T. A., Christianus, A., Chong, C. M., & Mahdi, M. A. (2024). Colloidal surface-enhanced Raman spectroscopic study of grouper epidermal mucus using acidified sodium sulphate as the aggregating agent. Spectrochimica Acta Part A: Molecular and Biomolecular Spectroscopy, 123974. https://doi.org/10.1016/J.SAA.2024.1239